Desenvolvimento, fabricação e aplicação de dispositivos eletroquímicos usando impressão 3D

Rafael Melo Cardoso

Universidade Federal de Uberlândia
Instituto de Química
Programa de Pós-Graduação em Química

Uberlândia
2020

Rafael Melo Cardoso

Desenvolvimento, fabricação e aplicação de dispositivos eletroquímicos usando impressão 3D

Tese de doutorado apresentada ao Programa de Pós-graduação do Instituto de Química da Universidade Federal de Uberlândia como parte dos requisitos para a obtenção do título de Doutor em Ciências.

Área de concentração: Quimica Analítica

Orientador: Rodrigo Alejandro Abarza Muñoz
Coorientador: Rodrigo Amorim Bezerra da Silva

Uberlândia
2020

Ficha Catalográfica Online do Sistema de Bibliotecas da UFU
com dados informados pelo(a) próprio(a) autor(a).

C268 Cardoso, Rafael Melo, 1988-
2020 Development, fabrication and application of electrochemical devices using 3D-printing [recurso eletrônico] : Desenvolvimento, fabricação e aplicação de dispositivos eletroquímicos usando impressão 3D / Rafael Melo Cardoso. - 2020.

Orientador: Rodrigo Alejandro Abarza Muñoz.
Coorientador: Rodrigo Amorim Bezerra da Silva.
Tese (Doutorado) - Universidade Federal de Uberlândia, Pós-graduação em Química.
Modo de acesso: Internet.
Disponível em: http://doi.org/10.14393/ufu.te.2020.723
Inclui bibliografia.
Inclui ilustrações.

1. Química. I. Muñoz, Rodrigo Alejandro Abarza ,1980-, (Orient.). II. Silva, Rodrigo Amorim Bezerra da,1983-, (Coorient.). III. Universidade Federal de Uberlândia. Pós-graduação em Química. IV. Título.

CDU: 54

Bibliotecários responsáveis pela estrutura de acordo com o AACR2:

Gizele Cristine Nunes do Couto - CRB6/2091

UNIVERSIDADE FEDERAL DE UBERLÂNDIA
Coordenação do Programa de Pós-Graduação em Química
Av. João Naves de Ávila, 2121, Bloco 5I - Bairro Santa Mônica, Uberlândia-MG, CEP 38400-902
Telefone: (34) 3239-4385 - www.cpgquimica.iq.ufu.br - cpgquimica@ufu.br

ATA DE DEFESA - PÓS-GRADUAÇÃO

Programa de Pós-Graduação em:	Química				
Defesa de:	Tese de Doutorado Acadêmico, 109, PPGQUI				
Data:	trinta de outubro de dois mil e vinte	Hora de início:	14:00	Hora de encerramento:	19:45
Matrícula do Discente:	11623QMI001				
Nome do Discente:	Rafael Melo Cardoso				
Título do Trabalho:	Desenvolvimento, fabricação e aplicação de dispositivos eletroquímicos usando impressão 3D				
Área de concentração:	Química				
Linha de pesquisa:	Eletroquímica Aplicada				
Projeto de Pesquisa de vinculação:	Novos materiais e estratégias para a produção de sensores eletroquímicos de alto desempenho.				

Reuniu-se por meio de webconferência, Plataforma GoogleMeet, https://meet.google.com/kqi-mgft-nhf, a Banca Examinadora, designada pelo Colegiado do Programa de Pós-graduação em Química, assim composta: Professores Doutores: João Flávio da Silveira Petruci, da Universidade Federal de Uberlândia; Lívia Flório Sgobbi, da Universidade Federal de Goiás; Iranaldo Santos da Silva, da Universidade Federal do Maranhão; Fabiana da Silva Felix, da Universidade Federal de Lavras e Rodrigo Alejandro Abarza Muñoz, orientador(a) do(a) candidato(a).

Iniciando os trabalhos o(a) presidente da mesa, Dr. Rodrigo Alejandro Abarza Muñoz, apresentou a Comissão Examinadora e o candidato(a), agradeceu a presença do público, e concedeu ao Discente a palavra para a exposição do seu trabalho. A duração da apresentação do Discente e o tempo de arguição e resposta foram conforme as normas do Programa.

A seguir o senhor(a) presidente concedeu a palavra, pela ordem sucessivamente, aos(às) examinadores(as), que passaram a arguir o(a) candidato(a). Ultimada a arguição, que se desenvolveu dentro dos termos regimentais, a Banca, em sessão secreta, atribuiu o resultado final, considerando o(a) candidato(a):

Aprovado(a).

Esta defesa faz parte dos requisitos necessários à obtenção do título de Doutor.

O competente diploma será expedido após cumprimento dos demais requisitos, conforme as normas do Programa, a legislação pertinente e a regulamentação interna da UFU.

Documento assinado eletronicamente por **Rodrigo Alejandro Abarza Munoz**, **Professor(a) do Magistério Superior**, em 30/10/2020, às 19:39, conforme horário oficial de Brasília, com fundamento no art. 6º, § 1º, do Decreto nº 8.539, de 8 de outubro de 2015.

Documento assinado eletronicamente por **Iranaldo Santos da Silva**, **Usuário Externo**, em 30/10/2020, às 19:40, conforme horário oficial de Brasília, com fundamento no art. 6º, § 1º, do Decreto nº 8.539, de 8 de outubro de 2015.

Documento assinado eletronicamente por **João Flávio da Silveira Petruci**, **Professor(a) do Magistério Superior**, em 30/10/2020, às 19:40, conforme horário oficial de Brasília, com fundamento no art. 6º, § 1º, do Decreto nº 8.539, de 8 de outubro de 2015.

Documento assinado eletronicamente por **Fabiana da Silva Felix**, **Usuário Externo**, em 02/11/2020, às 16:08, conforme horário oficial de Brasília, com fundamento no art. 6º, § 1º, do Decreto nº 8.539, de 8 de outubro de 2015.

Documento assinado eletronicamente por **Lívia Flório Sgobbi**, **Usuário Externo**, em 04/11/2020, às 09:29, conforme horário oficial de Brasília, com fundamento no art. 6º, § 1º, do Decreto nº 8.539, de 8 de outubro de 2015.

A autenticidade deste documento pode ser conferida no site https://www.sei.ufu.br/sei/controlador_externo.php?acao=documento_conferir&id_orgao_acesso_externo=0, informando o código verificador **2356366** e o código CRC **6AFF9C15**.

Referência: Processo nº 23117.065095/2020-57 SEI nº 2356366

Em memória de Célia de Andrade Melo

Agradecimentos:

Agradeço a Deus, que sempre olhou por mim e meus entes queridos.

Aos meus queridos pais Antônio e Elizete pela dedicação, amor e carinho em mim depositados, e minha irmã Bárbara.

À minha querida esposa que sempre esteve ao meu lado me apoiando incondicionalmente em todas as etapas deste trabalho, e à minha filha que foi um presente de Deus. Vocês são minha motivação diária e as amo muito.

Agradeço a todos que acreditaram e me ajudaram diretamente ou indiretamente em todas as etapas deste trabalho. Sou muito grato a todos estes e sei que Deus está olhando por todos nós.

Aos amigos do NUPE, por partilharem esta jornada comigo com crescimento em conjunto.

Aos queridos amigos de peito que sempre foram presentes em minha vida.

Ao Instituto de Química da Universidade Federal de Uberlândia, e todos seus funcionários de todos os níveis.

Aos órgãos de fomento CNPq, CAPES e FAPEMIG e FAU, em especial ao projeto CAPES pelo provimento de bolsa de estudos, e financiamento do projeto 88881.188561/2018-01 PDSE doutorado sanduiche.

O presente trabalho foi realizado com apoio da Coordenação de Aperfeiçoamento de Pessoal de Nível Superior – Brasil (CAPES) – Código de Financiamento 001

"Life is and will ever remain an equation incapable of solution, but it contains certain known factors."

(Nikola Tesla)

Resumo

Esta tese tem como foco o uso de recentes inovações em manufatura aditiva (impressão 3D) na confecção de células e sensores eletroquímicos. Como introdução este trabalho faz uma revisão completa sobre o tema, seguida de construção, caracterizações e aplicações de sensores e células impressas em 3D na eletroanalítica. A primeira delas é uma célula eletroanalítica para medidas hidrodinâmicas e estacionárias. A segunda se trata de sensores impressos por 3D baseado em um termoplástico condutivo, dopado com materiais carbonáceos (grafeno ou negro de fumo). A combinação destas células e eletrodos impressos em 3D contendo grafeno, foram aplicados na área forense na amostragem, identificação e quantificação do explosivo 2,4,6-trinitrotolueno, o conhecido TNT. O dispositivo foi proposto para amostragens em locais suspeitos de crimes que envolvam manuseio deste material. Um limite de detecção (LOD) de 0,4 $\mu molL^{-1}$ em uma faixa linear de 1 – 870 μmol L^{-1} foram reportados. Na área de bioanalítica, 3 moléculas foram analisadas em metodologias propostas. A primeira utilizando ou amperometria de múltiplos pulsos, para analise simultânea de nitrito e ácido úrico, em saliva e urina atingindo resultados de faixa linear de 0,5–250 μmol L^{-1} para ambos analitos e LODs de 0,02 e 0,03 μmol L^{-1} para ácido úrico e nitrito respectivamente, com precisão calculada de até RSD < 2,1 % e índices de recuperação de 70 - 120%. A modificação do sensor com a enzima glicose oxidase (GOx) foi proposta, atingindo LOD de 15 μmol L^{-1}, precisão intra-dia de 5% e índices de recuperação entre 90–105 % para glicose em plasma sanguíneo. Todos os dispositivos apresentaram custo inferior a U$0,50/unidade e alta precisão de fabricação (RSD = 4%). Por último esta tese também mostra como uma caneta 3D pode ser utilizada na construção de sensores com termoplástico condutivo contendo negro de fumo como material condutor. Em uma comparação o eletrodo impresso por impressora 3D apresentou melhores característica analíticas em comparação ao eletrodo 3 em 1 proposto usando a caneta 3D, porém características promissoras foram observadas como possibilidade de análise em uma gota, baixo consumo de plástico condutivo na construção e resultados voltamétricos comparáveis a eletrodos SPE's comerciais. Tudo isso com formato portátil e totalmente adaptável.

Palavras-chave: Impressão 3D; sensores eletroquímicos; forense; bioanálise, ácido polilático(PLA).

Development, fabrication and application of electrochemical devices using 3D-printing

Rafael Melo Cardoso

Universidade Federal de Uberlândia
Instituto de Química
Programa de Pós-Graduação em Química

Uberlândia
2020

Abstract

Recent advances in the manufacturing of electroanalytical sensors, cells and devices using 3D-printing is the focus of this work. This thesis introduces this theme/topic with a wide and critical literature freview, followed by several proposed applications at electroanalytical prototyping and sensing. The first of those is an electroanalytical cell, for hydrodynamic and stationary measurements, and 3D-printed sensors based on a conductive thermoplastic with carbonaceous materials (graphene or carbon black). The electrodes were applied in the forensic field by quantification, detection and sampling 2,4,6-trinitrotoluene, well known as TNT. The proposed device is a flexible sampler-sensor for suspect powders in crime scenes and presented proper analytical characteristics reaching a LOD of 0.4 μmol L^{-1} in a linear interval of $1 - 870$ μ molL^{-1} for TNT. This thesis also shows how a 3D pen can be used to fabricate electrochemical sensors, also proposed for TNT detection,presenting higher LOD, but interesting characteristics such as low volume in a drop of 100 μL, low conductive plastic consumption and voltammetric results similar to a commercial SPE. All this in portable shape cylindrical or three in one electrode. In the field of bioanalytics, glucose was a target molecule for 3D-printed electrodes modified with glucose oxidase, using chronoamperometry, reaching LOD of 15 μmolL^{-1}, inter-day and intra-day precision lower than 5 %, and adequate recovery values (90–105 %) for the analysis of blood plasma. A simultaneous method using amperometric detection of nitrite and uric acid within a linear range from 0.5–250 μmol L^{-1} for both analytes, LODs of 0.02 and 0.03 μmol L^{-1} for uric acid and nitrite, respectively, and high precision (RSD $<$ 2.1 % were obtained). This thesis also shows the first application of 3D-printed sensors and biosensors for the analysis of real biological samples with analytical features comparable to conventional modified electrodes.All the 3D-printed devices presented a unit cost lower than U$0.50 and high precision of fabrication (RSD = 4%).

Keywords: 3D-printing; additive manufacturing; electrochemical sensors; bioanalysis; forensics..

List of Figures

Figure 1 – The structure of this thesis. 26

Figure 2 – Schematics representation of extrusion (a and b) and bulk (c and d) 3D-printing methods: (a) fused deposition modeling (FDM); (b) direct ink writing (DIW); (c) digital light processing (DLP) and (d) selective laser melting (SLM). Adapted from (ELDER et al., 2020). 30

Figure 3 – (A) Scheme of horizontal and vertical 3D-printed electrodes using carbon black/ABS material; (B) Photographs of vertical printed (VP), horizontal printed rough surface (HPRS) and horizontal printed smooth surface (HPSS) electrodes. Reprinted with permission from (Bin Hamzah et al., 2018), Copyright (2018), Springer US. 39

Figure 4 – Representation of the 3D-printed graphene/PLA electrodes fabrication, proteinase K-mediated PLA digestion/activation and application for the 1-naphthol oxidation enzyme-mediated. Reprinted with permission from (MANZANARES-PALENZUELA et al., 2019), 2019), Copyright (2019), The Royal Society of Chemistry. 40

Figure 5 – (A) Representation of the 3D-printing procedure for the fabrication of the cell-on-a-chip device using a dual extruder 3D-printer; (B) Dimensions of the 3D-printed cell-on-a-chip device (in cm); (C) Real photograph of the device. Reprinted with permission from (KATSELI; ECONOMOU; KOKKINOS, 2020), Copyright 2020, Elsevier. 44

Figure 6 – Schematic 3D-printed (AM) electrochemical cell and the 3D-printing working electrode preparation by polishing. On right, SEM images of the 3D-printed surface after polishing and after electrochemical activation. Reprinted with permission from (RICHTER et al., 2019), Copyright (2019), American Chemical Society. 45

Figure 7 – Scheme of the proposed flow analysis device with (a) the representation of the dual extruder 3D-printer; (b) Orthogonal view of all 3D-printed flow device containing 2 electrodes: Working electrode (WE) and quasi-reference or counter electrode (QRCE); (c) perspective view of the device with embedded electrodes. Reprinted with permission from (O'NEIL et al., 2019), Copyright (2020), Elsevier. 47

Figure 8 – Image of the FDM 3D-printed electrodes where 1 is the printed hollow cube, 2 is the printed part with two faces removed (3 and 4), with 3 being the polished electrode and 4 the unpolished; 5 is the 1200grit sandpaper used 52

Figure 9 – (A) Scheme of the 3D-printed cell (transversal cut view) used for batch (1) and flow (2) electrochemical measurements; counter and reference electrodes are represented in A.1 while the use of SPE in A.2 dispenses the use of external counter and reference electrodes; (B) Components of the 3D-printed cell: (1) cell body, (2) bottom cover, (3) screws, (4) top cover; (5) micro-pipette adaptor; (6) O-rings with 2 different internal diameter: 5.28 mm (for any working electrode) and 7.65 mm (for the SPE strip); and (7) steel plate (for electric contact of working electrodes by their backside). Note that A.1 and A.2 show the same cell except to the micro-pipette adaptor (5) and pipette tip that is assembled for flow experiments (A.2). 53

Figure 10 – Cyclic voltammograms recorded in absence (blank electrolyte solution) and presence of 1.0 mmol L^{-1} TBHQ on carbon SPE (A), 1.0 mmol L^{-1} dipyrone on gold CDtrode (B), 1.0 mmol L^{-1} dopamine on GSE (C) and 1.0 mmol L^{-1} diclofenac on BDD electrode (D). Supporting electrolytes: 0.1 mol L^{-1} $HClO_4$ in A and C, 0.1 mol L^{-1} phosphate buffer (pH 7.2) in B and 0.1 mol L^{-1} H_2SO_4 in D. Counter and reference electrodes: Pt and Ag/AgCl/$KCl_{sat.}$, respectively, in B, C, and D. Scan rate: 50 mV s^{-1}. 56

Figure 11 – Amperometric responses (n = 3) obtained for solutions injected in increasing and decreasing concentration order: (A) TBHQ, (B) dipyrone (DIP), (C) dopamine (DOP), and (D) diclofenac (DIC). Concentration ranges: 1 – 1000 μmol L^{-1} (A, B, and C) and 5 – 50 μmol L^{-1} (D). Applied potentials: (A) +0.5 V (vs. pseudo Ag), (B) +0.6 V, (C) +0.9 V, (D) +1.2 V (*vs* Ag/AgCl/$KCl_{sat.}$). Injection volume: 100 μL (A, B, and C) and 50 μL (D); flow rate: 153 μL s^{-1} (A, B, and C) and 50 μL s^{-1} (3.0 mL min^{-1}) (D). Stirring rate (A, B, and C): 700 rpm. Supporting electrolytes and electrodes are the same of Figure 10 58

Figure 12 – Electrochemistry on conductive G-PLA electrode: (A) Cyclic voltammetry of 1 mmol L^{-1} $Ru(NH_3)_6$ $^{3+}$ at different scan rates (v) and (B) respective plots of i *vs.* $v^{1/2}$ in 0.1 mol L^{-1} phosphate buffer pH 7; (C) Cyclic voltammograms of 1 mmol L^{-1} of catechol and respective blank and (D) SWV scans for catechol from 5 to 300 μmol L^{-1} in 0.1 mol L^{-1} $HClO_4$ (frequency: 50 Hz, amplitude: 50 mV, step: 5 mV); and (E) BIA with amperometric detection (E = +1.2 V) of dopamine in a stirred 0.1 mol L^{-1} $HClO_4$ solution: successive injections from 1 to 400 μmol L^{-1}. 60

Figure 13 – (A) EIS spectra and (B) cyclic voltammograms (scan rate of 50 mV s^{-1}) obtained on the 3D-printed G-PLA electrode (black) and on bare GCE (red) in the presence of 1 mmol L^{-1} $Ru(NH_3)_6^{+3}$ in 0.1 mol L^{-1} KCl solution, in the frequency range between 0.1 Hz and 50.000 Hz with signal amplitude of 10 mV with 10 data points per frequency decade. Current density values were plotted in cyclic voltammograms for a better comparison. 61

Figure 14 – Infrared spectrum (ATR mode) of 3D-printed G-PLA surface. 62

Figure 15 – (A) Raman spectrum and (B) SEM image of 3D-printed G-doped PLA electrode. Inset in A: Lorentz deconvolution of D, G and D' bands. . . 64

Figure 16 – SEM images of G-PLA: (A) before and (B) after mechanical polishing. 71

Figure 17 – (A) FT-IR spectra and (B) XRD patterns for the polished 3D-printed G-PLA. 71

Figure 18 – Cyclic voltammograms of catechol 1 mmol L^{-1} (solid lines) and respective blank (0.1 mol L^{-1} HCl, dotted lines) on the 3D-printed G-PLA electrode before (black) and after (blue) mechanical polishing of the surface. 72

Figure 19 – Cyclic voltammograms on 3D-printed G-PLA electrode of blank solutions (dotted lines) and 1 mmol L^{-1} catechol after electrode surface polishing using different grit polishers: 600(black), 800 (red), 1200(purple) and 1500(blue). Electrolyte: 0.1 mol L^{-1} HCl, scan rate 50 mV s^{-1}, starting at 0.0 V. 73

Figure 20 – (Left) Square-wave voltammograms of increasing concentration of TNT solutions: a) 1; b) 2; c) 3; d) 4; e) 5; f) 10; g) 20; h) 29; i) 38 j) 47; k) 95; l) 188; m) 279; n) 369; o) 457; p) 543; q) 628; r) 711; s) 792; t) 873 μmol L^{-1} recorded on polished G-PLA electrodes and (Right) the respective analytical curve. Inset (left): 10 successive measurements for 100 µmol L^{-1} of TNT. Conditions: Step: 6 mV; Amplitude: 40 mV; Frequency: 40 Hz; Electrolyte: 0.1 mol L^{-1} HCl. 74

Figure 21 – Square-wave voltammograms (1st cycle) of residual TNT detection after swiping the 3D-printed sensor over (A) granite, (B) metallic and (C) glove surfaces (black). Blue lines correspond to blank experiments performed before TNT sampling. Conditions: Step 6 mV; Amplitude 40 mV; Frequency 40 Hz. Electrolyte 0.1 mol L^{-1} HCl. 75

Figure 22 – Atomic force microscopy measurements of the 3D-printed G-PLA surface in 5.0 × 5.0 μm dimension (rugosity value of 112 nm). 75

Figure 23 – Square-wave voltammograms of a blank solution (black) and in the presence of 100 µmol L^{-1} TNT (red), 2,4-dinitrotoluene (green), o-and p-nitrotoluene (dark blue) and nitrobenzene (light blue) recorded on polished G-PLA electrodes. Other conditions were similar to Figure 21 77

Figure 24 – Square-wave anodic stripping voltammograms of standard solutions of Pb(II) (a: 60, b: 120, c: 180, d: 240, e: 300 µg L^{-1}) and Cu(II) (a: 10, b: 20, c: 30, d: 40, e: 50 µg L^{-1}) on G-PLA electrode. Step: 4 mV; Amplitude: 40 mV; Frequency: 10 Hz; Deposition time: 90 s; Electrolyte: 0.1 mol L^{-1} HCl. 78

Figure 25 – Shows an example of a glucose electrochemical sensor using the classic Prussian Blue (PB) as mediator. Adapted with authorization from the literature (RICCI; PALLESCHI, 2005). 83

Figure 26 – Cyclic voltamogramms for solutions containing 1 mmol L^{-1} FCA in absence (red dashed line) and in the presence of 5 mmol L^{-1} glucose (black solid line). Supporting electrolyte: 0.1 mol L^{-1} phosphate buffer pH 7.0. Scan rate 50 mV s^{-1}. 86

Figure 27 – Representation of the GOx biosensor in two steps to convert glucose into glucolactone mediated by FCA 87

Figure 28 – Amperometric biosensor response as function of pH in 0.1 mol L^{-1} phosphate buffer, for 5 mmol L^{-1} glucose in presence of 1 mmol L^{-1} FCA. 88

Figure 29 – Amperometric biosensor response for different enzyme concentration values (1.0, 3.0, 5.0, 7.0 and 10.0 mg m L^{-1}) used in electrode modification. Measures performed in 0.1 mol L^{-1} phosphate buffer pH 7.0, for 5 mmol L^{-1} glucose in presence of 1 mmol L^{-1} FCA. 88

Figure 30 – Effect of different applied potential values (0.2, 0.3, 0.4, 0.5 and 0.6 V) on the amperometric biosensor response. Measurements performed in 0.1 mol L^{-1} phosphate buffer pH 7.0, for 5 mmol L^{-1} glucose in the presence of 1 mmol L^{-1} FCA. 89

Figure 31 – (A) Amperometric curves obtained in the presence of: a) 0; b) 0.5; c) 1.0; d) 1.8; e) 2.8; f) 4.6 and g) 6.3 mmol L^{-1} glucose. (B) Linear regression obtained from glucose concentration versus limit current. Supporting electrolyte: 0.1 mol L^{-1} phosphate buffer (pH 7.0) with 1 mmol L^{-1} FCA. Error bars obtained from the standard deviation of 5 replicates for each glucose concentration. 89

Figure 32 – Cyclic voltammograms for 1.0 mmol L^{-1} UA (A) and NIT (B) in 0.1 mol L^{-1} BR buffer pH 2 recorded on the 3D-printed G-PLA electrode (black), after mechanical polishing (green) and solvent-treated after polishing (blue). Dashed lines correspond to the respective blanks. Scan rate: 50 mV s^{-1}; step potential: 5 mV. 91

Figure 33 – SEM images of G-PLA surfaces: (A) untreated, (B) polished and (C) solvent treated after polishing. 93

Figure 34 – (A) Hydrodynamic voltammograms obtained by plotting peak current values as a function of the corresponding applied potential pulses (70 ms each pulse). The solutions contained 10 μmol L^{-1} of UA (•) and NIT (■). (B) Amperometric responses (n=5) of solutions containing only UA (20 μmol L^{-1}), only NIT (20 μmol L^{-1}) and UA + NIT (20 μmol L^{-1} each). Supporting electrolyte: BR buffer pH 2; dispensing rate: 280 μL s^{-1}; injection volume: 100 μL. 94

Figure 35 – Study of the injected volume (A) and dispensing rate (B) in the BIA system using the 3D-printed G-PLA electrode. Injections of 10, 30, 50, 75, 100 and 200 μL, dispensing rate 16.5, 33.2, 48.7, 78.1, 164, 213, 280 and 370 μL s^{-1} of standard solution of 20 μmol L^{-1} UA. Potential pulse: +0.70 V (■) and +1.0 V (•) for 50 ms. Correction factor (CF): iUA at +1.0 V / iUA at +0.7 V (•). Supporting electrolyte: 0.1 mol L^{-1} BR buffer solution (pH 2); in (A) dispensing rate: 280 μL s^{-1}; in (B) injection volume: 100 μL. 95

Figure 36 – Amperometric responses obtained after triplicate injections of solutions containing increasing concentrations of UA (0.5 to 500 µmol L-1) for study the correction factor. (B) Analytical curves obtained at () +0.7 V (0.5 - 350 molL-1) and at () +1.0 V (0.5 – 500 molL-1); the calculated correction factor for each concentration is plotted as blue (). Other conditions see Figure 34. 96

Figure 37 – (A) Amperometric responses obtained after triplicate injections of solutions containing increasing concentrations of NIT (0.5 to 500 μmol L^{-1}). (B) Analytical curve obtained at +1.0 V. Other conditions: see Figure 34. 97

Figure 38 – Amperograms obtained from alternating injections (n=12) of standard solutions containing 10 + 10 μmol L^{-1} and 25 + 25 μmol L^{-1} of UA and NIT. Supporting electrolyte: 0.1 mol L^{-1} BR buffer solution (pH 2); dispensing rate: 280 μL s^{-1}; injection volume: 100 μL. 97

Figure 39 – Amperometric responses obtained at (A) +0.7 V and (B) +1.0 V after triplicate injections of solutions containing only UA used to obtain the CF value, followed by the triplicate injection of ten standard solutions containing simultaneously increasing concentrations of UA and NIT (black line = i_{UA}) and (red line = $i_{UA+NIT)}$ (a-j: 0.5 – 250 μmol L^{-1}), and a triplicate injection of UA. (C) and (D) show the corresponding calibration curves for NIT and UA. Experimental conditions: see Figure 34. 98

Figure 40 – Simplified representation of internal parts of the 3D-Pen and a scheme of the customized 3D-printed substrate of the three-electrode device (TES): (1) Conductive thermoplastic filament; (2) geared mechanism (5 V) motor; (3) filament guide tube; (4) command buttons; (5) heated nozzle (190 °C); and (6) illustrative cut of the FDM 3D-printed device showing wires and template holes to be filled by the filament 106

Figure 41 – Schematic orthogonal view of the electrochemical devices fabricated using a 3D-Pen and customized 3D-printing structures: (1 and 2) Side and top views of cylindrical working electrodes with the body 3D-printed by FDM (WE-FDM) or DLP (WE-DLP). with the holes partially filled by the conductive filament using the 3D-Pen; (3 and 4) Top and transversal views of the three-electrode-systems (TES) on planar substrates 3D-printed by FDM (TES-FDM) or DLP (TES-DLP). Holes in the substrates (electrodes location) are illustrated with partial filled of the conductive filament to facilitate identification of these regions. . . . 107

Figure 43 – Images of the TES-DLP device: complete view (A); zoom pictures with a Digital USB 1000X microscope over the three electrodes before (B) and after (C) silver electrodeposition. A ruler was placed in (C) indicating 1 cm scale. 109

Figure 44 – AFM images for WE-FDM (A), WE-DLP (B), TES-FDM (C) and TES-DLP (D) (after electrochemical surface treatment) SPCE (E). . . 111

Figure 45 – SEM images (lower amplification on left and higher amplification on right) of the carbon black/PLA electrodes fabricated by 3D-Pen (A and B) and desktop 3D-printers (C and D), before (A and C) and after electrochemical surface treatment (B and D). 113

Figure 46 – SEM images (lower amplification on left and higher amplification on right) of the fabricated electrodes using the 3D-Pen (A and B) and using the desktop 3D-printer (C and D). These surfaces were electrochemically treated as described in the experimental section. 114
Figure 47 – Raman spectra for the 3D-Pen fabricated (WE-DLP) electrode before (blue) and after (pink) NaOH treatment and for the desktop FDM 3D-printed electrode before (black) and after (red) NaOH treatment. . 115
Figure 48 – Cyclic voltammograms recordings (vs carbon black/PLA pseudo-reference) in the presence of 1 mmol L^{-1} of dopamine before (black line) and after (red line) electrochemical activation of the TES-FDM; dashed lines are aqueous blank solutions (0.1 mol L^{-1} $HClO_4$). 116
Figure 49 – Amperogram profile obtained during the electrochemical activation (+1.4 V for 200 s followed by -1.0 V for 200 s in 0.5 mol L^{-1} NaOH). All the three electrodes of the TES-FDM device were connected as single working electrode vs Ag|AgCl|$KCl_{(sat)}$ to perform the electrochemical activation. 117
Figure 50 – Cyclic voltammetric recordings (from 1st to 50th cycles) of a stability experiment consisting of 50 continuous cycles in the presence of 1 mmol L^{-1} of the redox pair $[Fe(CN)_6]^{3-/4-}$ obtained on the TES-DLP device using the Ag|AgCl pseudo-reference electrode. Electrolyte: aqueous solution of 0.1 mol L^{-1} KCl; scan rate: 50 mV $s^{-}1$. 118
Figure 51 – Overlapping cyclic voltammograms of 1 mmol L^{-1} $[Fe(CN)_6]^{3-/4-}$ in aqueous 0.5 mol L^{-1} KCl obtained with: (A) WE-FDM; (B) WE-DLP; (C) TES-FDM; (D) TES-DLP; (E) SPE. Five responses correspond to the measures obtained in five different devices. Inset: real images of the devices. 119
Figure 52 – Baseline-corrected square-wave voltammograms of triplicate scans of single-drops (100 μL) of crescent concentrations of TNT (from 5 to 500 μmol L^{-1}). The inset corresponds to the respective analytical curve (R^2>0.99) obtained using the area of the first peak at around -0.35 V vs Ag|AgCl pseudo reference. Electrochemical parameters: step potential of 4 mV, amplitude of 4 mV, frequency of 30 Hz, and 0.1 mol L^{-1} HCl as background electrolyte in 1% (v/v) acetonitrile. 122

List of Tables

Table 1 – Different 3D-printed electrochemical sensors fabricated by FDM, highlighting the main contributions of each work. Carbon-based materials have been generally employed as conductive materials, mostly using commercial-available conductive filaments. 36
Table 2 – Different methods for surface activation/modification different proposed electrodes in order to increase the electron transfer rate. 41
Table 3 – Analytical performance (data obtained from Figure 11) of different sensors coupled to the 3D-printed cell for the amperometric detection of TBHQ, dipyrone (DIP), dopamine (DOP), and diclofenac (DIC) under hydrodynamic conditions (BIA or FIA with carrier recycle). 57
Table 4 – Comparison of analytical characteristics between the the proposed 3D-printed-PLA electrode at the detection of catechol (CAT) and dopamine (DOP). 60
Table 5 – Attributions of the infrared spectrum (ATR mode) of 3D-printed G-PLA surface. 62
Table 6 – Analytical characteristics of different G-PLA electrodes for TNT detection. 73
Table 7 – Analytical characteristics for the detection of Pb(II) and Cu(II) on the 3D-printed G-PLA sensor. 77
Table 8 – Analytical characteristics of GOx based biosensors, including the proposed 3D-printed G-PLA biosensor. 90
Table 9 – Concentration of glucose in blood plasma sample obtained by the 3D-printed G-PLA biosensor before (1) and after (2-5) spiking with known concentration of glucose, and recovery values (n=3) 90
Table 10 – Analytical parameters obtained by BIA-MPA. 99
Table 11 – Concentrations of UA and NIT obtained by BIA-MPA method, recovery values for the spiked biological samples and respective standard deviation values (n=3) using the standard addition method 100

Table 12 – Values (average ± SD) of peak-to-peak potential separation (ΔE), oxidation peak potential (Epa), current density (jpa), geometric measured area (A) and the respective relative standard deviation (RSD) values obtained from 5 units of each proposed device and compared with 5 units of commercial screen-printed electrodes (SPE). 120
Table 13 – Literature overview for electrochemical sensors of TNT produced on a range of electrochemical platforms employing disposable and semi-disposable electrodes. 122

Acronyms list

2D Two dimensional

3D Three dimensional

ABS Acrylonitrile-butadiene-styrene

AFM Atomic force microscopy

AM Additive manufacture

AMP Amperometry

ASV Anodic Stripping Voltammetry

ATM Automated Teller Machine

ATR Attenuate total reflectance

AWG American wire gauge

BDD Boron-doped diamond

BIA Batch injection analysis

CAD Computer-aided design

CAT Catechol

CF Correction factor

CNTs Carbon nanotubes

CONTRASP Confederação nacional dos trabalhadores de segurança privada

CoPc Cobalt phthalocyanine doped

CPE-GNP Carbon paste electrode modified with gold nanoparticles

CRGO Chemically Reduced Graphene oxide

CV Cyclic voltammetry

DIC Diclofenac

DIP Dipyrone

DIW Direct ink writing

DLP Digital light processing

DMF Dimethylformamide

DOP Dopamine

DPASV Differential pulse anodic stripping voltrammetry

DPV Differential-pulse voltammetry

EIS Electrochemical impedance spectroscopy

ERGO Electrochemically Reduced Graphene Oxide

FAD Flavin adenine dinucleotide

FADH2 Reduced flavin adenine dinucleotide

FCA ferrocene-carboxylic acid

FDM Fused Deposition Modeling

FEBRABAN Federação Brasileira de Bancos

FFF Fused filament fabrication

FIA Flow-injection analysis

FT-IR Fourrier transformed infrared

GCE Glassy-carbon electrode

Glyc-AgNPs glycine-stabilized silver nanoparticles

GNR Graphene nanoribbons

GOx Glucose oxidase

G-PLA Graphene doped-polylactic acid electrodes

GS graphite sheet

GSE Graphite sheet electrode

HMX Hexahydro-1,3,5-trinitro-S-triazine

HPLC High performance Liquid Chromatography

HPRS horizontal printed rough surface

IR Infrared

LOD Limit of detection

LSV Linear sweep voltammetry

MIP Molecularly imprinted polymer

MPA Multiple-pulse amperometry

MWCNT Multiwalled carbon nanotubes

NIT Nitrite

PB Prussian Blue

PBS Phosphate buffer solution

Pep Specific peptides

PETN Pentaerythritol tetranitrate

PLA Polylactic acid

PNC Preanodized nontronite clay-modified electrodes

PPf polyphenol film

PS II Photosystem II-enriched particles

QRCE Quasi-reference or counter electrode

RDX cyclotrimethylenetrinitramine

rGO Reduced graphene oxide

RSD Relative standard deviation

,

SCE Saturated calomel electrode

SEM Scanning electron microscopy

SLA Stereolithography

SLM Selective laser melting

SPCE screen-printed carbon electrode

SPE Screen-printed electrode

SPM Scanning probe microscope

STL Standard tessellation language

SWASV Square-wave anodic stripping voltammetry

SWV Square-wave voltammetry

TBHQ Tert-butylhydroquinone

TES three-electrode system

TES-DLP three-electrode system with body made with digital laser processing

TES-FDM three-electrode system with body made with fused deposition modeling

TNT Trinitrotoluene

UA Uric acid

UV Ultra-violet

WE Working electrode

WE-DLP working electrode body made digital light processing

WE-FDM working electrode body made with fused deposition modeling

WWW World Wide Web

XRD X-ray diffraction

Contents

1	**INTRODUCTION**	**25**
1.1	**Justification**	**27**
1.2	**Motivation**	**28**
1.3	**Objectives**	**29**
1.4	**3D-Printing**	**30**
1.4.1	FDM 3D-printed sensors	33
1.4.2	Surface treatment and modification of FDM 3D-printed electrodes	38
1.4.3	Fabrication of all-in-one electrochemical devices using 3D-printing	42
2	**3D-PRINTED CELLS AND SENSORS**	**49**
2.1	**Introduction**	**49**
2.2	**Experimental**	**50**
2.2.1	Reagents and solutions	50
2.2.2	Instrumental	50
2.2.3	Design and construction of the multiuse 3D-printed cell	52
2.3	**Results and Discussion**	**55**
2.4	**Conclusions**	**65**
2.5	**Acknowledgements**	**65**
3	**3D-PRINTED DEVICE COMBINING SAMPLING AND DETECTION OF TNT**	**67**
3.1	**Introduction**	**68**
3.1.1	2,4,6-Trinitrotoluene	68
3.2	**Experimental**	**68**
3.2.1	Reagents and solutions	68
3.2.2	Instrumentation	69
3.2.3	Fabrication of G-PLA electrodes	69
3.2.4	TNT sampling and detection	69

3.2.5 Safety note . . . 70
3.2.6 Lead and copper detection . . . 70
3.3 Results and Discussion . . . 70
3.4 Conclusions . . . 78
3.5 Acknowledgements . . . 79

4 3D-PRINTED SENSOR FOR BIOANALYSIS . . . 81
4.1 Introduction . . . 82
4.1.1 Detection of NIT and UA . . . 82
4.1.2 Glucose biosensing . . . 82
4.2 Experimental . . . 83
4.2.1 Chemicals and samples . . . 83
4.2.2 Electrochemical instrumentation and measurements . . . 84
4.2.3 Fabrication and treatment of 3D-printed G-PLA electrodes . . . 84
4.3 Results and Discussion . . . 85
4.3.1 Amperometric biosensing of glucose . . . 85
4.3.2 Voltammetric studies of UA and NIT . . . 91
4.3.3 Amperometric determination of UA and NIT . . . 92
4.4 Conclusions . . . 100
4.5 Acknowledgements . . . 100

5 3D-PEN VS DESKTOP FDM 3D-PRINTER . . . 103
5.1 Introduction . . . 104
5.2 Experimental section . . . 104
5.2.1 Reagents and solutions . . . 104
5.2.2 Instrumentation . . . 104
5.2.3 Fabrication of the electrodes using the 3D-Pen . . . 105
5.2.4 Fabrication of the electrodes using a desktop FDM 3D-printer . . . 109
5.3 Electrochemical measurements . . . 110
5.4 Microscopic and spectroscopic characterizations . . . 110
5.4.1 Safety note . . . 110
5.5 Results and discussion . . . 110
5.5.1 Morphological analysis of carbon black/PLA electrodes: 3D-printing pen versus desktop 3D-printer . . . 110
5.5.2 Electrochemical characterization of carbon black/polylactic acid electrodes fabricated using 3D-Pen . . . 116
5.5.3 TNT determination in a single drop on a planar three-electrode system (3D-Pen made) . . . 121
5.6 Conclusions . . . 124
5.7 Acknowledgements . . . 124

6 CONCLUSION 127
6.1 Addressal of objectives 127

BIBLIOGRAPHY 129

ANNEX 143

ANNEX A – CURRICULUM SUMMARY 145
A.1 Thesis related papers 145
A.2 PDSE - International visitor scholar related papers 146
A.3 Additional published papers 146
A.4 Book Chapters 147

ANNEX B – FRONT COVER ACA 149

ANNEX C – COPYRIGHT 151

I hereby certify that I have obtained all legal permissions from the owner(s) of each third-party copyrighted matter included in my thesis, and that their permissions allow availability such as being deposited in public digital libraries.

Rafael Melo Cardoso

Chapter 1

Introduction

Three-dimensional (3D)-printing technology used in analytical chemistry instrumentation is playing an important role on the innovation at sensors manufacture and prototyping, bringing the future of such area to a complete new level. This thesis aims to discuss, propose and apply this new trend technology in the electroanalytical field. The main proposed devices are: (1) Use of fused deposition modeling (FDM) 3D-printers for manufacture of a cheap and versatile electrochemical cell using insulator filament and sensors using conductive filaments; application of the 3D-printed sensor in (2) forensic area for sampling and detection of explosives and (3) bio-analysis in biological fluids; (4) use of 3D-pen as an alternative tool for sensors manufacturing. The thesis is divided into six chapters as follows:

Chapter I introduces the motivations about why keeping track of explosives like TNT is necessary for the forensic area, as well as the determination of glucose, nitrite and uric acid levels in biological samples, such as blood, saliva, and urine are important in a clinical perspective. By creating this background the use of additive manufacture (AM) is introduced as a tool to help overcoming electroanalytical challenges. A literature review on the use of 3D-printing in electroanalysis is presented as well with focus on the contributions of AM technology of fused deposition modeling (FDM) with current state of art. In the subsequent chapters (II to V) the proposed devices are detailed.

Chapter II shows how to use those machines at the manufacture of multi-use 3D-printed electrochemical cells of hydrodynamic or standard batch cells. The performance of this versatile cell is demonstrated for the amperometric detection of tert-butylhydroquinone, dipyrone, dopamine and diclofenac by flow injection analysis (FIA) and batch injection analysis (BIA) using different planar working electrodes. This chapter brings the proposition of a 3D-printed sensor graphene-containing polylactic acid electrode (G-PLA), which presented promising electroanalytical performance as working electrodes (e.g. submicromolar detection limit for dopamine and TNT).

Chapter III introduces the discussion on the use of a 3D-printed device for the forensic area. A planar shaped electrode is proposed for sampling and detection of an explosive at

crime scenes. Traces of TNT impregnated on different surfaces were abrasively sampled using the 3D-printed device and readily assembled in a portable electrochemical cell for rapid square-wave voltammetry scans in the presence of 0.1 mol L^{-1} HCl. The voltammetric response when compared to the characteristic TNT voltamogram will give a positive or negative response for the explosive. Lead and copper determination by stripping voltammetry was also demonstrated on the same device, highlighting the possibility of detecting gunshot residues with the sampling and sensor at the same device.

At Chapter IV, another application using (G-PLA) electrodes was developed for bio(sensing) of biological fluids. An enzymatic glucose biosensor fabricated on the G-PLA surface was developed and applied for glucose sensing in blood plasma using chronoamperometry. Oxygenated groups from the polymeric PLA matrix provides suitable condition to enzyme immobilization by cross-linking with glutaraldehyde. An amperometric sensor for nitrite and uric acid in urine and saliva samples is also demonstrated in this section.

Chapter V discusses another approach of producing low cost 3D-printed devices using a 3D-printing (or drawing) pen, a cheaper and portable instrumentation than 3D desktop printers. Three different designs were proposed, and a three electrode system (TES) was evaluated for TNT quantification in a single drop (100 μmol L^{-1}), advantage that is discussed as well, and compared with traditional 3D-printed devices proposed at previews chapters and discussed in this final result chapter. The structure of this thesis follows Figure 1.

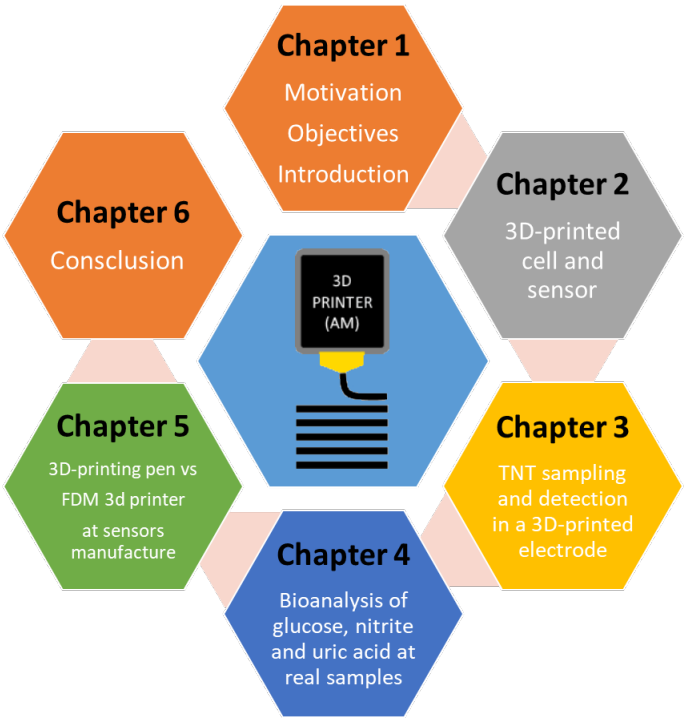

Figure 1 – The structure of this thesis.

In Chapter VI, the conclusions, advantages and disadvantages of this research are

discussed. Chapters I-V are adaptions of published papers during the Ph.D. period and can be accessed online.

1.1 Justification

In the last decade in Brazil the number of bank Automated Teller Machine (ATM) explosions became a frequent reported news on local and national media, especially in cities located far from metropolitan centers. According to Brazilian Bank Federation or "Federação Brasileira de Bancos" (FEBRABAN), since 2009, first time that this type of crime was reported, up to 2012 there was more than 2500 exploded ATM's in the union soil (TRIGUEIRO, 2012). From 2014 to 2018 the confederation of workers of private security (CONTRASP), released annually reports about the data of banks ATM's and trucks attacks. Per year the ATM's recorded violations reached 1306, 1251, 1050, 952 and 758 reports from 2014 to 2108 sequentially (CONTRASP, 2018). These decrease index represent more efficiency regarding the advances in monitoring technologies integrated with police intelligence forces. Nevertheless, low cost and alternative methods can be developed, once this type of crime still is a challenger situation for the banks and public security, bringing losses that reaches millionaires values.

The most common explosive employed for such criminal activity is the TNT, usually obtained by smuggled or diverted cargo of mining camping companies. In a public security point of view is important to keep track of those explosives, and innovations on new methodologies, procedures and assays are emerging as an alternative of other more expansive methods such as High Performance Liquid Chromatography (HPLC). One of the strategies is the use of an electrochemical sensor for TNT due to its electroactivity behavior, with a characteristic voltammetric peak profile. Simplicity, easy operation, low cost of instrumentation and consumables are the main positive characteristic of electrochemical devices. A classic example of electrochemical sensor is a pH meter, which after calibration, the equipment delivers fast results on measurements of H_3O^+ in aqueous solutions with impressive selectivity. An electrochemical response is briefly the electrical information of a target molecule at the interface between a conductive surface and solution.

Other field that demand fast answers on routine, trial or emergency cases is the clinical area. Our scenario regarding infra-structure of such instrumentation depends on location once the country contemplates a large territory. Clinical methods are generally widely described and normalized(OLIVEIRA; SOUTO, 2018), and assay and kits are well described with established methods. Nevertheless those new materials and technologies can contribute to portable or cheaper devices, specially on a pandemic situation where some reagents or device are missing on the manufacturer shelf. One classic and successful example of electrochemical device for a daily and important molecule target is the glucosimeter. Portable, fast and specific, this method is based on the electric response

information generated by a chain of reactions involving the glucose levels with the enzyme Glucose Oxidase(GOx) and other reagents. This technology is able to deliver in instants, results with no major intervention, helping the healthcare professionals make a faster and better decisions.

1.2 Motivation

For an analytical point of view, electrochemical devices have some advantages as mentioned before, and have the potential on overcoming both forensics and clinical areas. Tailoring analytical instrumentation innovations, various methods for prototyping/manufacturing electrochemical cells with the use of milling machines(TORMIN et al., 2012), flow analysis system with the use of acrylic and epoxy resin (MATSUMOTO et al., 1988), expansive machines such as laser cutting for cells constructions , allied with acrylic plates (KRONTHALER et al., 2012)or glassware have been reported.. The popularity of 3D-printer industry and the utility of this tool for rapid prototyping were the first characteristics that called the research group attention. Firstly for cells manufacturing, and then the possibility of new materials for electrodes such as conductive thermoplastic composites opened the possibility of integration of cells and sensors, and were the main target of this research.

Invented and patented in 1986 by Charles Hull (HULL, 1986) it was first called as stereolithography. By his definition, stereolithography is a system which through a cross sectional pattern creation, thin stacks of layers are deposited on each other (layer-by-layer) generating a three dimensional object. By curing thin layers of an UV-photosensitive resin sequentially programmed, the technology emerged with the first 3D-printer: SLA-1 and the first 3D-printing company (3D Systems) was funded.

The first 3D-printer is older than the creation of the World Wide Web (WWW) by the computer scientist Tim Berners-Lee. Chronologically means that both innovations evolved in a parallel path, and as well as internet, additive manufacture (AM) or 3D-printing is advancing exponentially once new materials and technologies are available in modern society. Nowadays, AM is massively used in many fields of industry and this exponential growth expands for many applications. To analytical chemistry is not different, once it can take advantage of the unique characteristics of the manufacture technique: modelling freedom and fast prototyping process. Other interesting characteristic that brings innovation to additive manufacture (AM) is the ability of local/on-demand solution, keeping industry and resarchers alert regarding 3D-printing new materials/techniques. These facts evidence a crescent demand on research at analytical instrumentation exploring this relatively new technology. Using electroanalysis to overcome analytical problems can play an important role in this scenario, attending with simple, cheap and reliable solutions. In this context, this thesis proposes to ally electroanalysis with 3D-printable platforms for

forensics and clinical applications.

Additionally, the cost of production and research development costs are tangible, depending on the technique it can reach values of 200$ (custom build FDM) for unit acquisition, and the same amount for one-year consumption of raw materials. In the past decade it is notable the vast quantity of reports on microfluidic devices (COCOVI-SOLBERG; WORSFOLD; MIRÓ, 2018; DIXIT; KADIMISETTY; RUSLING, 2018) with built in valves (ROGERS et al., 2015) or comparing different AM techniques (MACDONALD et al., 2017); colorimetric based arranges using spectroscopic methods and smartphones (ESCOBEDO et al., 2019), spectroelectrochemical cells (SANTOS et al., 2019), and electroanalytical devices (BROWNE et al., 2018; CARDOSO et al., 2019; GUSMÃO et al., 2019; KATSELI; ECONOMOU; KOKKINOS, 2019; RICHTER et al., 2019). Fused deposition modelling (FDM) has received higher attention in this thesis once FDM 3D-printing technique is the most affordable and accessible to research laboratories. Moreover, commercially-available conductive filaments containing graphene or carbon black enabled the fabrication of electrochemical sensors using FDM 3D-printing as reported by different research groups and will be discussed with more details, as well as recent advances in 1.3 of this first Chapter.

1.3 Objectives

The main objectives of this thesis is to investigate the usability of fused deposition modeling (FDM) 3D-printers at the development of electroanalytical cells, for hydrodynamic and stationary conditions, and to develop electrochemical sensors based on conductive thermoplastics using commercially-available filaments. Specific objectives follow:

1. To investigate the performance of additive manufactured batch-injection analysis cell towards detection of different analytes, using various planar working electrodes, in a wall-jet position;

2. Develop a working electrode based on conductive thermoplastic commercially available (Black Magic) and investigate its applicability in electroanalytical chemistry;

3. Investigate its applicability of 3D-printed sensor for direct sampling and electroanalysis of TNT powder on simulated surfaces. ;

4. Use the 3D-printed sensor for (bio)analysis at complex samples, such as urine and saliva, with target analytes nitrite and uric acid;

5. Develop a biosensor for glucose determination in blood plasma, modifying the 3D-printed substrate modified with glucose oxidase;

6. Introduce other approach of fabrication of 3D sensors, using a 3D pen, and compare and discuss its performance and reliability when compared to 3D-printers.

1.4 3D-Printing

There are several different additive manufacture methods, with different prices and raw materials, thus the most accessible one is the fused filament fabrication (FFF) or FDM, and is an extruded based technique. It works with a thermoplastic as a raw material, that when extruded through a hot nozzle (190 – 250º depending on the thermoplastic constitution) is deposited layer by layer with xy being the coordinates, and z is the layer step. The path, or coordinates that the machine executes in each level is the x and y-axes, propelled by a step motor and belts, and the z-axis perform the height steps of the process, until all layers are deposited and the model prototyped. FDM 3D-printers have already presented usefulness on space exploration due to the portability and versatility, which enables on-demand production of models and devices using a common raw material in order to save storage space and solve logistical challenges (PRATER et al., 2019). Figure 2, (a) and (b), shows a schematic operation of FDM, along with direct ink writing (DIW) which are extrusion based techniques. In DIW, the process is similar to FDM, despite the raw material is a paste ink extruded through by applying pressure in a piston.

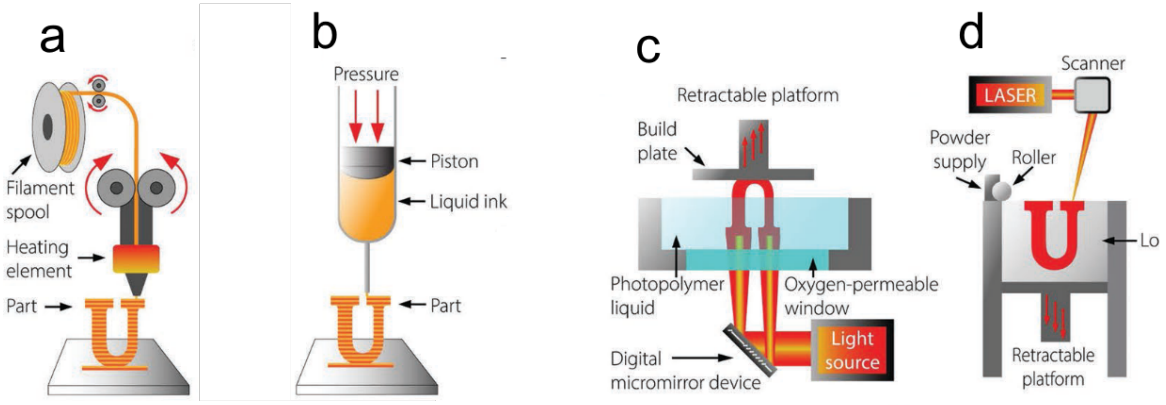

Figure 2 – Schematics representation of extrusion (a and b) and bulk (c and d) 3D-printing methods: (a) fused deposition modeling (FDM); (b) direct ink writing (DIW); (c) digital light processing (DLP) and (d) selective laser melting (SLM). Adapted from (ELDER et al., 2020).

Bulk methods such as digital light processing (DLP) and selective laser melting (SLM) have a different xy deposition. Both methods use an energy wave source, where in DLP, the UV light polymerizes a photocurable acrylate based resin, depositing it layer by layer in a top down build plate. On the other hand, SLM printers use a high-energy laser beam

that fuses a powder material, in a loose powder bed, and the steps go thought the z-axis. There are many other 3D-printing techniques, however the techniques presented in Figure 2 were used, or revised in this thesis.

Regarding the low cost and fast model prototyping, semi-conductive thermoplastic (carbon based) filaments are now available in the market or in custom formulations, which come to be a great feature to provide a good arsenal of tools with the possibility of multi-functional materials for electroanalytical instrumentation.

The 3D-printing technology has confirmed unique advantages in the fast prototyping of multifaceted structures with applications in aerospace, electronics, food and medicine. Analytical chemistry and electrochemistry have been recently benefited from the 3D-printing technology. Freedom of design enabled by 3D-printing opens up many possibilities for researchers to create novel materials and electrochemical sensing devices to be produced in large-scale, under desired geometry and minimal waste generation.

The process of 3D-printing or additive manufacturing involves the creation of solid 3D objects based on a controlled layer-by-layer deposition of a material. The first step of a 3D-printing process comprises the conception of a virtual image of the object, which is commonly obtained through computer-aided design (CAD) software. Next, the 3D design is converted to a STL file compatible with 3D-printer software, which converts the 3D image into sequential 2D layers of the initial object, resulting in a G-code file. From this point, the 3D-printer can create the 3D object by layer-by-layer material deposition. The working principles of different 3D-printing methods were schematically illustrated and discussed by Ambrosi and Pumera in a review article devoted to cover the main 3D-printing methods and some electrochemistry applications of 3D-printed materials (AMBROSI; PUMERA, 2016). The authors grouped the 3D-printing methods in four categories: a) photopolymerization, b) extrusion, c) powder-based and d) lamination.

The first group involves stereolithography (SLA) or digital light processing (DLP), which is a very disseminated method, especially in the development of miniaturized analytical systems and microfluidic devices (COCOVI-SOLBERG; WORSFOLD; MIRÓ, 2018). This method is based on resin formulations able to polymerize by UV light, which is controlled by an optic arrangement for the layer-by-layer deposition until the formation of the desired model. Nevertheless, to our knowledge, no applications were found at the fabrication of electrochemical sensors using this technique. The second group involves fused deposition modeling (FDM), which is the most affordable 3D-printing method and consequently the most employed by researchers in the development of new electrodes for sensing/biosensing and completely assembled electrochemical devices. The FDM is based on the extrusion of a semi-molten thermoplastic filament using a moving heated nozzle that deposits the polymeric material on a substrate, where it readily solidifies. Other layers are deposited over the first layer until the creation of the desired object. Hence, this review highlights FDM 3D-printed electrodes and electrochemical devices due to the low-

cost of 3D-printers and thermoplastic filaments. The third group covers the selective laser melting (SLM) technique that makes use of metal powders, which requires special careful handling, and expensive 3D-printers. Some examples of SLM 3D-printed electrochemical sensors are also presented in this review despite the disadvantages of this technique herein reported. Another powder-based 3D-printing method is the inkjet 3D-printing, which involves a droplet-based deposition of ink onto a solid substrate, such as plastic or paper. A wide range of powders can be processed depending on the selected binder in order to attend special requirements regarding surface tension, density viscosity of the resulting ink. For electrochemical applications, conductivity plays key role and thus conducting agents need to be mixed with the polymeric binder (PANG et al., 2020). The 3D-printed graphene aerogels have been reported and offer great promises for electrochemical sensing (ZHU et al., 2015).

Regarding other review articles focusing on 3D-printing technologies for sensing, Zhuang et al. presented a comprehensive review of the advances in (bio)sensing, fluidic and microfluidic devices using different types of cells and printing technologies, such as FDM, SLA, and SLM (NI et al., 2017). This review presents examples of physical sensors, biosensors, and chemical sensors, with a few examples of electrochemical sensors. The authors emphasized the benefits of 3D-printing to replace time-consuming fabrication steps and expensive instrumentation and protocols to fabricate sensors.

In the field of electrochemical sensors, Patel et al. reported a mini-review on the use of conductive materials for 3D-printing of electrodes of different geometries (HAMZAH et al., 2018). The authors highlight the potential applications of 3D-printing technology for electroanalytical applications with some examples reported in the literature (around thirty references). In the field of energy conversion and storage, Tian and collaborators reported a detailed review on the development of energy storage devices using 3D-printing (TIAN et al., 2017). The authors presented basic considerations on the 3D-printing process, how batteries and electrochemical capacitors work and strategies to develop high-performance electrochemical energy storage devices using 3D-printing.

A search in the Web of Science® database using as keywords 3D-printing and *electrochem**, it can be observed a first paper published in 2012 and an exponential increase in the next years, reaching 167 papers in 2019 in a total number of 533 papers with more than 8,400 citations (information obtained on 02^{nd} March 2020). These data indicate a relevance to the use of 3D-printing for electrochemistry applications, which include electrochemical sensing. In this context, this thesis presents a revision article dedicated to recent contributions of 3D-printing technology to the development of electrochemical sensors. Special attention is given to the FDM technique that has been the most employed technique for this aim. Most investigations using FDM 3D-printed electrochemical sensors have reported the need for surface treatment before electrochemical measurements, thus a section is devoted to critically discuss the different protocols reported in the liter-

ature to improve the electrochemical characteristics of 3D-printed electrodes. Examples of immobilization of chemical catalysts and biomolecules to develop improved sensors and biosensors are presented. Finally, prototypes of 3D-printed electroanalytical devices (comprising the three-electrode system and electrochemical cell) are shown as examples of potential applications of 3D-printing in the fabrication of complete electrochemical sensing devices.

1.4.1 FDM 3D-printed sensors

The literature has demonstrated the use of commercially available desktop 3D-printers to fabricate low-cost and functional objects (GNANASEKARAN et al., 2017). For electrochemical and electroanalytical applications, this approach has been explored for the 3D-printing of electrodes, electrochemical cells, microfluidic systems, electrochemical microscopes, spectroelectrochemical cell and others.

The morphological and structural characteristics of the electrochemical devices or sensors can be modulated according to the printing parameters. The material, composition, and the pretreatment of the filaments are also important in the process of the preparation of the electrodes. The customization and design of 3D materials can also be established according to the 3D-printing technique. In FDM 3D-printers process is based on the melting of polymeric filaments followed by deposition on a substrate. As a consequence, this technique provides a low-cost and good precision in 3D-printing. FDM has been widely reported for 3D-printing electrochemical devices based on polymer and conductive composites. The extruded filament is layer-by-layer deposited and a printing platform moves in different directions (x, y), while the stage moves on the z axes, which allows for the creation of versatile three-dimensional objects with modulable shapes and dimensions (DUL; FAMBRI; PEGORETTI, 2016; WANG et al., 2017).

The 3D-printing can be performed with different thermoplastic polymers, wherein the polylactic acid- (PLA) and acrylonitrile-butadiene-styrene(ABS)-based filaments in the conductive form are the most used for electrochemical devices. The PLA consists of (bio)polyesters and it is biodegradable, and thus considered as an environmentally-friendly safe material. This one can be produced in large-scale since it has an affordable price, around 5 Euros per kg (RODRÍGUEZ-PANES; CLAVER; CAMACHO, 2018). The PLA filaments are widely used to fabricate materials using the FDM technique and present a melting temperature of around 200°C (RAVI; DESHPANDE; HSU, 2016). The ABS is mainly used in the industrial area and presents good mechanical properties, ease of processing, reuse possibility (BRYDSON, 1999), and is produced worldwide (POLLI et al., 2009). The range of ABS extrusion temperature is between 200–300º C depending on the composition (MILENIUS, 1979). In order to evaluate the characteristics of both materials, Rodríguez-Panes et al. (RODRÍGUEZ-PANES; CLAVER; CAMACHO, 2018) reported a comparative analysis between ABS and PLA pieces produced by the FDM

technique. The ABS filament showed more ductile than PLA, but the latter is more rigid and has more tensile strength. Thus, regarding the several parameters, such as infill, layer height and orientation, the PLA presents greater variability than ABS and the PLA pieces behave more rigidly. Properties of both materials are distinct and thus the preference by one of them as polymeric matrix will depend on the desired characteristics of the material.

Conductive filaments based on PLA and ABS are obtained by the incorporation of conductive materials into the polymer matrix. Composites are necessary to improve the electrical properties of the 3D-printed devices and the percentage of the conductive materials in the non-conductive thermoplastics (ABS and PLA) must be optimized to achieve appropriate conductivity and effective 3D-printability. In general, conductive carbonaceous materials are used for this purpose, mainly nanomaterials, such as carbon nanotubes, carbon black and graphene. The choice of these is due to the high surface area, good thermal and mechanical resistance, high chemical inertia, possibility of functionalization and high electrical conductivity.

Commercial filaments containing carbon black particles (Bin Hamzah et al., 2018; KATSELI; ECONOMOU; KOKKINOS, 2019; KATSELI; ECONOMOU; KOKKINOS, 2020; RICHTER et al., 2019) are used for this approach due to their high electrical conductivity and low-cost since they can be obtained as a byproduct from the combustion of petroleum products (DONNET et al., 2018). In addition to these characteristics, this material is biocompatible and consequently can be an alternative in the development of electrochemical sensors and biosensors (SILVA et al., 2017). Also, some works have reported the use of graphite (FOSTER et al., 2020), carbon nanofibers and carbon nanotubes (CNTs) (GNANASEKARAN et al., 2017; HONEYCHURCH; RYMANSAIB; IRAVANI, 2018; RYMANSAIB et al., 2016). Among these, CNTs deserve special mention. First reported by Iijima in 1991 (IIJIMA, 1991), the structure of CNTs is formed by one or more rolled-up graphene sheets in a hemispherical arrangement of sp^2 carbon atoms. High surface area, elasticity and high electrical conductivity are the hallmarks of this material (WONG et al., 2017). Therefore, CNTs are an excellent alternative for obtaining conductive filaments as it will be further discussed in the text. However, conductive filaments containing CNTs are still not commercially-available and probably, for this reason, no papers using such filaments are described for electrochemical sensors. On the other hand, commercially-available graphene-based filaments are the most used material for electrode construction by the FDM technique (CARDOSO et al., 2018; SANTOS et al., 2019). Graphene, as CNTs, presents sp^2 hybridized carbon atoms, but in a 2D single sheet. Graphene-based materials present high surface area, excellent conductivity and high mechanical strength. Therefore, these materials have revealed interesting electrochemical properties, enabling the electrochemical detection of several species (RAYMUNDO-PEREIRA et al., 2018; ROCHA et al., 2018; SHAO et al., 2010).

Table 1 shows the different 3D-printed electrochemical sensors fabricated by FDM,

highlighting the main contributions of each work. Carbon-based materials have been generally employed as conductive materials, mostly using commercial-available conductive filaments.

Table 1 – Different 3D-printed electrochemical sensors fabricated by FDM, highlighting the main contributions of each work. Carbon-based materials have been generally employed as conductive materials, mostly using commercial-available conductive filaments.

Conductive filament *	3D-printer	Analyte/probe	Technique	Main target	Ref.
ABS/carbon black	Wanhao Duplicator 4	Ferrocene and serotonin	CV	Evaluation of different printing directions on the electrochemical behavior of electroactive species	(Bin Hamzah et al., 2018)
PLA nanographite-loaded	ZMorph®	Pb^{2}+ and Cd^{2+}	SWV	Different electrode designs; use of solvents to produce the nanograhite/PLA composite	(FOSTER et al., 2017)
Polystyrene/carbon nanofiber/graphite	Custom-built	Pb^{2+}	DPASV	Dual extrusion using self-fabricated conductive filament	(RYMANSAIB et al., 2016)
Polystyrene/carbon nanofiber–graphite	Custom-built	Zn^{2+}	CV and DPASV	Fabrication of filaments	(HONEYCHURCH; RYMANSAIB; IRAVANI, 2018)
Commercial graphene-based (Black Magic®)	TRIBLAB printer	Picric acid and ascorbic acid	CV	DMF activation of 3D-printed-electrodes	(MANZANARES-PALENZUELA et al., 2018)
Commercial PLA/ graphene-based (Black Magic®)	TRIBLAB	$[Fe(CN)_6]^{4^{-}/3^{-}}$	CV	DMF and electrochemical activation of 3D-printed electrodes	(BROWNE et al., 2018)
Commercial carbon black-based (Proto-pasta®)	ZMorph VX Multi-Tool 3D-printer	Dopamine	CV and SWV	Electrochemical treatment of 3D-printed surface in NaOH and production of a novel pseudo-reference	(RICHTER et al., 2019)
Commercial graphene-based (Black Magic®)	RepRap3D	Dopamine	CV and DPV	Electrochemical treatment of 3D-printed surface in phosphate buffer	(SANTOS et al., 2019)
Commercial PLA/ graphene-based (Black Magic®)	Prusa clone	Dopamine and catechol	SWV and amperometry coupled with BIA	Proposed 3D-printed cell for BIA using planar 3D-printed electrodes (or other planar electrodes)	chapter 2 (CARDOSO et al., 2018)
Commercial PLA/ graphene-based (Black Magic®)	Prusa clone	TNT	SWV	Single 3D-printed device for sampling TNT residues and further detection	chapter 3 (CARDOSO et al., 2020)
Commercial PLA/ graphene-based (Black Magic®)	Designex3D Alpha	Cu^{2+}	Photoelectrochemistry/ Chronoamperometry	Low-cost approach to mass producing electrode materials for supercapacitors and photoelectrochemical sensor	(FOO et al., 2018)

Commercial graphene-based (Black Magic®)	Prusa i3 MK3 printer	$[Fe(CN)_6]^{4-/3-}$ and $[Ru(NH3)_6]^{2+/3+}$	CV	3D-build pseudo-reference	(ROHAIZAD et al., 2019)
Commercial graphene-based (Black Magic®)	Prusa clone	H_2O_2	Chronoamperometry and CV	Prussian blue electrodeposition after electrochemical treatment of 3D-printed surface	(KATIC et al., 2019)
Commercial (graphene-based Black Magic®)	TRILAB 3D	1-naphthol	CV	Use of proteinase K for electrode treatment for the development of a biosensor	(MANZANARES-PALENZUELA et al., 2019)
Commercial carbon black-based (Proto-pasta®)	Creator Pro	Caffeine, Hg^{2+} and glucose biosensor	DPV, SWASV and amperometric	Fabrication of an analytical device entirely by 3D-printing using dual extrusion	(KATSELI; ECONOMOU; KOKKINOS, 2019)
Commercial ABS carbon-loaded 3DEdge®, PLA carbon-loaded (Proto pasta®) and (Amolen®)	Flashforge	Caffeine and paracetamol	DPV	Fabrication of an electrochemical cell-on-a-chip concept using a dual extrusion	(KATSELI; ECONOMOU; KOKKINOS, 2020)
Commercial graphene-based (Black Magic®)	Makergear M2 Dual printer	Ferrocene and Catechol	LSV	Single-step fabrication of a fluidic flow cell with electrochemical detection with 2 electrodes 3D-printed within the channel	(O'NEIL et al., 2019)
Commercial graphene -based (Black Magic®)	Prusa clone	Nitrite, uric acid and glucose	MPA	Combination of mechanical polishing and solvent immersion of 3D-printed surface for the analysis of biological samples and glucose biosensing	chapter 4 (CARDOSO et al.,)
Commercial graphene-based (Black Magic®)	RepRap3D	Dopamine	DPV	3D-printed surface immersed in DMF for 30 min (different procedures were compared) - analysis of biological samples	(KALINKE et al., 2020)
Commercial graphene-based (Black Magic®)	Custom-built	Hg^{2+}, Cd^{2+}, Pb^{2+}	ASV	Silver ink to promote WE contact. Microparticles of Bi to improve LOD's against metal detections	(WALTERS et al., 2020)
Commercial carbon black-based (Proto-pasta®)	Prusa clone	Cd^{2+}, Pb^{2+}	ASV	30-fold current increase after alkaline pre-treatment towards metals detection	(ROCHA et al., 2020a)
Commercial carbon black-based (Proto-pasta®)	Prusa clone	Cu^{2+}	ASV	Metal detection in fuel bioethanol using an electrochemically-treated 3D-printed electrode	(JOÃO et al., 2020)

In this sense, a conductive polystyrene filament modified with carbon nanofibers and graphite microparticles was proposed (RYMANSAIB et al., 2016). The electrochemical performance of the polymer composites was investigated by cyclic voltammetry using the printed electrodes made with different compositions in ferrocene methanol. The electrodes prepared with 10 % (wt%) of carbon nanofibers and graphite presented satisfactory conductivity with proper mechanical resistance and printing characteristics. This composition was satisfactory to maintain the percolation thresholds and good electrical conductivity. The method was successfully applied for the anodic stripping detection of lead. The work also shows the capability to reuse the electrode after surface polishing. A 3D-printed electrode fabricated using a conductive filament containing nanographite was proposed (FOSTER et al., 2020). The amount of nanographite within the filament was evaluated and characterized by thermogravimetric, morphological and physicochemical analyses. The authors found an effective percolation and high conductivity with 25 wt% nanographite. Above this amount, the electrode showed a fragile and non-reproducible behavior, affected by the decrease of PLA amount. Raman analysis showed that the printing step did not change the thermoplastic characteristics of the 3D-printed electrode. Also, the nanographitized electrode presented a low functionalized surface, as observed by the low amount of defects, which did not affect the electrochemical response of the obtained electrode. The 3D-printed electrode was successfully applied for the simultaneous determination of lead and cadmium by square-wave stripping voltammetry, presenting low limit of detection (LOD) values (7.40 x 10^{-9} and 1.96 x 10^{-8} mol L^{-1}, respectively).

Besides the filament material, the 3D-printing orientation of electrodes can also influence their electrochemical behavior (Bin Hamzah et al., 2018). 3D-printed ABS/carbon black electrodes were fabricated by printing under horizontal and vertical directions (See Figure 3). The evaluation of electrodes revealed that horizontal direction printing resulted in a smooth surface (lateral side of the 3D-printed object) and a comparatively rougher surface of 3D-printed ABS/carbon black electrodes (top surface of the same 3D-printed object). The vertical direction 3D-printed electrode led to a reduced charge transfer resistance and uncompensated solution resistance, enhancing the electrochemical performance in the presence of ferrocene and serotonin. This was attributed to the conductive pathways orientation from electrical connection to solution interface, i.e. the internal structure of the vertical direction printed electrodes.

1.4.2 Surface treatment and modification of FDM 3D-printed electrodes

As previously stated, the use of commercial conductive filaments is attractive due to low-cost, design versatility (shape and size) and the possibility of fast decentralized production of conductive or semi-conductive substrates for different electrochemical ap-

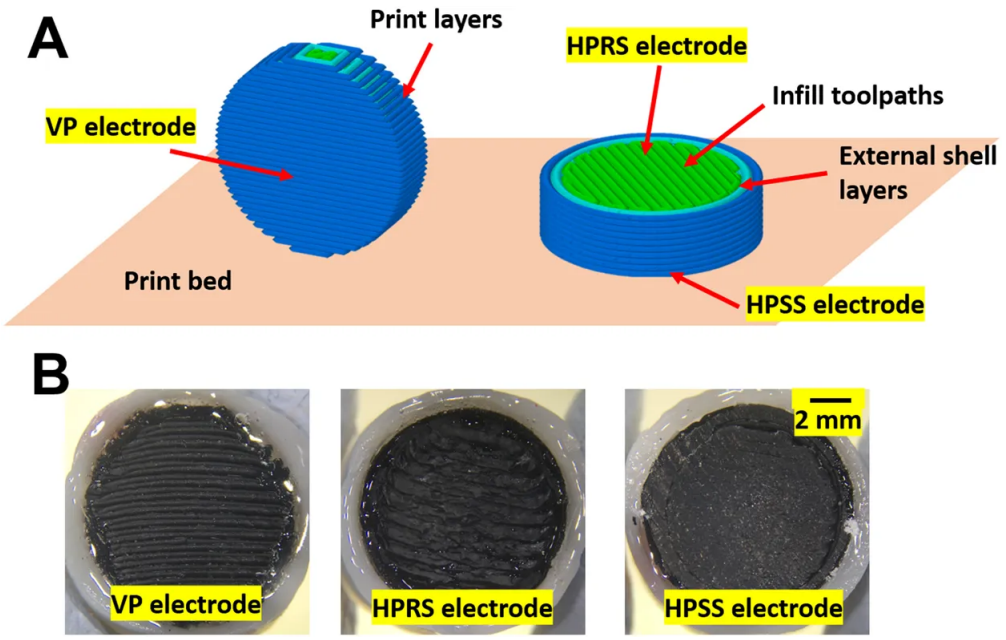

Figure 3 – (A) Scheme of horizontal and vertical 3D-printed electrodes using carbon black/ABS material; (B) Photographs of vertical printed (VP), horizontal printed rough surface (HPRS) and horizontal printed smooth surface (HPSS) electrodes. Reprinted with permission from (Bin Hamzah et al., 2018), Copyright (2018), Springer US.

plications. Some researchers (FOSTER et al., 2017) showed the possibility of using commercial graphene/PLA filaments in the development of 3D-printed electrodes for many applications, including capacitors, lithium-ion batteries and water splitting processes. Afterwards, using the same conductive material (graphene/PLA),3D-printed sensors were proposed (MANZANARES-PALENZUELA et al., 2018; FOO et al., 2018), and as proofs-of-concept, the electrochemical detection of copper and several redox species were carried out, respectively. However, in both works, the electrode response was relatively poor (high impedance values) if compared to other carbonaceous surfaces (glassy-carbon, carbon-paste, etc.). This behavior was attributed to a high amount of insulating PLA and low graphene content (8 % wt) in the used filaments (FOSTER et al., 2017; MANZANARES-PALENZUELA et al., 2018). So, to overcome this disadvantage, two strategies that are very common in literature at electrochemical devices were used: electrode activation and/or modification.

Pumera research group introduced the DMF treatment in 2018 (BROWNE et al., 2018) and the electrochemical activation as well (MANZANARES-PALENZUELA et al., 2018). By adding 10 minutes step of solvent exposition immersing the electrodes into DMF, a peak separation for $[Fe(CN)_6]^{4-/3-}$ of 527 mV was obtained for 3D-printed pin electrodes. The electrochemical activation proposed step was carried out applying a constant potential optimized to 1.5 V during 150 s at 0,1 mol L^{-1} phosphate buffer solution, reducing

the peak-to-peak separation to 171 mV. The improved performance of the sensors after activation in such reports were attributed to: to availability of graphene based structures to act as a transducer by removing superficial plastic matrix (PLA) with the solvent, and the different fictionalized carbon groups present at the electrode new surface. Those activation data where confirmed when dos Santos compared different activation methods since simple mechanical polishing, electrochemical procedures in phosphate buffer media, or immersion in concentrated acid and alkaline solution (SANTOS et al., 2019).

More sophisticated strategies are presented in literature such as the use of a proteinase-K enzyme as a removal agent of PLA during a 24 hour exposition, witch consequently expose the graphene sites and increase it ratio along the sensor (MANZANARES-PALENZUELA et al., 2019) as shown in Figure 4. Thermal annealing strategy using high temperatures on a porous electrode pattern was presented aiming explosives detection, showing how 3D-printed complex model structures can be prototyped, or even produced with 3D-printing technology. Both activation procedures, showed satisfactorily results in terms of voltammetric performance of the electrodes, but the lengthy procedure for both to obtain the final surface can be a bottleneck in case of any on-demand necessity.Table 2 compares different methods of activation and/or modifications of different proposed 3D-printed electrodes.

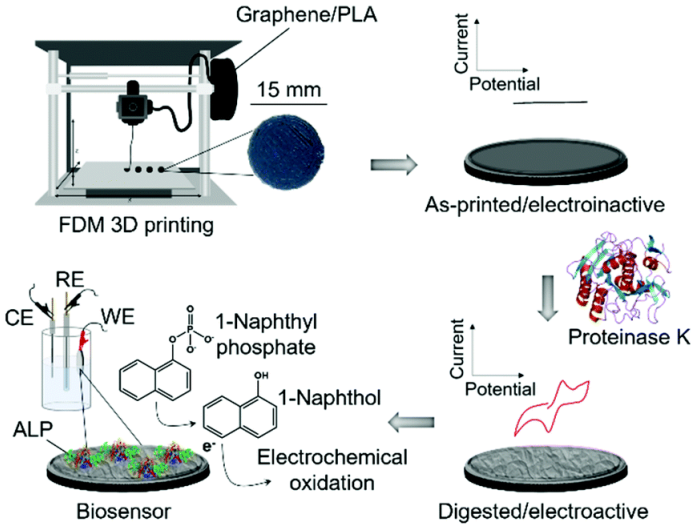

Figure 4 – Representation of the 3D-printed graphene/PLA electrodes fabrication, proteinase K-mediated PLA digestion/activation and application for the 1-naphthol oxidation enzyme-mediated. Reprinted with permission from (MANZANARES-PALENZUELA et al., 2019), 2019), Copyright (2019), The Royal Society of Chemistry.

Table 2 – Different methods for surface activation/modification different proposed electrodes in order to increase the electron transfer rate.

Commercial Filament	Activation	Observations	Available online	Reference
Black Magic®	Immersion in DMF	Picric acid and ascorbic acid detection with first activated 3D-printed electrode	Apr. 2018	(MANZANARES-PALENZUELA et al., 2018)
Black Magic®	10 min in DMF, and 250s with 2V atPBS solution	Hollow circular pin electrodes with ΔEpeak= 171 mV for $[Fe(CN)_6]^{4-3-}$	Oct. 2018	(BROWNE et al., 2018)
Black Magic®	EC activation of ±1.8V vs SCE; 900s;PBS 0.1 mol L^{-1}; DMF and Acetone activation	Dopamine detection with 2 linear ranges for dopamine and LOD of 0.24 μmol L^{-1}	Nov. 2018	(SANTOS et al., 2019)
Black Magic	24h hours proteinase K-mediated PLA hydrolysis	ΔEpeak= 350 mV for $[Fe(CN)_6]$ $^{4-3-}$	Jun. 2019	(MANZANARES-PALENZUELA et al., 2019)
Proto-pasta® and Black Magic®	Strong alkaline solution immersion compared to DMF	Propose a mechanism in alkaline media, where the saponification of PLA groups occur	Mar. 2019	(WIRTH et al., 2019)
Black Magic®	Mechanical polishing with 1200 grit sandpaper	0.4 μmol L^{-1} LOD for TNT detection, from 1-870 by SWV	Apr. 2019	Chapter 4 (CARDOSO et al.,)
Black Magic®	DMF, Acetone	ΔEpeak= 296 mV for $[Fe(CN)_6]^{-4-3}$ for acetone immersed electrode	Apr. 2019	(GUSMÃO et al., 2019)
Black Magic®	Porous hollow 3D pattern design with thermal annealed activation	Nitro-aromatic explosives detection in a solvent free activated electrode with fine details desing	Sep. 2019	(NOVOTNÝ et al., 2019)
Proto-pasta®	Mechanical and Electrochemical: +1.4 V/ 200 s, -1.0 V/200 s in NaOH 0.5 mol L^{-1}. Silver paint at the reference electrode	Complete FDM cell and sensor apparatus with Epeak reaching 150mV. Dopamine detection	Sep. 2019	(RICHTER et al., 2019)
Proto-pasta®	10 V applied during 60s 0.3 mol L^{-1} Na_2SO4 in in a U-shaped glass cell	ΔEpeak around 85mV using $Ru(acac)_3$ probe	Dec. 2019	(VANĚČKOVÁ et al., 2020b)
Black Magic®	Compare solvent method, with alkaline media/electrochemical activation	30 min of alkaline media followed by EC activation showed more promissor results; Dopamine sensor with LOD of 3.5 μmol L^{-1}	Dec. 2019	(KALINKE et al., 2020)
Electrifi Conductive ®	10 V applied during 60s 0.3 mol L^{-1} Na_2SO4 in in a U-shaped glass cell. Electroplated using 6V for 32 minutes between 3D-printed electrode at a U shaped cell, filled with 0.1 mol L^{-1} $Cu(NO_3)^2$	Cu2+electroplating reaching Epeak for $[Ru(NH_3)_6]^{3+}$ of ~69 mV	Dec. 2019	(VANĚČKOVÁ et al., 2020a)
Black Magic®	10 min in DMF and 2V for 250s at PBS solution. Overnight encubation of Au nanoparticlesand/or horseradish peroxidase	25-100 μmol L^{-1} for H_2O_2 direct eléctron transfer detection	Dec. 2019	(López Marzo; MAYORGA-MARTINEZ; PUMERA, 2020)
Proto-pasta®	Mechanical and EC by +1.4 V/ 200 s; -1.0 V 200 s in NaOH 0.5 mol L^{-1}	Cd-2+ and Pb2+ detection at biological samples using in a complete AM cell.	Jan. 2020	(ROCHA et al., 2020b)

Aiming to shed light on the varied protocols reported for surface treatment of 3D-printed graphene/PLA electrodes, different procedures, including mechanical polishing, electrochemical and chemical treatments and combination of them, were compared using dopamine as the model analyte (KALINKE et al., 2020) [42]. The best electrochemical sensing properties for dopamine detection were obtained after immersion of the 3D-printed electrodes in 1.0 mol L^{-1} NaOH for 30 min, which degrades excess of PLA exposing graphene sites. The LOD values of 3.5, 2.2 and 1.7 mmol L^{-1} were obtained using cyclic voltammetry, differential-pulse voltammetry and square- wave voltammetry, respectively. Biological samples (synthetic urine and blood serum) were analyzed by differential pulse voltammetry (DPV), as the dopamine peak was better separated from the ascorbic acid and uric acid peaks using this technique, with recovery values ranging between 89 and 98%. However, this investigation was carried out only for 3D-printed graphene-PLA electrodes. A similar investigation is required for the evaluation of 3D-printed carbon black/PLA electrodes. The work by Richter et al and Rocha et al proposed the electrochemical treatment in alkaline medium (RICHTER et al., 2019; ROCHA et al., 2020a). They affirm that this procedure involves the chemical/electrochemical treatment due to the action of NaOH by consuming PLA whereas electrochemical activation probably provides functional groups on the active conducting sites.

Tailoring the electrode surface using chemical modifiers or by the immobilization of bio-molecules for specific recognition of species has been widely investigated in the development of electrochemical sensors or biosensors since the pioneering work of Murray (MURRAY, 1980). Considering 3D-printed electrodes, their surface can also be modified with electrocatalyst to produce electrochemical sensors with enhanced detectability, sensitivity and selectivity (KATIC et al., 2019; ROCHA et al., 2020a). Similarly, electrochemical biosensors can be developed by immobilizing different bio-molecules on the surface of 3D-printed surfaces. This section highlights the works published in the literature showing how 3D-printed surfaces can be modified to develop novel and improved electrochemical sensors and biosensors. Table 2 brings all implemented methods of activation or modification to improve performance or obtain more efficient sensor towards a specific molecule, and its main characteristics.

1.4.3 Fabrication of all-in-one electrochemical devices using 3D-printing

A great benefit of 3D-printing technology in modern analytical chemistry is the feasibility of a single-step fabrication of miniaturized analytical systems in the desired geometry and for large-scale production in a reproducible manner. Considering the FDM technique as the most accessible and affordable 3D-printing technique and the many strategies pointed out in this review to fabricated 3D-printed electrochemical sensors, the

development of integrated and miniaturized electroanalytical systems in a single-step for the analysis of reduced sample volumes using portable instrumentation (e.g., point-of-care tests, on-site environmental measurements and so on) is an increasing demand in many research areas that can be addressed by the 3D-printing technology. This section shows some preliminary examples already reported with this aim, all of them using the FDM 3D-printing technique.

One challenge to overcome concerns is the fabrication of reference electrodes with no potential variations. In this context, a method for printing a graphene/PLA pseudo-reference electrode was reported (ROHAIZAD et al., 2019). Printed-electrodes were submitted to a silver electrodeposition to obtain Ag/AgCl electrodes. In this regard, the electrode was immersed in silver ions solution and a potential of −0.9 V (*vs* an external Ag/AgCl reference electrode) was applied for 800 s. The performance of the proposed electrode was compared with a commercial conventional reference electrode (Ag/AgCl/KCl 3.5 mol L^{-1}) by open circuit using a multimeter and by cyclic voltammetry using two electrochemical probes ($[Fe(CN)_6]^{3-/4-}$ and $[Ru(NH_3)_6]^{2+/3+}$). The obtained voltammograms for each system have similar behaviors and current intensities, however with a shift to more negative values of potential. Also, the proposed pseudo-reference electrode was considered a simple and low-cost alternative to commercial reference electrodes.

Integrated electrochemical systems are attractive since they increase operational simplicity. In this context, 3D-printing can be applied for the construction of the three conventional measuring electrodes (working, counter and reference electrodes) in the same device manufactured by a single step. This purpose was presented in the paper published by (KATSELI; ECONOMOU; KOKKINOS, 2019). For this, three conductive electrodes (working, auxiliary and pseudo-reference) were printed from a carbon-loaded PLA filament. Additionally, an electrode holder was printed from non-conductive PLA filament, developing a single integrated electrochemical system. The analytical performance of the proposed 3D-printed sensor was similar or better than other electrodes and high reproducibility of fabrication was verified (RSD < 10 %). This proposed electrode was applied for three different applications: determination of Hg^{2+} by square-wave anodic stripping voltammetry, organic molecules (caffeine) by differential-pulse voltammetry and glucose biosensing using amperometric determination by incorporation of glucose oxidase on the working electrode. LOD values of 9.5 x 10^{-9} molL^{-1} for Hg^{2+} ions, 9.3 x 10^{-6} mol L^{-1} for caffeine, and a linear range from 2.0 x 10^{-3} to 2.8 x 10^{-2} mol L^{-1} for glucose were obtained.

Other recent work (KATSELI; ECONOMOU; KOKKINOS, 2020) explored the dual extruder 3D-printing for a lab-on-a-chip device construction, wherein the electrochemical cell was printed with PLA filament. The representation of the proposed device is shown in Figure 5. Different conductive filaments were studied (3D Edge carbon-ABS, carbon black-PLA Proto-pasta and Amolen carbon-PLA), wherein carbon-ABS showed higher

sensitivity and better background characteristics. The proposed device was successfully used for the simultaneous determination of paracetamol and caffeine by differential-pulse voltammetry. After the optimization of parameters, the device showed LOD values of 2.8 x 10^{-6} and 2.0 x 10^{-6} mol L^{-1} for paracetamol and caffeine, respectively. Electrodes also presented an adequate manufacturing reproducibility. The analytes were determined in pharmaceutical tablets and urine samples, showing recovery values between 96 and 103 %.

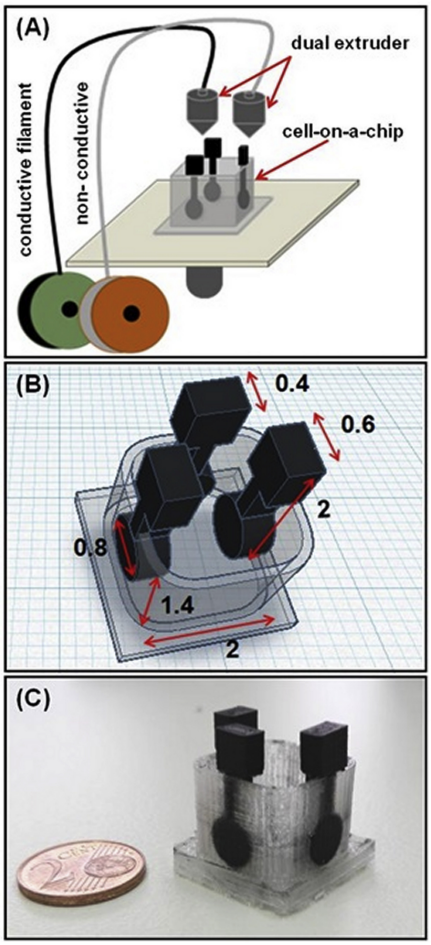

Figure 5 – (A) Representation of the 3D-printing procedure for the fabrication of the cell-on-a-chip device using a dual extruder 3D-printer; (B) Dimensions of the 3D-printed cell-on-a-chip device (in cm); (C) Real photograph of the device. Reprinted with permission from (KATSELI; ECONOMOU; KOKKINOS, 2020), Copyright 2020, Elsevier.

A completely fabricated 3D-printed electrode using carbon nanofiber, graphite and polystyrene filament was reported (HONEYCHURCH; RYMANSAIB; IRAVANI, 2018). The new proposed electrochemical device was applied for the determination of zinc ions by differential-pulse anodic stripping voltammetry with low background currents even without the presence of bismuth, mercury or other metallic films. The sensor showed a LOD of 2.9 x 10^{-8} molL^{-1} and an average recovery of 98 % for tap water sample fortified

with 3.3 x 10^{-6}molL^{-1} of zinc. In addition, the fabrication of 3D-printed fluidic electrochemical cells with ABS and electrochemical sensing devices with graphene/PLA filament were proposed (CARDOSO et al., 2018). Those results will be discussed furthermore in chapter 2.

The fabrication of a complete electroanalytical system which consisted of 3D-printed conductive electrodes (working, auxiliary and pseudo-reference electrodes) and the 3D-printed non-conductive electrochemical cell (different 3D-printed parts to generate the assembled electroanalytical system) was demonstrated (RICHTER et al., 2019). The 3D-printed electrochemical cell and the working electrode preparation procedures can be seen in Figure 6. The electrodes were fabricated by FDM 3D-printing using a carbon black/PLA filament. The performance of the working electrode was evaluated after polishing on sandpaper and simultaneous chemical/electrochemical activation in a 0.50 mol L^{-1} NaOH solution. This treatment led to PLA removal by saponification, exposing the carbon black microparticles (Figure 6). The considerable improvement in the electrochemical behavior for dopamine determination was verified. The proposed device showed excellent results with LOD of 1.0 x 10^{-7} mol L^{-1} and good reproducibility (RSD = 0.4 %) between successive measurements.

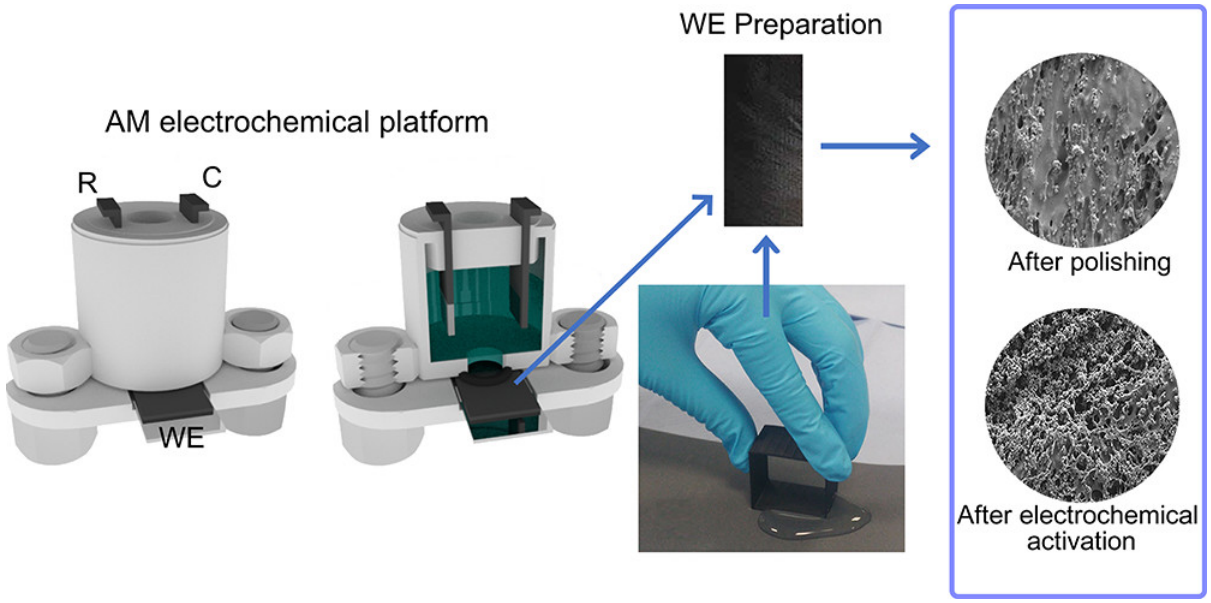

Figure 6 – Schematic 3D-printed (AM) electrochemical cell and the 3D-printing working electrode preparation by polishing. On right, SEM images of the 3D-printed surface after polishing and after electrochemical activation. Reprinted with permission from (RICHTER et al., 2019), Copyright (2019), American Chemical Society.

A spectroelectrochemical cell coupled to a Raman spectrometer and a potentiostat for in situ mapping of the Prussian blue redox process was developed (SANTOS et al., 2019). The spectroelectrochemical device was printed using non-conductive ABS filament

and the working electrode using conductive graphene/PLA filament. The proposed cell enabled the Raman mapping in real-time, and the investigation of the structural changes of Prussian blue during electrochemical measurements. In this approach, the 3D-printed cell proved to be a low-cost and easily adaptable system. Another example of the construction of a coupled cell for electrochemical and spectroscopic measurement was recently reported, in this case, an UV/Vis spectroelectrochemistry cell using FDM 3D-printed electrodes (VANĚČKOVÁ et al., 2020c). These examples show that electrochemical devices can be easily fabricated using the 3D-printing technology, allowing them to obtain the most varied systems and shapes, according to the intended application.

The single-step fabrication of 3D-printed devices for flow analysis combined with electrochemical detection using a dual extruder FDM 3D-printer was proposed (O'NEIL et al., 2019). The device consisted of a hydrodynamic fluidic channel with inlet and outlet, on which 2 electrodes are printed along the channel using a conductive filament (graphene/PLA) as shown in Figure 7 the first electrode served as a working electrode while the second one was used either as pseudo-reference or as a counter electrode, depending on the experiment (Figure 7 (b) and (c)). Hydrodynamic voltammograms were performed using ferrocene methanol as the redox probe under different flow rates (from 0.5 to 3.5 mL min^{-1}) using the second electrode as the pseudo-reference electrode. It was not mentioned by the authors how the flow rate and injections were controlled. Other experiments for ferrocene methanol and catechol as model analytes were performed using an Ag/AgCl wire introduced at the outlet tubing as a pseudo-reference electrode. For the catechol detection in an artificial fluid buffer (to simulate a more complex medium), it was necessary to modify the 3D-printed working electrode with gold by electrodeposition. Certainly, the low responses obtained on unmodified 3D-printed surfaces were verified due to the need for the surface treatment of such surfaces as previously discussed in this review (such as mechanical polishing, chemical or electrochemical treatments). Hence, this work reveals the potential of FDM 3D-printing to fabricate all-in-one flow electroanalytical devices with great promises for on-site determinations.

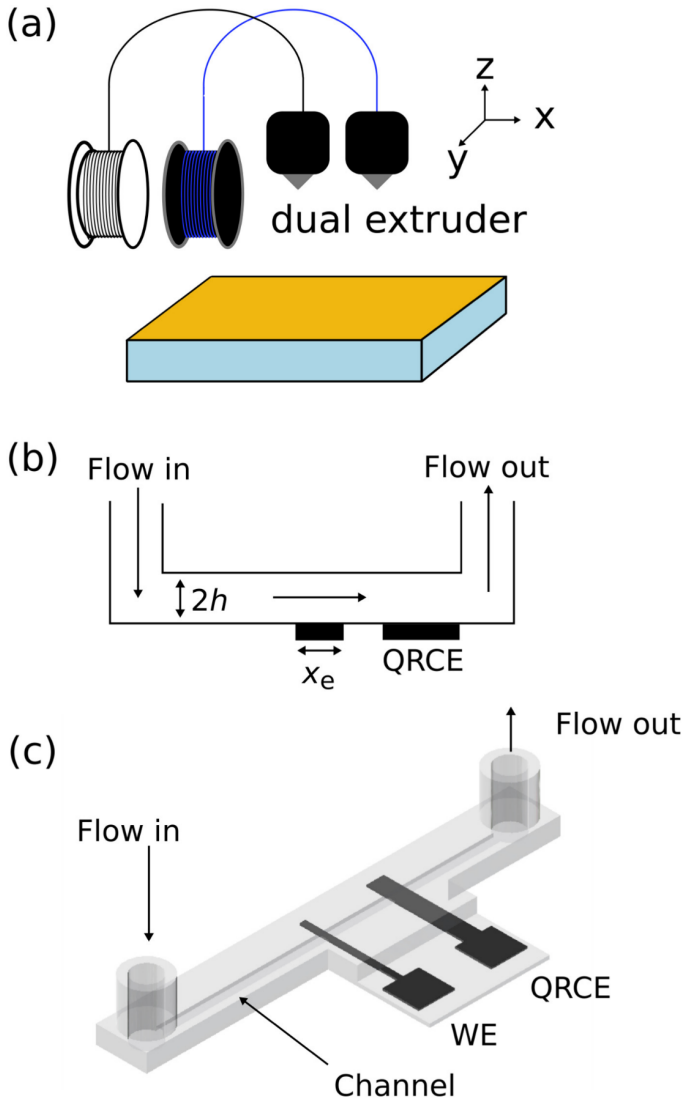

Figure 7 – Scheme of the proposed flow analysis device with (a) the representation of the dual extruder 3D-printer; (b) Orthogonal view of all 3D-printed flow device containing 2 electrodes: Working electrode (WE) and quasi-reference or counter electrode (QRCE); (c) perspective view of the device with embedded electrodes. Reprinted with permission from (O'NEIL et al., 2019), Copyright (2020), Elsevier.

Chapter 2

3D-printing for electroanalysis: From multiuse electrochemical cells to sensors

This Chapter contain an adaption of the published article entitled "3D-printing for electroanalysis: From multiuse electrochemical cells to sensors" Rafael M. Cardoso, Dianderson M. H. Mendonça, Weberson P. Silva, Murilo N. T. Silva, Edson Nossol, Rodrigo A. B. da Silva, Eduardo M. Richter, Rodrigo A. A. Muñoz available online .

Graphical Abstract

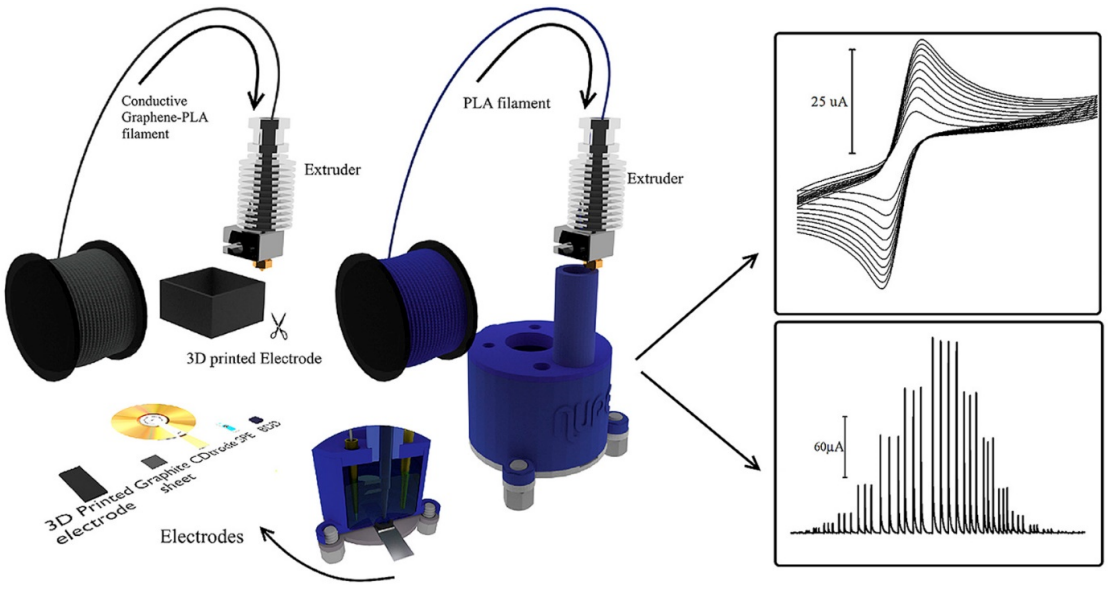

2.1 Introduction

Analytical equipment normally are prototyped using classic and very known methods such as milling machines and injected molded parts. Concerning electroanalytical

instrumentation, holders, cells, channels and other apparatus are normally commercially obtained, or developed inside a research lab, and executed normally by a third part that have the machinery. This many steps can delay and bring costs to a analytical equipment prototyping process. Additive manufacture are a new player in this field, and big industries or small companies are taking advantage of this easy and cheap new tool. This chapter propose an electrochemical cell for BIA/FIA electroanalysis, and demonstrate the possibility of a 3D-printed sensor using conductive thermoplastics commercial formulation.

2.2 Experimental

2.2.1 Reagents and solutions

All solutions were prepared with deionized water (resistivity not lower than 18 MΩ cm) obtained from a Milli-Q water purification system (Millipore, Bedford, MA, USA) and analytical grade reagents. Catechol (95% w/w), dopamine (98% w/w) and tert-butylhydroquinone (TBHQ, 98% w/w) were obtained from Acros (New Jersey, USA); dipyrone (98% w/w), diclofenac (98% w/w) and hexaammineruthenium (III) chloride (98% w/w) from Sigma Aldrich (Milwaukee, WI, USA); perchloric acid (70% w/w), phosphoric acid (85% w/w) and sulfuric acid (98% w/w) from Reagen (Rio de Janeiro, Brazil).

Perchloric acid solution (0.1 mol L^{-1}) was used as supporting electrolyte for the determination of the phenolic compounds catechol, dopamine and TBHQ. Sodium phosphate buffer (0.1 mol L^{-1}; pH 7.2) and sulfuric acid (0.1 mol L^{-1}) were used as supporting electrolytes for the determination of dipyrone and diclofenac, respectively. All stock solutions were freshly prepared by dissolution in the respective electrolyte. Working standard solutions were prepared before use by suitable dilution in electrolyte solution.

2.2.2 Instrumental

Electrochemical measurements were performed with a μ-AUTOLAB type III potentiostat / galvanostat (Eco Chemie, Utrecht, Netherlands) interfaced to a microcomputer and controlled by NOVA 1.12 software. The proposed 3D-printed cell with a three-electrode configuration was used for all electrochemical measurements. All measurements were performed at room temperature (25ºC) and in the presence of dissolved oxygen.

A platinum wire and a lab-made Ag/AgCl/KCl_{sat}.(PEDROTTI; ANGNES; GUTZ, 1996) were used as auxiliary and reference electrodes, respectively. Five working electrodes have been evaluated in the 3D-printed cell: gold thin film electrode obtained from compact discs (gold CDtrode), graphite sheet electrode (GSE), boron-doped diamond (BDD), a carbon screen-printed electrode (SPE) and the 3D-printed conductive substrate. The gold CDtrode was obtained by cutting a small piece (1 cm x 5 cm) of a recordable compact

disc (Mitsui, Japan) containing a highly pure gold thin film (≈ 100 nm) and removing the polymer protection after exposure of the disc surface on concentrated nitric acid (65 % m/m) for 3 min (ANGNES et al., 2000). 5-cm length of a CDTrode is necessary to make the electric contact directly over the conducting gold surface. The GSE was obtained by cutting a small piece (1 cm x 1 cm) of a commercial graphite paper-based sheet (Longteng Sealing, Shandong, China) followed by mechanical polishing (abrasive paper and alumina suspension). A small piece (1 cm x 1 cm) of polycrystalline silicon wafer containing a BDD film with 8000 ppm of doping level was purchased from Neocoat (La Chaux-de-Fonds, Switzerland). Before electrochemical measurements, the BDD electrode was cathodically pretreated by applying -0.1 A for 300 s in 0.5 mol L^{-1} sulfuric acid. A SPE strip containing the three-electrode setup in which the working electrode was a carbon electrode (4 mm diameter) was obtained from DropSens^{ő} (Oviedo, Spain). The integrated auxiliary (printed carbon ink) and pseudo-reference (printed silver ink) of the SPE strip were used, dispensing other external electrodes. Prior to use, each SPE was activated by successive voltammetric cycling in the respective supporting electrolyte until reaching stable background currents.

The 3D-printed sensor was produced using a conducting G-PLA filament purchased from Black Magic 3D (New York, USA). 3D hollow square tubes (4.0 cm x 4.0 cm) with wall thickness of 0.6 mm were printed with G-PLA filament using a 0.5 mm hotend nozzle and 220^{o}C of heated bed temperature (recommended by the fabricant). Finally, pieces of planar substrates (10 cm x 20 cm) were cut and divided in smaller units (2 cm x 3 cm) to be used as working electrodes.Figure 8 show a picture of the proposed sensor.

As no information on the weight proportion of graphene or chemicals was given by the fabricant, Raman spectra of the G-PLA sensor were obtained using a LabRAM HR Evolution - Horiba (λ=532 nm). Moreover, scanning electron microscopy (SEM) performed in a Vega 3 -Tescan equipment at 20 kV was carried out to confirm the presence of graphene and determine its nature.

Electrochemical impedance spectroscopy (EIS) measurements were carried out in the presence of 1 mmol L^{-1} of hexaammineruthenium (III) chloride in a 0.1 mol L^{-1} KCl solution using as working electrode the 3D-printed sensor and a bare glassy-carbon electrode (GCE), in the frequency range between 0.1 and 50000 Hz with signal amplitude of 10 mV and 10 data points per frequency decade. The diameter of the semicircle of Nyquist plot is proportional to the charge transfer resistance (Rct value), which was obtained by the electrochemical circle fit option of Nova software using the equivalent circuit consisting of Rct, solution resistance (Rs), and Warburg impedance (W).

Infrared (IR) spectroscopy measurements were performed using a Perkin Elmer Spectrum 2 (Waltham, EUA) spectrometer on attenuate total reflectance (ATR) mode. Measurements were obtained in the range between 4000-600 cm-1 with a resolution of 4 cm^{-1}.

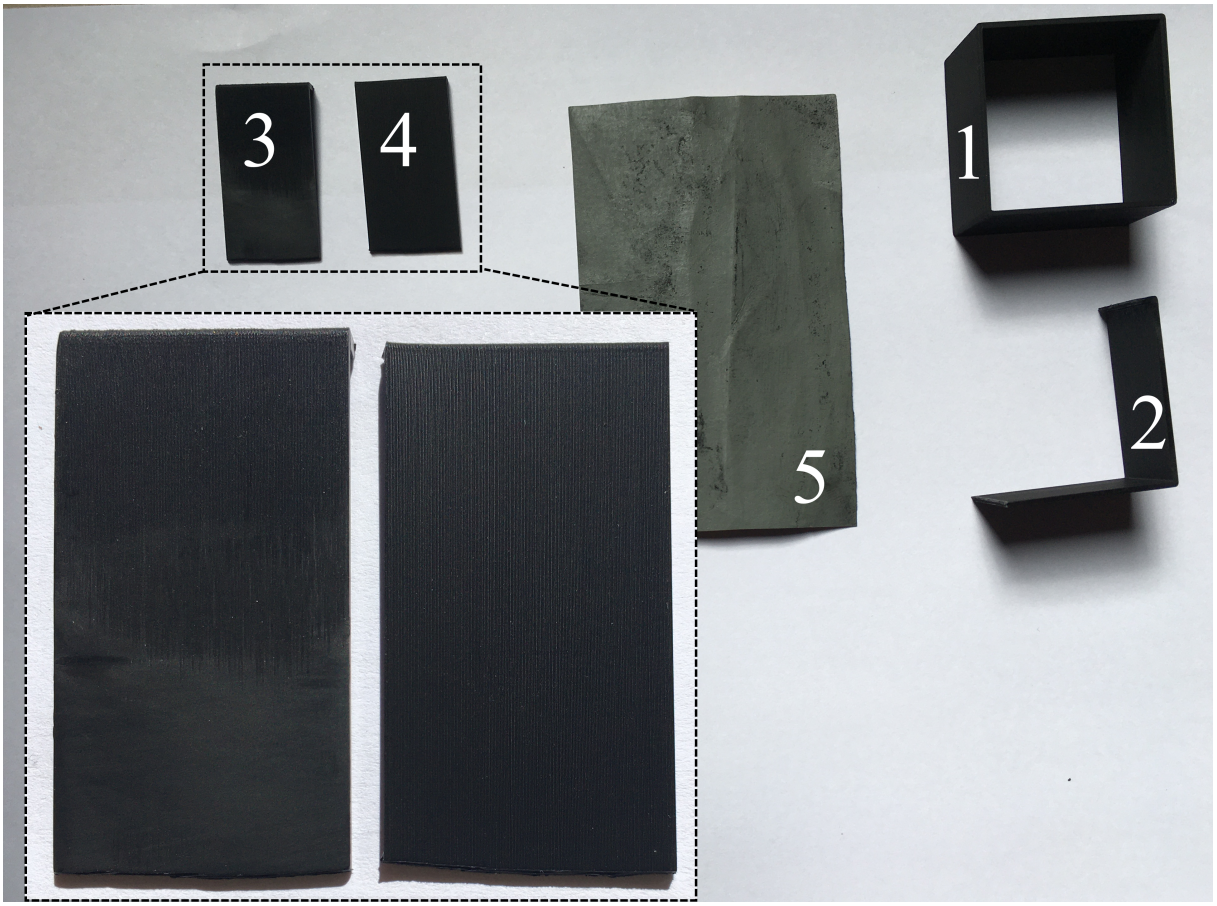

Figure 8 – Image of the FDM 3D-printed electrodes where 1 is the printed hollow cube, 2 is the printed part with two faces removed (3 and 4), with 3 being the polished electrode and 4 the unpolished; 5 is the 1200grit sandpaper used

2.2.3 Design and construction of the multiuse 3D-printed cell

The design of the electrochemical cell was obtained using Simplify 3D software and the standard tessellation language file (STL file) was used by the 3D-printer (Core A1 (GT-Max3D®), Campinas, Brazil) to manufacture the cell (FDM technology). The printing material was an ABS filament (3Dfila; 1.75 mm) and the 3D-printing parameters were set to high resolution of 0.1 mm per layer, hotend nozzle temperature of 230 ºC and heated bed temperature of 110 ºC, with no need of supports. The STL model file was designed using Blender®software, and then sliced on Simplify3D®to generate the .GCODE file to perform the printing.

The 3D-printed cell (transversal cut view) for applications in stationary conditions for voltammetric measurements is presented in Figure 9.A.1 (highlighting the positioning of external counter and reference electrodes) while the same 3D-printed cell with additional accessories to perform measurements under flow conditions (FIA and BIA) is presented in Figure 9.A.2 (this image shows the insertion of a SPE strip containing the three electrode

system that dispenses external counter and reference electrodes presented in Figure 9.A.1). Figure 9.B shows the image of all components of the 3D-printed cell: 1) Cell body, which includes a small round hole that allows the contact of the working electrode (or the SPE strip) with the internal solution, and the three screw nuts equidistant at the external region of cell body; (2) Bottom cover containing three holes for the insertion of 3D-printed screws (3) to enable the pressure control against the O-ring to assemble the cell; there is a rectangular thin cavity to accommodate the steel plate or SPE strip; (4) Top cover (to be firmly fitted on the cell) containing two orifices to introduce auxiliary and reference electrodes, a hole for liquid manipulation (or introduction of a mechanic stirrer) and another small hole to insert the micro-pipette adapter (presented in 5); (6) rubber-made O-rings with 2 different internal diameters, 5.28 mm (for any plate working electrode) and 7.65 mm (to cover the entire SPE strip), and (7) steel plate (for electric contact of working electrodes by their backside). Note that A.1 and A.2 show the same cell except to the micro-pipette adaptor (5) and pipette tip that is assembled for flow experiments (A.2). The 3D-printing process, cell assembling using a BDD electrode as example, and batch-injection of a model analyte and obtaining the current responses by a portable potentiostat (microStat, Dropsens, Spain) monitored on a notebook screen is available online (click here) in a video format.

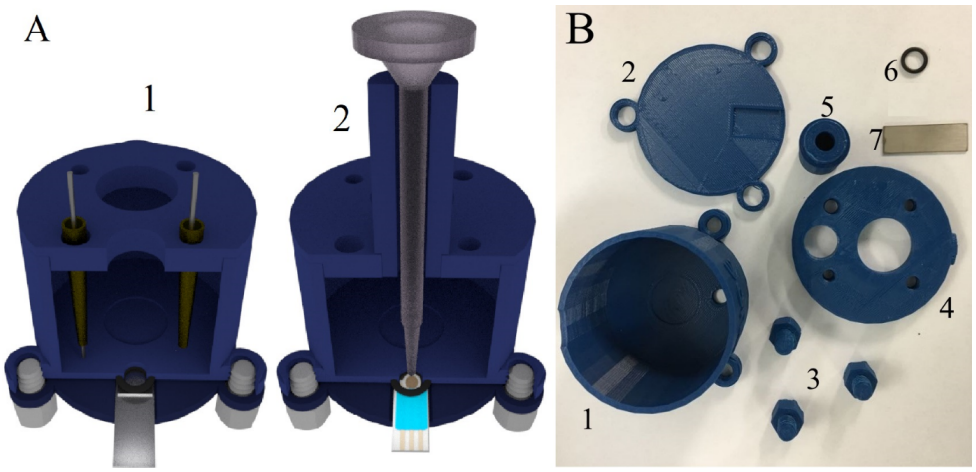

Figure 9 – (A) Scheme of the 3D-printed cell (transversal cut view) used for batch (1) and flow (2) electrochemical measurements; counter and reference electrodes are represented in A.1 while the use of SPE in A.2 dispenses the use of external counter and reference electrodes; (B) Components of the 3D-printed cell: (1) cell body, (2) bottom cover, (3) screws, (4) top cover; (5) micro-pipette adaptor; (6) O-rings with 2 different internal diameter: 5.28 mm (for any working electrode) and 7.65 mm (for the SPE strip); and (7) steel plate (for electric contact of working electrodes by their backside). Note that A.1 and A.2 show the same cell except to the micro-pipette adaptor (5) and pipette tip that is assembled for flow experiments (A.2).

The planar working electrode (gold CDtrode, GSE, BDD or 3D-printed platform) is

positioned over a steel board. After that a rubber-made O-ring is placed over the working electrode and then the upper part of the cell is assembled using 3D-printed screw nuts (to prevent leaks and delimiters the working electrode area, A = 2.7 cm^2 using the smaller O-ring, while the working electrode area of SPE is defined by the manufacturer, A = 0.126 cm^2). The electric contact can be made directly through the topside or the backside of the substrate (the only exception is for the gold CDtrode as it consists of a gold thin film deposited on polycarbonate and thus the electric contact can only be assessed by the topside). The applied pressure on the working electrode is defined by the screwing level. When using commercial SPEs, the contact of three electrodes is made using a special cable produced by the SPE manufacturer (DropSens, Oviedo). The region where the three electrodes come in contact with the solution is limited by the larger O-ring (7.65 mm diameter). The total internal volume of the 3D-printed cell is around 80 mL, typical volume used for flow analysis. For measurements under non-stirred solutions, the cell was filled with 10 mL of electrolyte.

The 3D-printed cell to be operated under hydrodynamic conditions (FIA or BIA) works in a wall-jet configuration with the micro-pipette tip closely placed to the working electrode. As presented in Figure 9.A.2, an additional support containing a central hole was fixed above the top cover of the cell (concentric with the working electrode placed at the bottom of the cell) for introduction of the micro-pipette tip (syringe shape). Hydrodynamic conditions were explored using two systems: 1) BIA: The solutions were directly injected onto working electrode surface by an electronic micro-pipette (Eppendorf®Multipette stream) maintained at a fixed distance (2 mm between the working electrode and the tip, Multipette Combitip®) and 80 mL of electrolyte was added to the cell before injections and measurements. This system was applied for the detection of TBHQ, dipyrone and dopamine on carbon SPE, gold CDtrode and GSE, respectively; 2) FIA with carrier recycling: A polyethylene tube (i.d. = 1.0 mm) was fixed on the thinner end of the Combitip®, the electrolyte solution was carried by a peristaltic pump (Gilson Miniplus 3) under a flow rate of 3.0 mL min^{-1} and the solutions were injected onto the working electrode surface by an acrylic injector connected inline. This FIA system allows the re-circulation of the carrier solution by fixing a tube inside the cell containing 80 mL of the electrolyte solution. In this case, the FIA cell contains a large volume of solution (electrolyte plus huge diluted residues) in its own reservoir, similarly to the BIA system. This configuration presents a very low reagent consumption and waste generation, even under high flow rates. Overall description of this system was previously reported by Franco et al. (FRANCO et al., 2016). In this work, the FIA system with carrier recycling was used for detection of diclofenac on BDD.

2.3 Results and Discussion

As a proof of concept of the 3D-printed cell, electrochemical measurements of four target analytes were performed using distinct plate-shaped working electrodes assembled on the same cell for batch or flow conditions. The choice of electrodes and analytes were based in similar works previously reported: TBHQ on carbon SPE (TORMIN et al., 2012), dipyrone on gold CDtrode (MUÑOZ; MATOS; ANGNES, 2001), dopamine on GSE (OLIVEIRA; MUNOZ; ANGNES, 2010) and diclofenac on BDD electrode (GIMENES et al., 2011). Finally, results obtained with a 3D-printed sensor (using the G-PLA filament) are also shown. Disposable SPE combines all three electrodes (working, auxiliary and pseudo-reference) on the same planar support, being attractive due to simplicity, reproducibility, relative low cost and robustness (LI et al., 2012; METTERS; KADARA; BANKS, 2011). Gold CDtrodes (ANGNES et al., 2000) are a disposable and low cost electrode source and has been proposed for several applications as described in a recent review (HONEYCHURCH, 2017). GSE is another source of low-cost sensors not so explored as SPEs or CDtrodes although this material presents attractive features for sensor applications, such as low electrical resistance, good flexibility, favorable mechanical performance, and thus infinite possibilities of electrode designs (OLIVEIRA; MUNOZ; ANGNES, 2010). The BDD electrode presents special electroanalytical properties, such as high stability of surface (low poisoning of electroactive species), wide potential window and low capacitive currents, which make this sensing platform feasible to investigate electrochemical oxidation processes occurred at high positive potentials (BROCENSCHI et al., 2017; IRKHAM; WATANABE; EINAGA, 2017; OLIVEIRA et al., 2016). Conductive surfaces can also be easily obtained by direct 3D-printing of graphene-based conductive material (FOSTER et al., 2017). The 3D-printing conductive surfaces were adapted to the 3D-printed cell forming a set with significant desirable characteristics, such as low cost, good mechanical strength, countless possibilities of cell or sensor designs, as well as use of conductive filaments of different compositions.

Figure 10 presents the cyclic voltammetric experiments using the 3D-printed cell under non-stirred solutions (scheme of Figure 9.A.1) for each analyte on the respective working electrode. These experiments were performed in absence and presence of 1.0 mmol L^{-1} of each analyte using 10 mL of electrolyte solution inside the cell. The electrochemical oxidation of TBHQ follows a quasi-reversible behavior ($\Delta Ep \approx 400$ mV) on carbon SPE (Figure 10.2A) as well as for dopamine ($\Delta Ep \approx 300$ mV) on GSE (Figure 10.2C). However, high background currents on GSE can be observed and are probably due to higher resistivity of the GSE in comparison with carbon SPE. Cyclic voltammograms of dopamine on GSE were also performed using different scan rates (1-900 mVs^{-1}), in which was obtained a highly linear dependence ($R^2 > 0.99$) between current peak and the square root of scan rate, characteristic of a diffusion controlled process, which is similar to the results presented for paracetamol using similar electrodes (OLIVEIRA; MUNOZ;

ANGNES, 2010).The cyclic voltammetry of dipyrone presented two irreversible anodic peaks on gold CDtrode at around +0.4 and +0.6 V (Figure 11.3B) similar to a previous work (ANGNES et al., 2000), while the voltammetry of diclofenac revealed three irreversible oxidation peaks on the BDD electrode at around +0.9, +1.3 and +1.7 V (Figure 11.3D). These results indicate the successful use of the 3D-printed cell for electrochemical measurements under unstirred solution using different working electrodes.

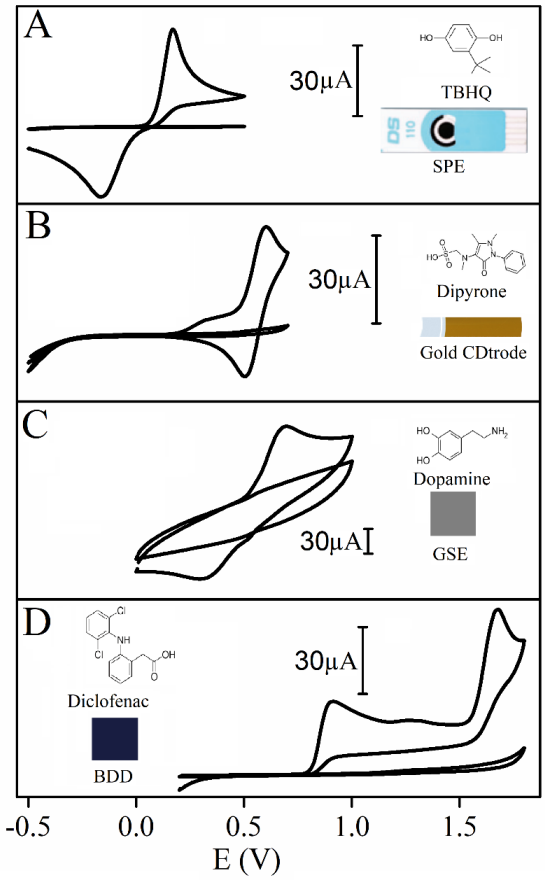

Figure 10 – Cyclic voltammograms recorded in absence (blank electrolyte solution) and presence of 1.0 mmol L^{-1} TBHQ on carbon SPE (A), 1.0 mmol L^{-1} dipyrone on gold CDtrode (B), 1.0 mmol L^{-1} dopamine on GSE (C) and 1.0 mmol L^{-1} diclofenac on BDD electrode (D). Supporting electrolytes: 0.1 mol L^{-1} $HClO_4$ in A and C, 0.1 mol L^{-1} phosphate buffer (pH 7.2) in B and 0.1 mol L^{-1} H_2SO_4 in D. Counter and reference electrodes: Pt and $Ag/AgCl/KCl_{sat.}$, respectively, in B, C, and D. Scan rate: 50 mV s^{-1}.

The performance of the proposed 3D-printed cell was also evaluated using flow ("wall-jet" configuration) conditions (scheme on Figure 9.A.2). The three electrode/analyte systems presented in Figure 10 were investigated using the same printed cell for BIA with amperometric detection (A-C). BIA parameters, flow rate, injection volume and stirring rate were set to 153 μL s^{-1} 100μL and 700 rpm. The used FIA parameters were optimized to 50 μL of injection plug with3.0 mL min^{-1} of flow. The applied potential for each target

molecules were defined by the voltametric responses. Figure 11 (A – C) presents the amperometric responses for triplicate injections of solutions containing each target analyte (1 - 1000 μmol L^{-1}) in ascending and descending orders. All calibration curves showed satisfactory linearity between analyte concentration and anodic peak current (R > 0.99) in the investigated concentration range. Moreover, all experiments showed absence of memory effects, as the slopes for ascending and descending orders presented very similar values (the difference was lower than 2.3%). The high precision of the BIA system was also observed in a repeatability study, performed by injections of solution containing 10 μmol L^{-1} (n = 10) alternated to 100 µmol L^{-1} (n = 10) of each target analyte (results not shown). In these investigations, the obtained RSD values for injections of lowest and highest analyte concentrations did not exceed 5 % and 6 %, respectively.

Optionally, the amperometric detection of diclofenac on the BDD electrode was performed using the 3D-printed cell operating under a FIA system with carrier recycling (FRANCO et al., 2016). Under optimized conditions, solutions of diclofenac (5 – 50 μmol L^{-1}) in increasing and decreasing concentrations were injected in triplicate. As presented (Figure 11.3D), high linearity (R > 0.99) and absence of carryover effects were also observed in the investigated concentration range. The obtained RSD values for twenty successive alternated injections of 12.5 μmol L^{-1} and 20 μmol L^{-1} were 7 % and 2 %, respectively (amperogram not shown). Table 3 summarizes the analytical performance of the "wall-jet" systems (BIA and FIA with carrier recycle) with amperometric detection coupled to the 3D-printed cell.

Table 3 – Analytical performance (data obtained from Figure 11) of different sensors coupled to the 3D-printed cell for the amperometric detection of TBHQ, dipyrone (DIP), dopamine (DOP), and diclofenac (DIC) under hydrodynamic conditions (BIA or FIA with carrier recycle).

Working Electrode	**Analyte**	**Slope** (μ**A**/μ**mol L**$^{-1}$)	**LR** (μ**mol L**$^{-1}$)	**RSD** (%)	**LOD** μ**mol L**$^{-1}$	**AF**^{c} **h**$^{-1}$	**R**
SPE	TBHQ	0.164^{a}/0.165^{b}	1 – 1000	2 / 6^{d}	0.18	134	0.999
Gold CDtrode	DIP	0.066^{a}/0.066^{b}	1 – 1000	4 / 2^{d}	0.73	108	0.998
Graphite sheet	DOP	0.188^{a}/0.186^{b}	1 – 1000	5 / 2^{d}	0.50	128	0.999
BDD	DIC	0.058^{a}/0.056^{b}	5-50	7 / 3^{e}	0.23	178	0.999

LR: Linear range; RSD: Relative standard deviation; LOD: Limit of detection; AF: Analytical frequency. Slope in ascending^{a} and descending^{b} orders, RSD concentration of 10/100 μmol L^{-1} ^{d}, and 13 and 20 μmol L^{-1} ^{e}

The 3D-printed electrode (planar substrate) based on the conductive G-doped PLA filament was assembled on the 3D-printed cell to perform electrochemical measurements under quiet solution and hydrodynamic conditions using the BIA system. Figure 12 presents the electrochemical measurements performed using this novel sensor. The cyclic voltammetry of the redox probe $Ru(NH_3)_6$ $^{+3}$ (Figure 12.4A) shows an electrochemical reversible process controlled by diffusion of the redox probe species as revealed by the linear behavior of the peak current as function of the square root of scan rate (Figure 12.4B).

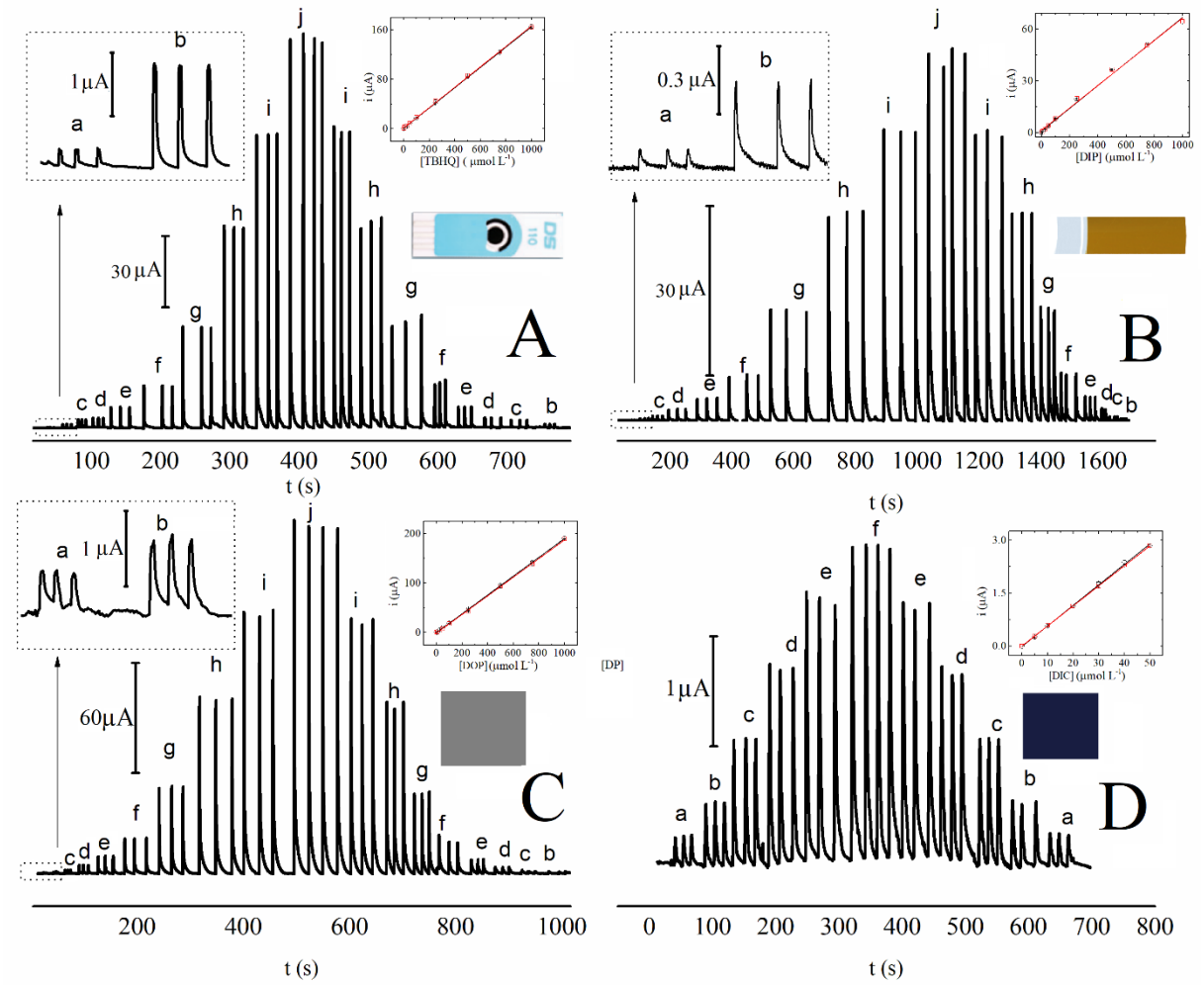

Figure 11 – Amperometric responses (n = 3) obtained for solutions injected in increasing and decreasing concentration order: (A) TBHQ, (B) dipyrone (DIP), (C) dopamine (DOP), and (D) diclofenac (DIC). Concentration ranges: 1 – 1000 μmol L^{-1} (A, B, and C) and 5 – 50 μmol L^{-1} (D). Applied potentials: (A) +0.5 V (vs. pseudo Ag), (B) +0.6 V, (C) +0.9 V, (D) +1.2 V (*vs* Ag/AgCl/KCl$_{sat.}$). Injection volume: 100 μL (A, B, and C) and 50 μL (D); flow rate: 153 μL s^{-1} (A, B, and C) and 50 μL s^{-1} (3.0 mL min^{-1}) (D). Stirring rate (A, B, and C): 700 rpm. Supporting electrolytes and electrodes are the same of Figure 10

This result is a preliminary evidence of the potential use of the 3D-printed sensor using the PLA filament containing graphene. Figure 12.4C and 4D show the cyclic voltammetry and square-wave voltammetry (SWV) scans for catechol, respectively. The peak-to-peak separation observed in the cyclic voltammetry indicates a quasi-reversible system, which typically occurs on a glassy-carbon electrode (CARDOSO et al., 2015). SWV scans from 5 to 300 μl L^{-1} of catechol shows the linear behavior and high detectability of this sensor compared with a graphene oxide-modified electrode (ROCHA et al., 2018). Figure 12.4E shows BIA with amperometric detection of dopamine on the 3D-printed electrode within a linear range between 1 and 400 μmol L^{-1}, and a detection limit of 0.18 μmol L^{-1} (3-fold the standard deviation of baseline divided by the slope value). Comparing these analytical features with those obtained on glassy-carbon electrodes modified with unmodified glassy-carbon and modified with reduced graphene oxide (rGO) (ROCHA et al., 2018) or multiwalled carbon nanotubes (MWCNT) (CARDOSO et al., 2015; STEFANO et al., 2017), the proposed 3D-printed sensor presented comparable performance for dopamine detection. Table 4 compares analytical performance of the 3D-printed sensor for the detection of catechol by SWV and dopamine by BIA with amperometric (AMP) detection with previous works reported in the literature for the same purpose. The 3D-printed sensor produced with G-PLA filament may not present superior performance in comparison to GCE modified with MWCNT or rGO, but it presents better results than unmodified GCE. Considering the low cost and availability of G-PLA filament for the 3D-printing of several units of this sensor at once, the proposed 3D-printed sensor is a promising source of electrodes that may replace GCE for a large variety of applications including electroanalysis.

EIS measurements were obtained on the 3D-printed sensor produced with G-PLA and on a bare GCE surface for comparison. Figure 13 shows the respective Nyquist plots in the presence of 1 mmol L^{-1} of hexaammineruthenium(III) chloride in 0.1 mol L^{-1} KCl and Figure 13 shows the cyclic voltammograms obtained in the same solution obtained on both electrodes. The selection of this redox probe is due to it being an outer-sphere electron transfer redox probe and consequently it is only dependent on the electronic structure of the carbon surface (BROWNSON; KELLY; BANKS, 2015).

Impedance spectra revealed different profiles for each surface. The bare GCE surface presented lower impedance and thus lower resistance to charge transfer in comparison to the 3D-printed G-PLA sensor. The Rct value obtained on the 3D-printed sensor was 552 Ω while a negligible value was verified on the bare GCE (the absence of a semicircle in the Nyquist plot did not enable the estimation of the Rct value). Additionally, the heterogeneous electron transfer rate constant (k_0) of both surfaces using the same redox probe was calculated by the Nicholson method (BROWNSON; KELLY; BANKS, 2015; NICHOLSON, 1965) and the values obtained for GCE and 3D-printed G-PLA sensor were 0.0184 and 0.00510 cm $s^{-}1$, respectively, which is in agreement with the EIS data. These

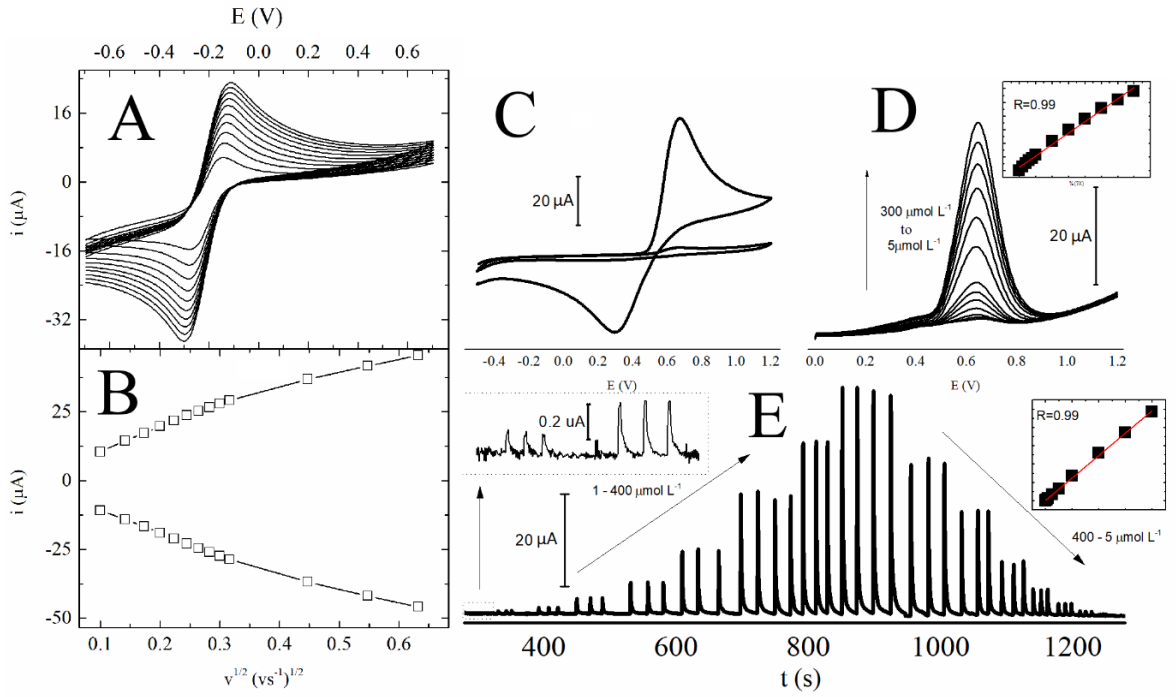

Figure 12 – Electrochemistry on conductive G-PLA electrode: (A) Cyclic voltammetry of 1 mmol L^{-1} $Ru(NH_3)_6$ $^{3+}$ at different scan rates (v) and (B) respective plots of i *vs.* $v^{1/2}$ in 0.1 mol L^{-1} phosphate buffer pH 7; (C) Cyclic voltammograms of 1 mmol L^{-1} of catechol and respective blank and (D) SWV scans for catechol from 5 to 300 μmol L^{-1} in 0.1 mol L^{-1} $HClO_4$ (frequency: 50 Hz, amplitude: 50 mV, step: 5 mV); and (E) BIA with amperometric detection (E = +1.2 V) of dopamine in a stirred 0.1 mol L^{-1} $HClO_4$ solution: successive injections from 1 to 400 μmol L^{-1}.

Table 4 – Comparison of analytical characteristics between the the proposed 3D-printed-PLA electrode at the detection of catechol (CAT) and dopamine (DOP).

Electrode	**Technique**	**Analyte**	**LR / μmol L^{-1}**	**LOD / μmol L^{-1}**	**Ref.**
CPE-GNP	SWV	CAT	30 - 1000	0.031	(TASHKHOURIAN; DANESHI; NAMI-ANA, 2016)
PNC	SWV	CAT	0-0.7 / 0.7-15	0.0001	(ZEN; CHEN, 1998))
ERGO-GCE	DPV	CAT	10 - 100	0.004	(ROCHA et al., 2018)
CRGO-GCE	DPV	CAT	1 - 100	0.001	(ROCHA et al., 2018)
GCE	DPV	CAT	10 - 100	0.17	(ROCHA et al., 2018)
G-PLA	SWV	CAT	5 - 300	0.04	This work
MWCNT	BIA-AMP	DOP	0.1 - 1000	0.030	(CARDOSO et al., 2015)
ERGO-GCE	BIA-AMP	DOP	1 - 1000	0.030	(ROCHA et al., 2018)
CRGO-GCE	BIA-AMP	DOP	1 - 1000	0.055	(ROCHA et al., 2018)
GCE	BIA-AMP	DOP	1.0 – 1000	0.331	(ROCHA et al., 2018)
G-PLA	BIA-AMP	DOP	1 - 400	0.1	This work

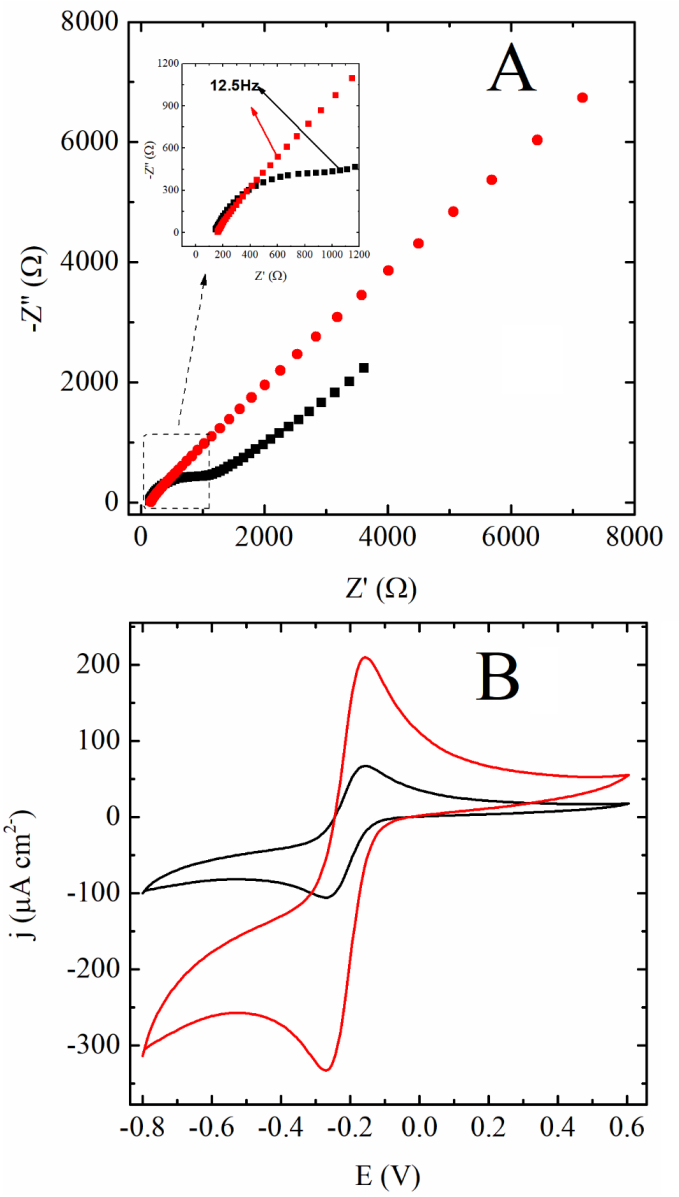

Figure 13 – (A) EIS spectra and (B) cyclic voltammograms (scan rate of 50 mV s^{-1}) obtained on the 3D-printed G-PLA electrode (black) and on bare GCE (red) in the presence of 1 mmol L^{-1} $Ru(NH_3)_6^{+3}$ in 0.1 mol L^{-1} KCl solution, in the frequency range between 0.1 Hz and 50.000 Hz with signal amplitude of 10 mV with 10 data points per frequency decade. Current density values were plotted in cyclic voltammograms for a better comparison.

results indicate that the GCE surface should provide a faster electron transfer of the redox molecule to the electrode surface in comparison with the 3D-printed sensor. Therefore, the improved electroanalytical sensing properties of the 3D-printed electrode is likely due to the surface effects of the 3D-printed G-PLA composite towards the electrochemistry of the phenolic compounds evaluated in this work. To confirm this hypothesis, IR spectroscopy measurements of the G-PLA printed surface (Figure 14 and Table 5) were obtained.

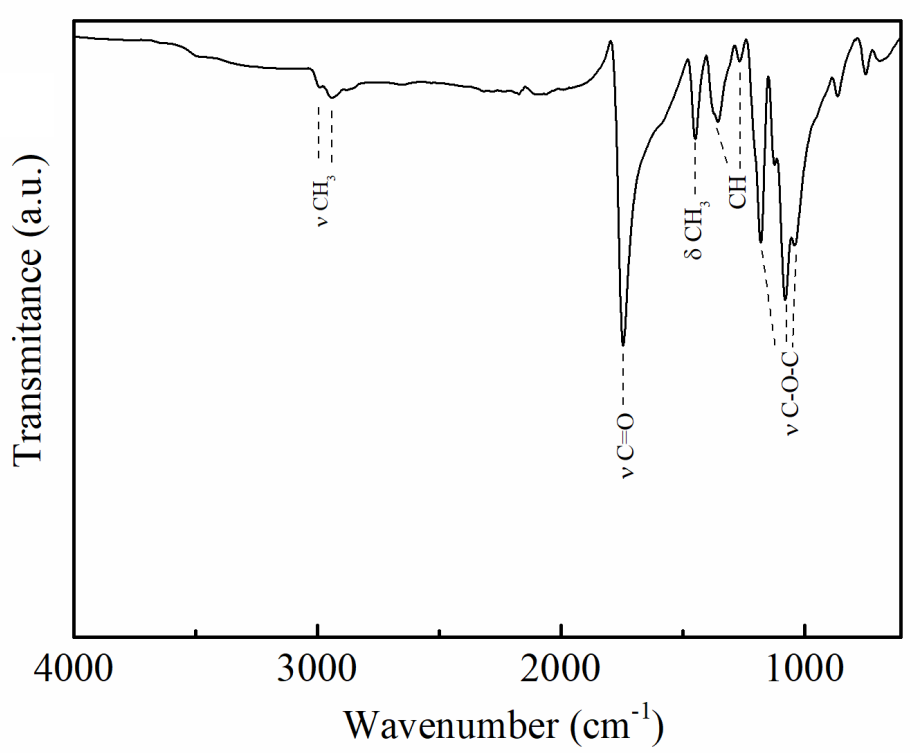

Figure 14 – Infrared spectrum (ATR mode) of 3D-printed G-PLA surface.

Table 5 – Attributions of the infrared spectrum (ATR mode) of 3D-printed G-PLA surface.

Wavenumber (cm^{-1})	**Attribution**
2998 – 2932	CH_3 antisymmetric and symmetric stretching
1746	C=O stretching
1446	CH_3 antisymmetric bending
1385 – 1352	CH deformation and symmetric bending
1179	C-O-C stretching
1079	C-O-C stretching
1039	C-O-C stretching
866	Amorphous phase
752	Crystalline phase

The IR spectrum presented antisymmetric (2998 cm^{-1}) and symmetric (2932 cm^{-1}) CH_3 stretching vibrations related to the polymeric matrix. The presence of the bands at 1746 and 1179 cm^{-1}, corresponding to C=O vibration and C-O-C stretching, respectively, reveal the presence of oxygenated groups at the sensor interface due to the PLA matrix. Intense bands between 1079 and 1039 cm^{-1} also indicate the C-O-C stretching, related to PLA structure (WANG; RHIM; HONG, 2016). Oxygenated functional groups, especially carboxylic group, identified at the 3D-printed conductive G-PLA surface may be responsible for the facilitated electrochemistry of catecholamine molecules as previously described in the literature (CREVILLEN et al., 2009) and may explain the improved response to catechol and dopamine in comparison with bare GCE and the comparable sensing performance with other nanocarbon-based electrodes, such as rGO and MWCNT, as highlighted in Table 4

Next, the presence of graphene in the 3D-printed electrode was confirmed by Raman spectroscopy and SEM. The spectrum for the electrode in Figure 15.A reveals the presence of D (1356 cm^{-1}), G (1586 cm^{-1}), D' (1623 cm^{-1}) and 2D (2700 cm^{-1}) bands. The observed intense D band can be associated with the presence of defects, such as edges, heteroatoms, vacancies, grain boundaries, and sp^3 type hybridization. The D' band is also associated with defects and the I(D)/I(D') intensity ratio can be used to probe the nature of the defect (ECKMANN et al., 2012). For the 3D-printed G-PLA electrode the calculated value of 3.22 indicates that boundary-like defects are present in majority in the carbon material. The G band is attributed to the presence of sp^2 carbon and 2D signal is related with two-dimensional order in the graphene plane. Therefore, Raman data indicates the presence of graphene nanoribbons (GNRs) in the electrode (ECKMANN et al., 2012). This result is confirmed by SEM image presented in Figure 15.B, showing the GNRs dispersed along the PLA polymer matrix. The I(D)/I(D') ratio of 3.22 is higher than values presented for rGO-based sensor (from 1.73 to 1.38) (ROCHA et al., 2018) and MWCNT-modified electrodes (from 2.52 to 1.38) (CARDOSO et al., 2015; STEFANO et al., 2017), which indicates a higher degree of defects of the carbon material within the 3D-printed G-PLA electrode.

The total cost of the multiuse cell is around $ 6.00 and takes 6 h for 3D-printing production, while 16 sensor strips (1 x 2 cm each one) are printed in 10 min at a cost of $ 1.00 each strip (disposable electrodes). The FDM 3D-printing technology can provide large-scale production and reproducible electrochemical cells and electrodes at a reduced cost in comparison to other strategies reported in the literature (CHEN et al., 2016; GROSS et al., 2014; WAHEED et al., 2016), especially considering the low-cost of a FDM 3D-printer (around $120.00) and that can be produced anywhere. Importantly, there are many open sources FDM printers available and thus this technique reached an affordable level, being used for household or laboratory prototyping applications. Therefore, the design and construction of inexpensive lab-made devices, including the electrochemical

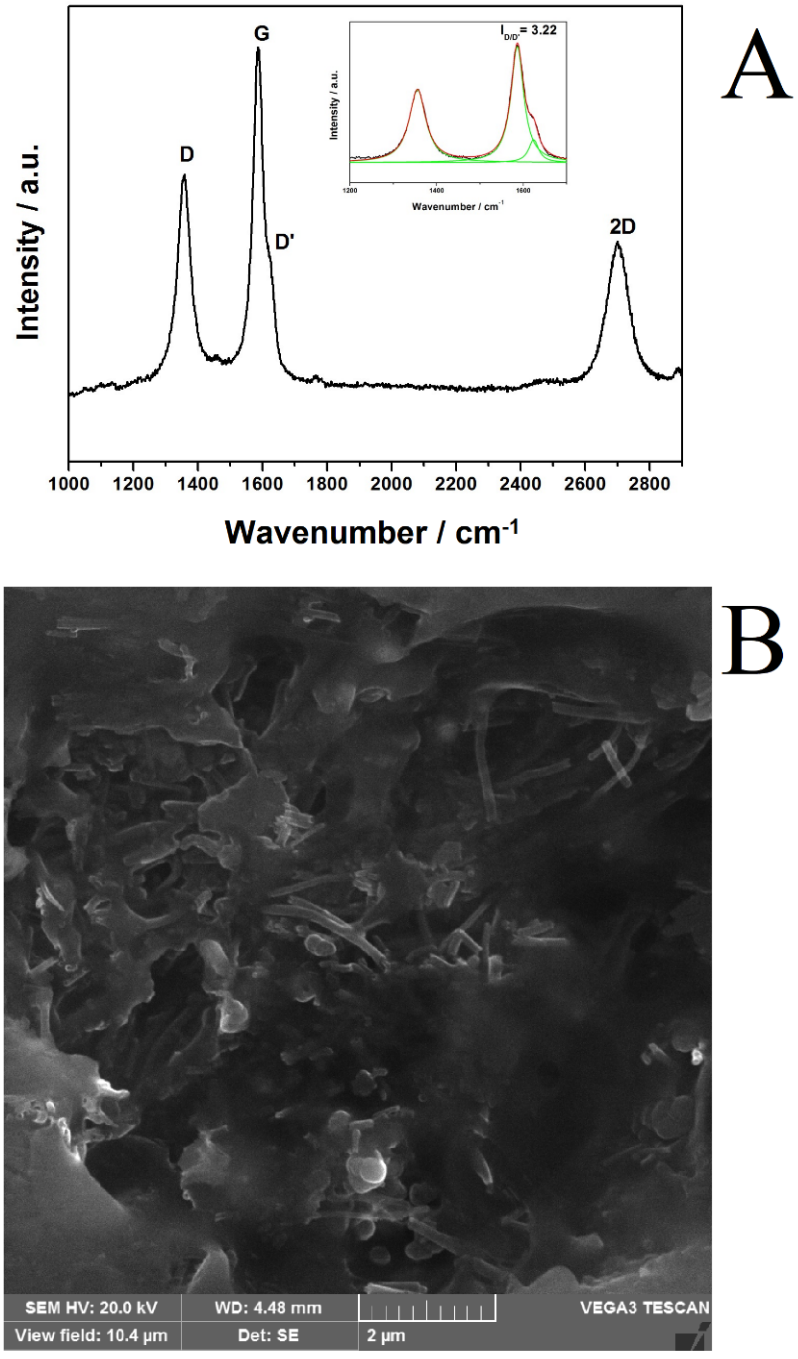

Figure 15 – (A) Raman spectrum and (B) SEM image of 3D-printed G-doped PLA electrode. Inset in A: Lorentz deconvolution of D, G and D' bands.

cells and sensors presented in this work, can be accessed using homemade FDM 3D-printers and the respective prototypes obtained through file sharing between laboratories worldwide.

2.4 Conclusions

This work demonstrates how the 3D-printing technology can be used to produce electrochemical cells and sensors for applications using quiet solutions or flow analysis (FIA and BIA systems) for voltammetric or amperometric measurements. A simple protocol to build a multiuse 3D-printed cell using ABS filament to operation under stationary or hydrodynamic conditions using different electrodes was presented. Using a PLA filament containing graphene, electrochemical sensors were 3D-printed, with attractive electroanalytical properties demonstrated for the analysis of phenolic compounds, such as dopamine and catechol. The performance of the 3D-printed sensor was superior in comparison with a bare GCE and comparable to modified electrodes with rGO or CNTs. Although the electrochemical characterization of the 3D-printed G-PLA sensor showed lower electron transfer kinetics than a bare GCE (based on k0 and IES data), the superior performance of this novel sensor for dopamine and catechol may be explained by the oxygenated functional groups presented at the G-PLA surface that play key role on the electrochemistry of phenolic compounds. Such an oxygen-rich surface offers great promise for other applications, such as trace metal determination. Another important feature of such 3D-printed sensors and cells is the total cost of production (lower than $4.00).

Considering that 3D-printers can be built using the 3D-printing technology, the expansion of 3D-printers for several applications, including research and education laboratories worldwide, can make possible the obtaining of electrodes and cells for education purposes as well as for routine applications and on-site analyses. Future effort to address a simple strategy to produce a single unit containing the three-electrode system or/and flow cells containing such three-electrode systems in large-scale using the 3D-printing technology is under investigation.

2.5 Acknowledgements

The authors are grateful to CNPq (478081/2010-3, 305227/2010-6, and 307271/2017-0), FAPEMIG (01856-10, 01537-14, and 02118-15) and CAPES (23038.007073/2014-12) for financial support. INCTBio (CNPq 465389/2014-7) is kindly acknowledged for the grant. The authors also would like to thank Multiuser Laboratory of Chemistry Institute at the Universidade Federal de Uberlândia for assistance in obtaining SEM images (equipment acquired with FINEP grant) and to thank Multiuser Laboratory of the Institute of Physics at Federal University of Uberlândia for assistance in obtaining Raman data. This

study was financed in part by the Coordenação de Aperfeiçoamento de Pessoal de Nível Superior – Brasil (CAPES) – Finance Code 001

Chapter 3

3D-printed device combining sampling and detection of TNT

This Chapter contains an adaption of the recently published article entitled "3D-printed flexible device combining sampling and detection of explosives" by Rafael M. Cardoso, Sílvia V. F. Castro, Murilo N. T. Silva, Ana P. Limaa, Mário H. P. Santana, Edson Nossol, Rodrigo A. B. Silva, Eduardo M. Richter, Thiago R. L. C. Paixão, Rodrigo A. A. Muñoz available online

Graphical Abstract

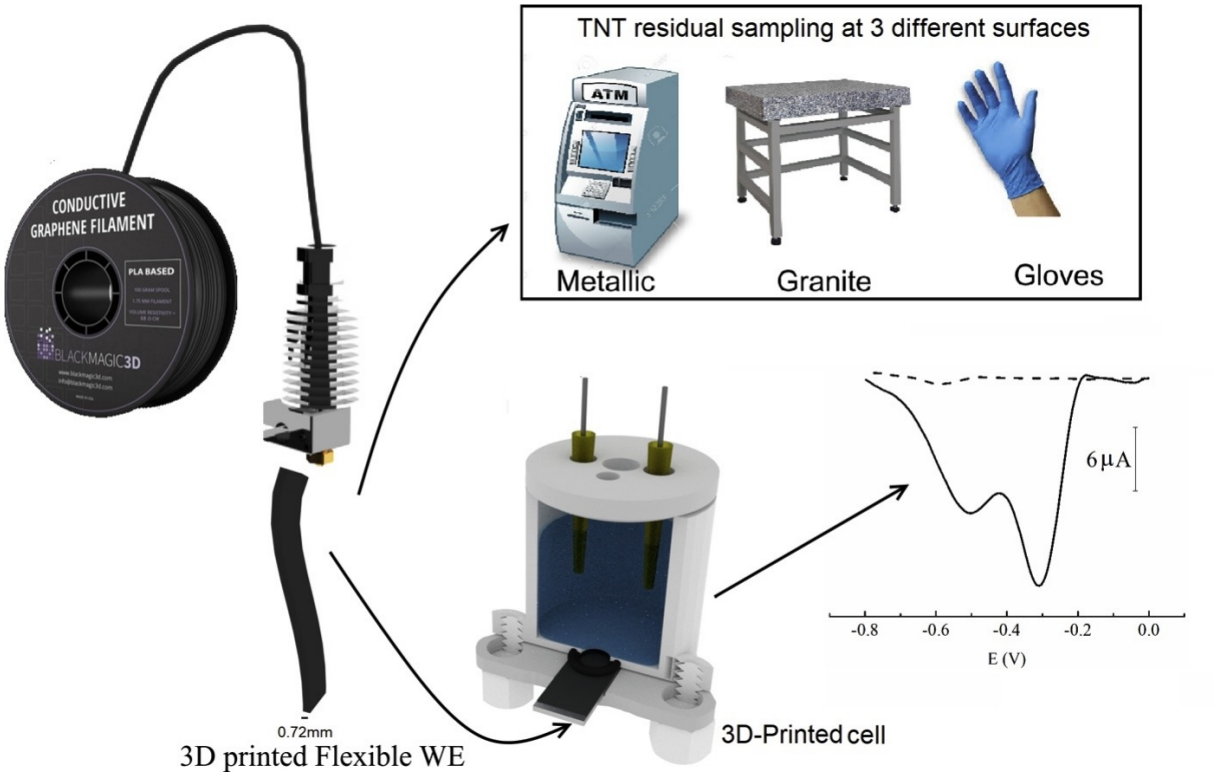

3.1 Introduction

The aim of this chapter is evaluate the applicability of G-PLA as a tool at sampling and detection the explosive more common in ATM's explosions in Brazil.

3.1.1 2,4,6-Trinitrotoluene

The 2,4,6-Trinitrotoluene is a nitroaromatic compound widely used in many areas such as military, mining and construction (building implosions). Unfortunately, due to its explosive characteristic, this compound is also used to harm people, or used in criminal activities. In a public security point of view, the detectability of this compound is very important to prevent global terrorism, especially if the method can be field-deployable. In Brazil, crimes like electronic bank terminals robberies by exploding it with TNT were frequently reported by the media in the past decade.

The detection of TNT or other explosives using electroanalytical methodologies has being explored due to the electroactivity of TNT. Different carbonaceous materials such as graphite sheet (CASTRO et al., 2019), glassy carbon modified with gold nanoparticles (SAGLAM et al., 2018), diamond electrodes (SANOIT et al., 2009) have been reported as working electrodes, but for the first time we propose a detection and sampling of TNT in simulated surfaces by a 3D-printed device.

3.2 Experimental

3.2.1 Reagents and solutions

All solutions were prepared with deionised water (resistivity not lower than 18 M cm) obtained from a Milli-Q water purification system (Millipore, Bedford, MA, USA) and analytical grade reagents. Hydrochloric acid (37% w/v) and nitrobenzene (98% w/w) were purchased from Synth (São Paulo, Brazil). Stock solutions (1000 mg L^{-1}) of lead and copper were purchased from Quimlab (Jacareí, Brazil). TNT, cyclotrimethylenetrinitramine (RDX), Hexahydro-1,3,5-trinitro-S-triazine (HMX) and entaerythritol tetranitrate (PETN) were provided by the military police of Minas Gerais (Brazil) with purities higher than 96% (w/w).

A mixture of *o*- and *p*-nitrotoluene and 2,4-dinitrotoluene were obtained according to the protocol described by Hermann et al. (HERMANN; GEBAUER; KONIECZNY,). The products of the reaction were characterised by ^{1}HNMR. The following reagents were used for the synthesis: benzene and nitrobenzene (98% m/m) from Synth (Diadema, Brazil), and toluene (99.5% m/m), sulfuric acid (95–97%, m/m), nitric acid (65%, m/m), sodium bicarbonate (99.0%, m/m), sodium sulfate (99.0%, m/m), ethyl acetate (99.5%, m/m), and *n*-hexane (95%, m/m) from Vetec (São Paulo, Brazil).

3.2.2 Instrumentation

Electrochemical measurements were carried out using a μ-AUTOLAB type III potentiostat/galvanostat (Metrohm Autolab B. V., Utrecht, Netherlands) interfaced to a microcomputer and controlled by NOVA 1.12 software. A 3D-printed cell with a three-electrode configuration was used for all electrochemical measurements. A platinum wire and a laboratory-made Ag/AgCl/KCl_{sat}. electrode were used as auxiliary and micro-reference electrodes, respectively.

Scanning electron microscopy (SEM) was performed with Vega 3-Tescan equipment at 20 kV to confirm the presence of graphene in the G-PLA printed material. Atomic force microscopy (AFM) images were obtained with a Shimadzu scanning probe microscope (SPM-9600) using the tapping mode to study the sample surface.

Fourier transformed infra red FT-IR spectra in attenuated total reflectance (ATR) mode were obtained using Frontier MIR/FIR PerkinElmer equipment using an ATR accessory from Pike Technologies. The X−ray Diffraction (XRD) pattern was obtained using ShimadzuXRD 6000 X-ray diffraction equipment with a Cu Kα radiation source (λ= 1.5406 Å).

3.2.3 Fabrication of G-PLA electrodes

Using an open-source Graber i3 RepRap 3D-printer ("Graber i3 - RepRap", [s.d.]), hollow cubes (4 cm × 4 cm) with wall thickness of 0.72 mm were printed using a conducting graphene-doped PLA (G-PLA) filament purchased from Black Magic3D-(New York, USA). All printing was performed using a 0.5 mm hotend nozzle and 220^{o}C heated bed temperature. 3D-printer parameters were set to 1 (0.6 mm, top) and 0 (bottom layer), and 0% of infill. Before use, the four sides of the hollow cube were polished for 30 s with abrasive paper (3 M 1200 Grit) with deionised water (for exposure of graphene). Other abrasive paper (600, 800 and 1500 Grit) were evaluated, applying the same polishing time. Then, pieces of planar substrate (2 × 3 cm) were cut and used as integrated collector and sensor. For comparison, the performance of the printed G-PLA was also evaluated without polishing. After use, the electrode could be cleaned by repeating the surface polishing.

3.2.4 TNT sampling and detection

TNT powder (10 mg) was spread randomly on granite or metallic surfaces and then spread by swiping with the own hands using gloves to impregnate TNT on the surfaces. The excess TNT powder was removed from the surfaces until no material was visible to the naked eye. Next, a 3D-printed device (2 × 3 cm) was used to perform abrasive sampling of the residual powder present on the different surfaces (granite, metal or gloves) by swiping the flexible device over the surfaces (a single swipe only). Before sampling,

the 3D-printed G-PLA electrodes were mechanically polished, as described previously, to expose the graphene. After collection, the device was inserted into the 3D-printed cell (up to 20 mL capacity) and 5 mL of supporting electrolyte was added to perform the SWV measurements. SWV operating conditions were 6 mV (step), 40 mV (amplitude), and 40 Hz (frequency). A solution of HCl (0.1 mol $L^{\breve{}1}$) was used as supporting electrolyte for TNT detection. SWV measurements were performed in the presence of dissolved oxygen.

3.2.5 Safety note

TNT powder is insensitive to shock or friction, which reduces the risk of accidental detonation. In this work, few milligrams of the explosive were safely handled to prepare stock solutions in acetonitrile.

3.2.6 Lead and copper detection

Simultaneous determination of Pb^{2+} and Cu^{2+} was performed in 0.1 mol $L^{\breve{}1}$ HCl (supporting electrolyte) by square-wave anodic stripping voltammetry (SWASV) after polishing of the 3D-printed electrode surface without any electrochemical or solvent pre-treatment. SWV operating conditions were 4 mV (step), 40 mV (amplitude), and 10 Hz (frequency); metal deposition occurred under stirring (250 rpm for 90 s) provided by a magnetic bar under the application of a voltage of –0.3 V. SWV measurements were performed in the presence of dissolved oxygen.

3.3 Results and Discussion

Previous works have demonstrated the presence of graphene nanoribbons in sensors printed with G-PLA filament by using SEM and Raman spectroscopy (CARDOSO et al., 2018). Palenzuela et al. reported the surface treatment of G-PLA by immersion in dimethylformamide (DMF) for 10 min to expose the graphene nanoribbons and improve the electrochemical performance of the material (MANZANARES-PALENZUELA et al., 2018). Dos Santos et al. reported an electrochemical treatment based on oxidation at +1.8 V *vs* Saturated calomel electrode(SCE) followed by reduction through cyclic voltammetric scanning between 0 and –1.8 V *vs.* SCE to improve the electrochemical response of the G-PLA electrode; faster electron transfer was verified and attributed to a higher density of defects and oxygenated groups (SANTOS et al., 2019). Herein, we propose a simpler, faster and greener manner to expose the graphene nanoribbons based on mechanical polishing for 30 s with 3M abrasive paper (1200 grit) wet with deionised water. Figure 16 shows SEM images (A) before and (B) after mechanical polishing of the surface, which clearly show the appearance of the graphene nanoribbons at the material surface.

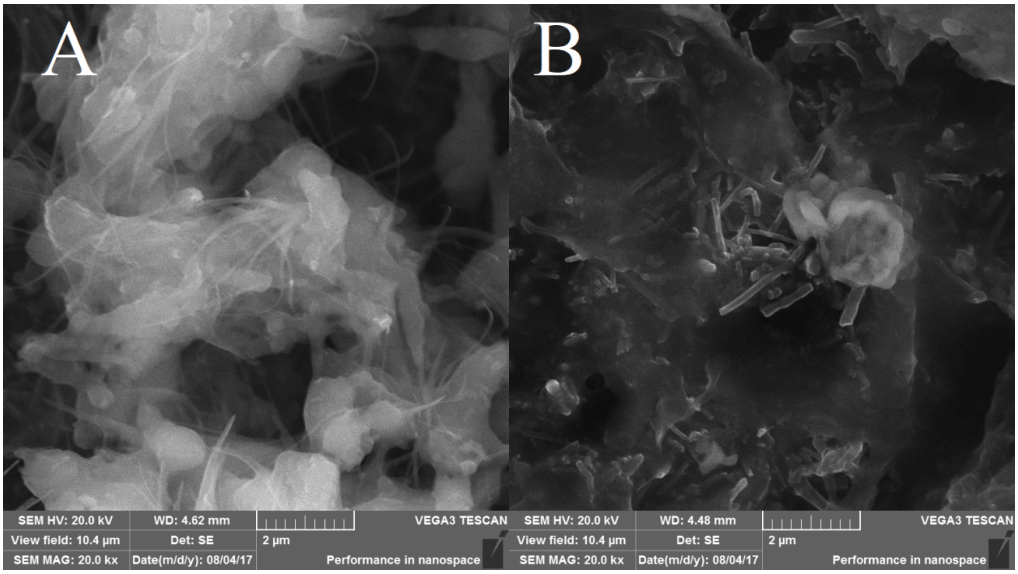

Figure 16 – SEM images of G-PLA: (A) before and (B) after mechanical polishing.

The IR spectrum of the 3D-printed G-PLA polished electrode Figure 17 shows a series of bands referring to stretching and deformation modes associated with the PLA matrix, as follows: 2995 and 2948 $^{-1}$, corresponding to CH_3 stretching vibrations; C=O vibration at 1745 cm^{-1}; C–H deformations at 1446 , 1353 and 1270 cm^{-1}; and C–O–C stretching at 1176 , 1073 and 1036 cm^{-1} (CARDOSO et al., 2018; CHIENG et al., 2014). The XRD patterns for the 3D-printed G-PLA polished electrode are shown in Figure 17.B. The diffractogram exhibits a broad peak from 10° to 25º attributed to the semi-crystalline PLA. It also shows a peak at 26º related to the graphitic (002) plane and associated with the structure of graphene (CHIENG et al., 2014; ZHAO et al., 2008).

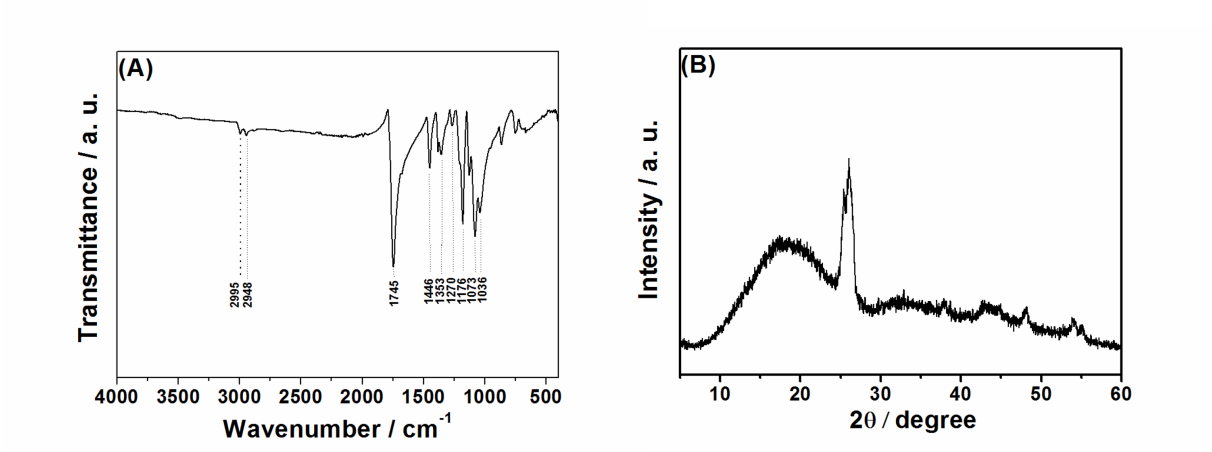

Figure 17 – (A) FT-IR spectra and (B) XRD patterns for the polished 3D-printed G-PLA.

In order to show the effect of mechanical polishing on the electrochemical response, Figure 18 presents the cyclic voltammograms recorded in 1 mmol L^{-1} catechol using the

G-PLA before (black line) and after (red line) the treatment. The respective blanks are also shown. The electrochemical profile obtained for the untreated G-PLA sensor shows sluggish electron transfer due to the low number of graphene nanoribbons available. On the other hand, the polished G-PLA sensor exhibits a similar response to that obtained by an unmodified glassy-carbon electrode (ROCHA et al., 2018) ($\Delta E = 400$ mV), which indicates a faster electron transfer. Abrasive papers of different grits were evaluated (600, 800, 1200 and 1500 grit). Figure 19 shows cyclic voltammograms for catechol on 3D-printed G-PLA electrodes after mechanical polishing using different papers for 30 s.

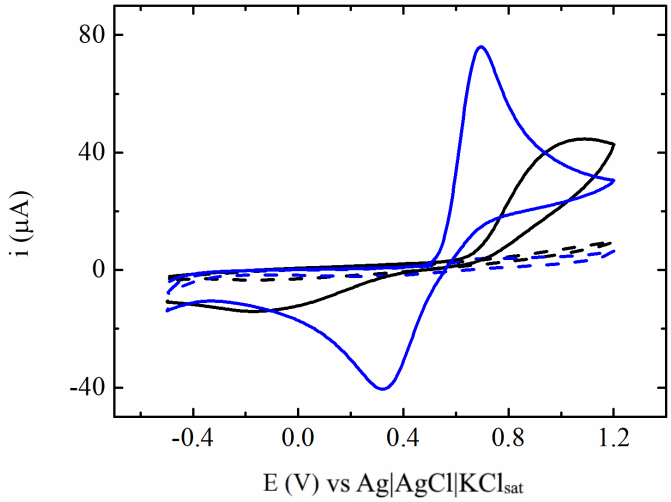

Figure 18 – Cyclic voltammograms of catechol 1 mmol L^{-1} (solid lines) and respective blank (0.1 mol L^{-1} HCl, dotted lines) on the 3D-printed G-PLA electrode before (black) and after (blue) mechanical polishing of the surface.

Each experiment was performed using a different 3D-printed G-PLA surface. Slightly higher current was verified for the 3D-printed G-PLA surface polished with 1200 grit, while lower currents were verified when the surface was polished with 600 and 800 grit papers. For this reason, 1200 and 1500 grit papers are recommended. Another point to be taken into consideration is the current variation between different surfaces (inter-electrode precision), which also contributes to the results observed in Figure 19. Hence, in this study, we selected 1200 grit paper for the further experiments. Inter-electrode precision, as well as other analytical characteristics of the proposed sensor, will be discussed further.

Next the 3D-printed G-PLA polished sensor was evaluated for TNT sensing. Figure 20 shows square-wave voltammograms for increasing concentrations of TNT (left) and the respective analytical curves (right). Inset are shown 10 overlapping SWV measurements, which were performed consecutively in the presence of 100 µmol L^{-1} TNT. SWV parameters and electrolyte were selected based on a previous investigation of TNT determination by a graphene-based sensor (CASTRO et al., 2018). The analytical characteristics of the proposed sensor are shown in Table 6.

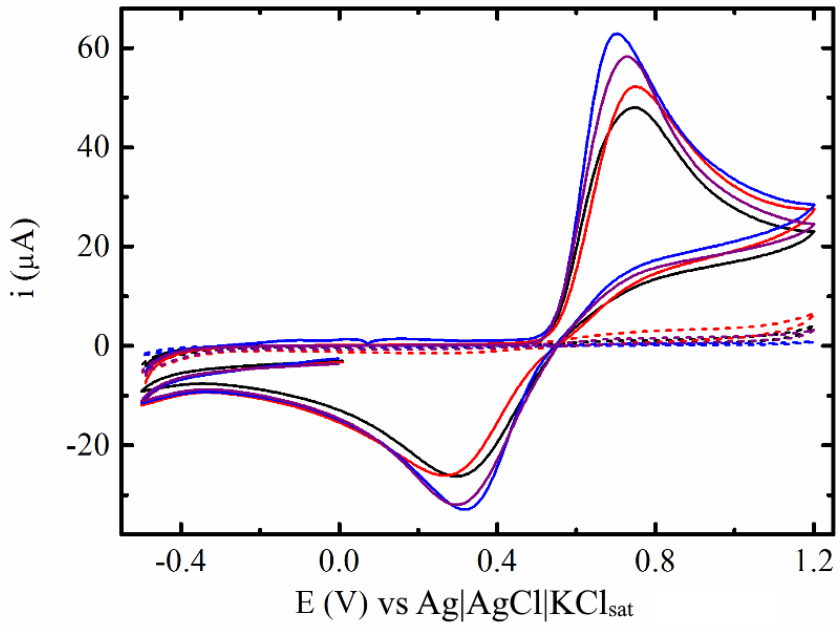

Figure 19 – Cyclic voltammograms on 3D-printed G-PLA electrode of blank solutions (dotted lines) and 1 mmol L^{-1} catechol after electrode surface polishing using different grit polishers: 600(black), 800 (red), 1200(purple) and 1500(blue). Electrolyte: 0.1 mol L^{-1} HCl, scan rate 50 mV s^{-1}, starting at 0.0 V.

Table 6 – Analytical characteristics of different G-PLA electrodes for TNT detection.

	Slope (μA V/μmol L^{-1})	**Linear range** (μmol L^{-1})	**LOD** (μmol L^{-1})	**R**	**ST**[a] (h^{-1})	**RSDintra**[b] (%)	**RSDinter**[c] (%)
G-PLA	0.0129	1.00 – 870	0.4	0.998	132	<1	8.9

[a] ST: sample troughputb / [b] RSD for n=10 / *c* RSD for n=3

The 3D-printed sensor presented satisfactory performance for TNT sensing. Each SWV scanning voltammetric detection took less than 30 s and the estimated sample throughput was calculated as 132 measurements per hour. A linear range from 1.00 to 870 µmol L^{-1} was obtained, with a detection limit estimated at 0.40 μmol L^{-1}. High precision and stable responses were obtained, as the RSD values (intra-electrode precision) were lower than 1.0% (n = 10). Analysing the response obtained using three different electrodes, the RSD value was 8.9% (inter-electrode precision for n = 3). These results indicate that the polished 3D-printed G-PLA sensor is an excellent candidate for TNT sensing. The analytical characteristics of the proposed sensor can be compared with those of conventional carbon disc electrodes modified with a reduced graphene oxide-multiwalled carbon nanotube electrode nanocomposite, which presented a LOD value of 0.019 μmol L^{-1} within a linear range of 0.500–1100 μmol L^{-1} (CASTRO et al., 2018); with hydrogenated graphene, resulting in LOD values of 1.8–2.2 μmol L^{-1} (SEAH et al., 2014); or with PtPd concave nanocubes anchored on graphene nanoribbon reaching an LOD of 0.0040 µmol L^{-1} with linear range of 0.040–13.2 μmol L^{-1}, after accumulation of

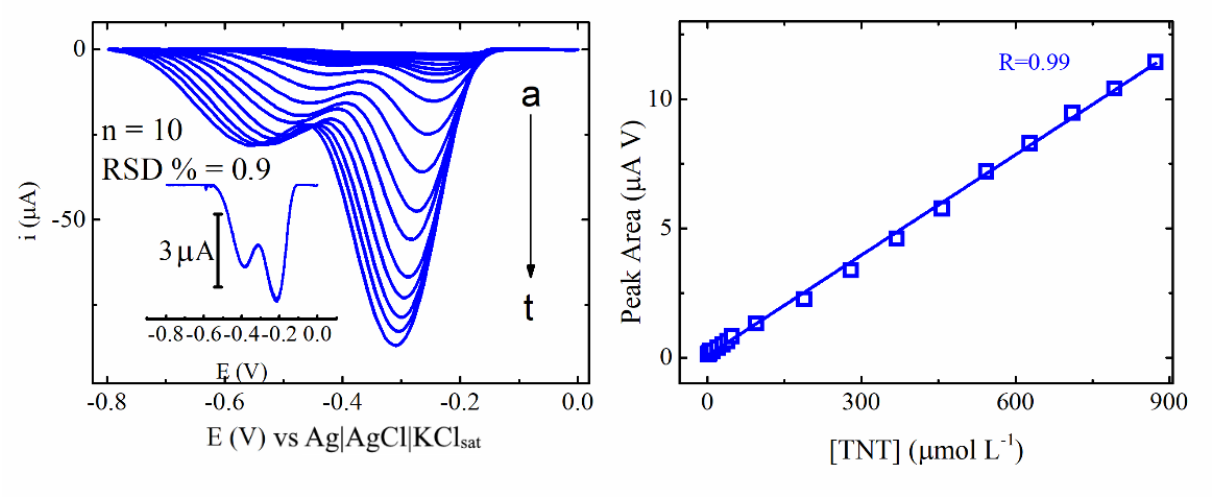

Figure 20 – (Left) Square-wave voltammograms of increasing concentration of TNT solutions: a) 1; b) 2; c) 3; d) 4; e) 5; f) 10; g) 20; h) 29; i) 38 j) 47; k) 95; l) 188; m) 279; n) 369; o) 457; p) 543; q) 628; r) 711; s) 792; t) 873 μmol L^{-1} recorded on polished G-PLA electrodes and (Right) the respective analytical curve. Inset (left): 10 successive measurements for 100 µmol L^{-1} of TNT. Conditions: Step: 6 mV; Amplitude: 40 mV; Frequency: 40 Hz; Electrolyte: 0.1 mol L^{-1} HCl.

TNT for 150 s before voltammetric measurement (ZHANG et al., 2015). All LOD values were obtained according to IUPAC.

Due to the additional flexible properties of the 3D-printed platform, the sensor was evaluated as a sampler of TNT residues found on different surfaces. Hence, the same 3D-printed device could be used for sampling and fast sensing of explosives. Three different 3D-printed G-PLA electrodes were mechanically polished and used for sampling TNT residues from metallic and granite surfaces and plastic gloves previously contaminated with TNT. Before the three surfaces were sampled by the 3D-printed G-PLA sensors, no TNT powder residue could be observed by the naked eye. Figure 21 presents the SWV measurements obtained for the three 3D-printed devices after TNT sampling over the different surfaces, which were assembled on the 3D-printed cell followed by electrolyte addition and scanning.

The G-PLA sensor detected TNT residues on all surfaces, as the SWV measurements presented the typical voltammetric profile of the explosive (similar to the profile shown in Figure 20). The metallic surface simulates a typical electronic bank terminal, a granite countertop can be found in manipulation laboratories, and gloves can contain TNT residues due to manipulation of the explosive. Therefore, a simple swipe by the 3D-printed device was efficient in sampling TNT residues from the different surfaces. The high surface roughness of the 3D-printed G-PLA device may contribute to the high efficiency in TNT sampling. AFM measurements of the G-PLA surface revealed the high rugosity of

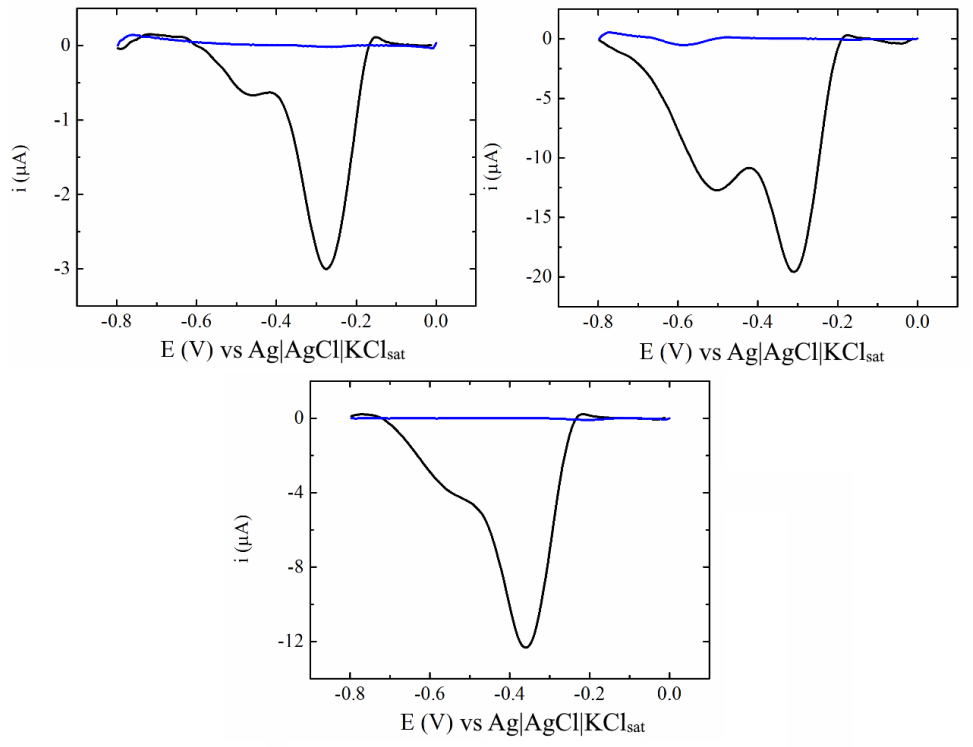

Figure 21 – Square-wave voltammograms (1st cycle) of residual TNT detection after swiping the 3D-printed sensor over (A) granite, (B) metallic and (C) glove surfaces (black). Blue lines correspond to blank experiments performed before TNT sampling. Conditions: Step 6 mV; Amplitude 40 mV; Frequency 40 Hz. Electrolyte 0.1 mol L^{-1} HCl.

the surface (Figure 22).

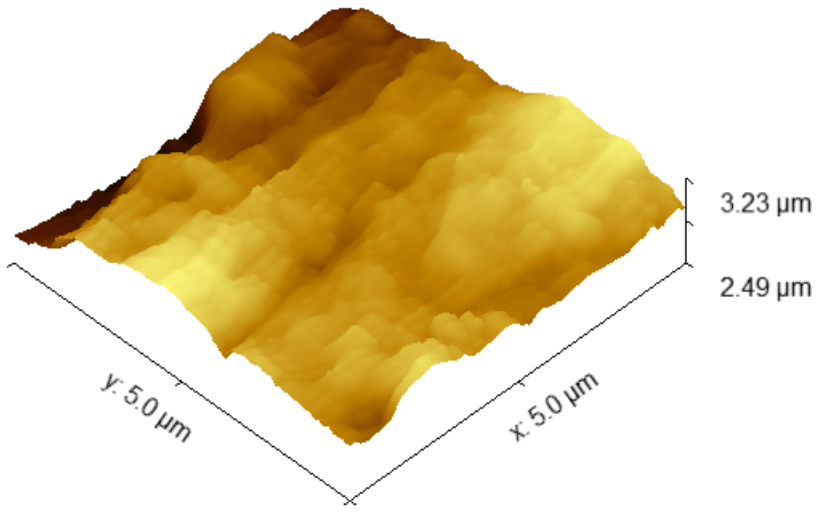

Figure 22 – Atomic force microscopy measurements of the 3D-printed G-PLA surface in 5.0 × 5.0 μm dimension (rugosity value of 112 nm).

For a comparison, the rugosity value obtained for a 5 µm × 5 µm area of the 3D-printed surface was 112 nm, which is higher than the value obtained (90 nm) for a glassy-carbon electrode modified with reduced graphene oxide dispersion (0.5 mg mL^{-1}) by dropcasting of a 20μL aliquot (ROCHA et al., 2018). The voltammetric response observed Figure 21 is due to the TNT particles abrasively immobilised on the G-PLA surface. Therefore, an external calibration curve or the standard addition method would not be the most accurate way to quantify TNT, as the voltammetric responses of TNT in standard solutions (Figure 21) is proportional to the diffusion-controlled transfer of TNT species to the G-PLA surface. In the case of sampling and scanning, the voltammetric response is related to the adsorbed TNT species on the G-PLA surface. The electroactivity of the sensor relies on the graphene nanoribbons distributed throughout active sensor area of the plastic matrix of the 3D-printed G-PLA. Once graphene nanoribbons are exposed on the surface, the electron transfer responsible for the electrochemical response of TNT is improved. The rough surface of the 3D-printed electrode is an additional feature of the device for the collection of trace explosives by simple swiping of the 3D-printed platform over different surfaces in crime scene scenarios. The concentration of TNT immobilised on the G-PLA sensor detected by SWV was estimated using the Faraday equation (m = MM * Q / 96,485.3329 * n), in which Q corresponds to the charge (area of the respective SWV recording), MM to the molecular weight, n to the number of electrons involved in the reduction (for TNT, n = 6), and m is the mass. The estimated mass of TNT detected on granite, metal and glove surfaces were 3.2, 20 and 15 ng, respectively, using the Faraday equation, highlighting the possibility of detecting small amounts of explosive by directly sampling with the proposed device. This novel approach enabled the determination of TNT amount immobilised on the electrode surface by the simple calculation of charge from the SWV recording. Other innovative features of using a 3D-printed material are its flexibility, light weight and roughness, which contribute to its successful use as a collector. Moreover, FDM printing is easily accessible due to the low cost of printers, and the resulting 3D-printed G-PLA device is low-cost, disposable, biodegradable and reproducible, which makes it very promising for the investigation of different crime scene scenarios.

Figure 23 shows a study of potentially interfering species: the nitroaromatic explosive 2,4-dinitrotoluene, which is the main impurity present in commercial TNT; a mixture of o- and p-nitrotoluene; and nitrobenzene (which may also be present as an impurity in commercial TNT). All potentially interfering species undergo a similar electrochemical reduction process (reduction of the nitro groups). The electrochemical reduction of 2,4-dinitrotoluene takes place at more negative potentials than the first electrochemical reduction of TNT and therefore did not interfere with TNT detection. The same is true for o- and p-nitrotoluene and nitrobenzene, which undergo electrochemical reduction at –0.5 V. Other nitro-explosives, such as RDX and HMX, did not present any voltammetric

Table 7 – Analytical characteristics for the detection of Pb(II) and Cu(II) on the 3D-printed G-PLA sensor.

Metals	Slope (μA L μg^{-1})	Linear range (μg L^{-1})	R	LOD (μg L^{-1})	ST[a] (h^{-1})
Pb(II)	0.00037	60-300	0.987	36.2	20
Cu(II)	0.00153	10-60	0.995	8.8	20

a ST: sample throughput or analytical frequency.

response under these conditions on the polished G-PLA sensor; hence, it can be assumed that they do not interfere with TNT detection.

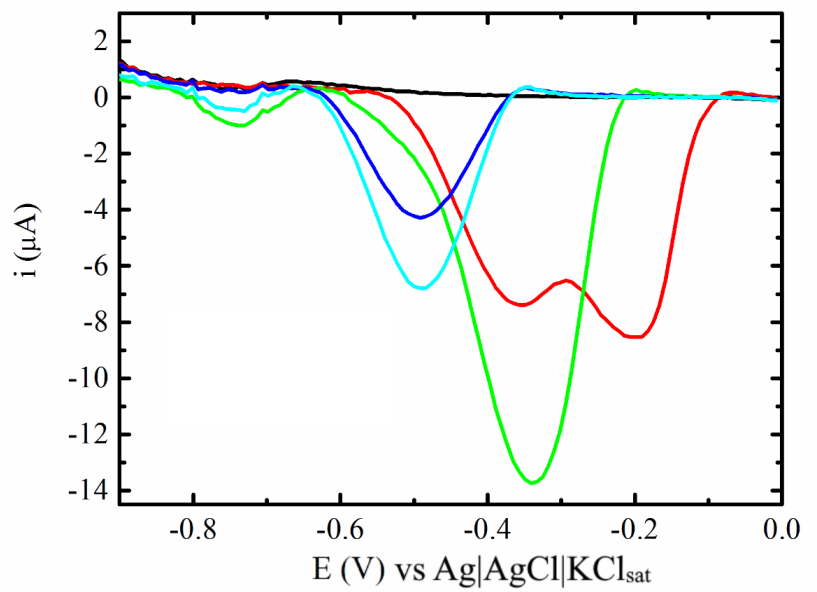

Figure 23 – Square-wave voltammograms of a blank solution (black) and in the presence of 100 µmol L^{-1} TNT (red), 2,4-dinitrotoluene (green), o-and p-nitrotoluene (dark blue) and nitrobenzene (light blue) recorded on polished G-PLA electrodes. Other conditions were similar to Figure 21

Another possible application of the 3D-printed G-PLA sensor is metal detection using anodic stripping voltammetry, which can be extended to the analysis of gunshot residues on hands or gloves. Figure 24 shows SWASV recordings for increasing concentrations of Cu(II) and Pb(II) obtained by a treated G-PLA sensor. Table 7 summarises the analytical characteristics of the 3D-printed G-PLA sensor for the detection of Pb(II) and Cu(II). This preliminary result indicates the feasibility of the 3D-printed G-PLA sensor for metal determination, which needs further investigation for the analysis of gunshot residues.

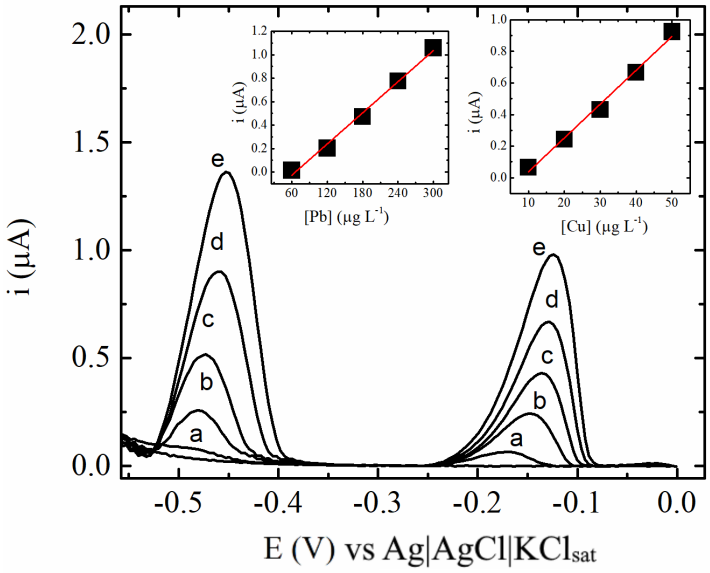

Figure 24 – Square-wave anodic stripping voltammograms of standard solutions of Pb(II) (a: 60, b: 120, c: 180, d: 240, e: 300 μg L^{-1}) and Cu(II) (a: 10, b: 20, c: 30, d: 40, e: 50 μg L^{-1}) on G-PLA electrode. Step: 4 mV; Amplitude: 40 mV; Frequency: 10 Hz; Deposition time: 90 s; Electrolyte: 0.1 mol L^{-1} HCl.

3.4 Conclusions

We have demonstrated the versatile application of 3D-printed flexible devices for the sampling and sensing of explosive residues. Improved electrochemical performance was verified after mechanical polishing of the G-PLA surface for 30 s, which was able to expose the graphene nanoribbons that act as an active surface carbon-based substrate. The sensor was sensitive to TNT detection using standard solutions, as well as for sampling and detection of small amounts of TNT powder residue found on different surfaces (granite, metal and glove surfaces). The flexible G-PLA device enabled TNT sampling by simply swiping the sensor on the different surfaces. The unique voltammetric profile of the 3D-printed G-PLA sensor towards TNT sensing makes possible the identification of TNT in the presence of other nitroaromatic species as well as other nitro-explosives. For the first time, an FDM 3D-printed graphene-based sensor was demonstrated to identify and estimate quantities of the explosive on simulated surfaces using the peak profiles and total transfer charge of the analyte concerned. The same G-PLA sensor was sensitive to Pb(II) and Cu(II) using SWASV, which offers great promise for metal detection in gunshot residues using a similar approach. Hence, 3D-printed G-PLA devices are a novel platform for the sampling and sensing of different species of forensic interest.

3.5 Acknowledgements

The authors are grateful to CNPq (478081/2010–3, 305227/2010–6, and 308174/2013–5), FAPEMIG (01856–10, 01537–14, and 02118–15), FAPESP (2017/10522–5), CAPES (CAPES Pró-Forense 25/2014 23038.007073/2014–12 and CAPES 001), INCTBio (CNPq grant no. 465389/2014–7) for financial support, and to the Multiuser Laboratory of the Chemistry Institute at the Universidade Federal de Uberlândia, supported by FINEP, for providing the equipment and technical support for material characterisation.This study was financed in part by the Coordenação de Aperfeiçoamento de Pessoal de Nível Superior – Brasil (CAPES) – Finance Code 001

Chapter 4

Biosensing of glucose in blood plasma and uric acid and nitrite in saliva and urine

This Chapter contains an adaption of the recently published article entitled " 3D-Printed graphene/polylactic acid electrode for bioanalysis: Biosensing of glucose and simultaneous determination of uric acid and nitrite in biological fluids" by Rafael M. Cardoso, Pablo R. L. Silva, Ana P. Lima, Diego P. Rocha, Thiago C. Oliveira, Thiago M. do Prado, Elson L. Fava, Orlando Fatibello-Filho, Eduardo M. Richter, Rodrigo A. A. Muñoz available online.

Graphical Abstract

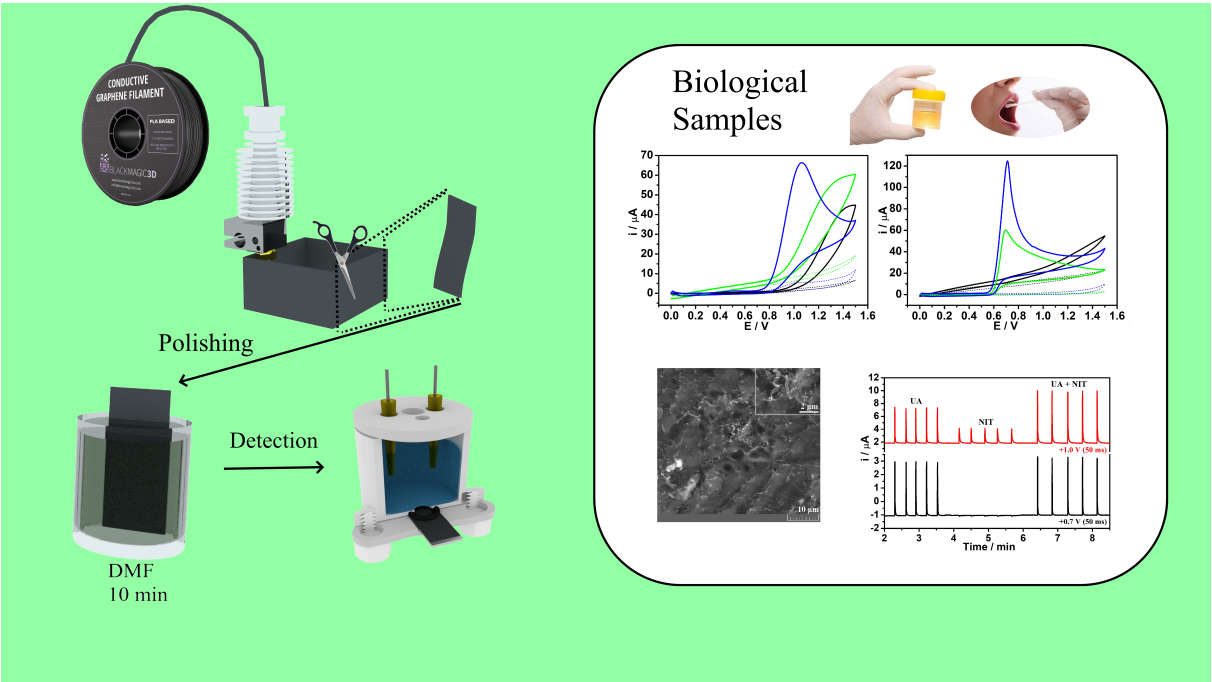

4.1 Introduction

Electroanalytical sensors are commonly reported in the medical and clinical area and the aim of this chapter is to propose and discuss the use of 3D-printed electrode at amperometric detection of activated G-PLA, and modified bio-sensor for glucose monitoring.

4.1.1 Detection of NIT and UA

Inorganic nitrate in the organism are formed by Nitrate-Nitrite-Nitric Oxide pathway, and is an important metabolite and its variations can indicate numerous diseases, such as obesity (CAETANO et al., 2018). This component can act as a modulator of heart diseases or metabolite dysfunction (BRYAN et al., 2005; MONTI et al., 2003; ROBERTS et al., 2015). Its electroactivity is evidenced and there are several methods of detecting nitrite using electrochemical sensors (CAETANO et al., 2018; HU et al., 2012; METTERS; KADARA; BANKS, 2012).

Other important organism metabolite is the uric acid, which is the final product of purine metabolism (GAO et al., 2019). Although uric acid plays an important role as an anti-oxidant in human body, high levels of this component in our system can lead to urates formation duo to the purine pathway. Thus, an imbalance of this compound in our organism represents a pathological scenario (STOZHKO et al., 2018) thus new methodologies to detect this analyte should be improved. The standard screening tests for uric acid can be a non-enzymatic and an enzymatic method, and both are based on spectrophotometric (UV region) methods after some sample treatment (GUO, 2016). These steps can lead to time consumption methods, and electroanalytical methods to directly detect uric acid is very recurrent in with the utilization of carbon electrodes (LUO et al., 2012) or modified (MADHUVILAKKU et al., 2020; TASHKHOURIAN; DANESHI; NAMI-ANA, 2016; ZEN; CHEN, 1997).

4.1.2 Glucose biosensing

Glucose sensing is widely important in applications from biological samples to the food chain industry. In the medical area for instance, an early detection of high levels of glucose can prevent the further complications in a diabetic patient. That necessity of fast response brings up the convenience of having a point of care sensor. There are many transducers for glucose detection, thus the electrochemical based methods are dominant in the market (NEWMAN; TURNER, 2005) in which blood samples are the main target.

Between different types of electroanalytical glucose sensors, the ones using Glucose oxidase (GOx) immobilized on an electrode surface are widely reported (DIAS et al., 2016; FIORITO; BRETT; Córdoba De Torresi, 2006; KATIC et al., 2019; LIU; JU, 2003). Further reports show GOx immobilized amperometric biosensors that work by

monitoring the electrons during the oxidation process of the enzyme substrate (glucose), in a reversible process through a mediator and converted to analytical data. Figure 25 shows an example of a glucose electrochemical sensor.

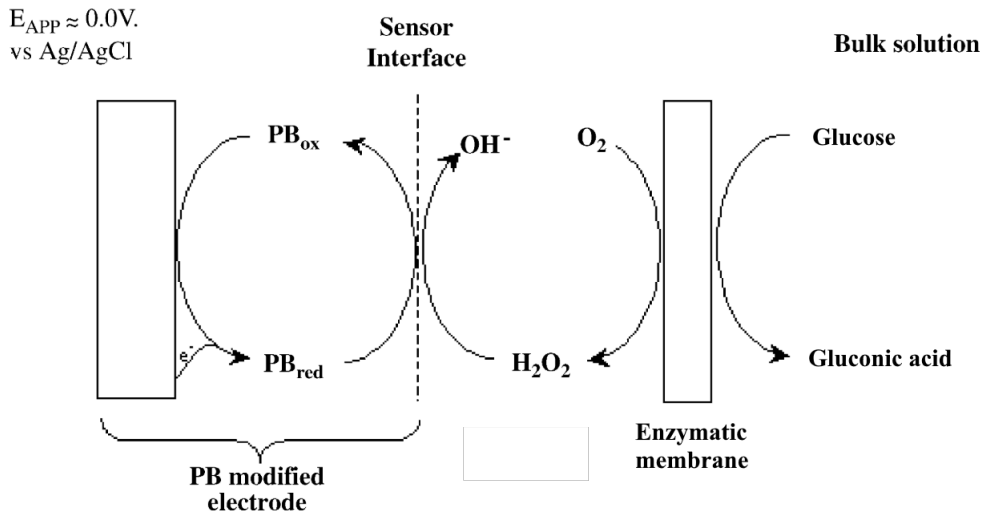

Figure 25 – Shows an example of a glucose electrochemical sensor using the classic Prussian Blue (PB) as mediator. Adapted with authorization from the literature (RICCI; PALLESCHI, 2005).

In this context, this chapter describes the use of 3D-printed G-PLA electrodes for bioanalytical applications. First, the simultaneous determination of uric acid and nitrite using multiple-pulse amperometric detection is demonstrated and applied for the analysis of saliva and urine. Second, a glucose biosensor was fabricated on the 3D-printed G-PLA platform immobilizing the GOx enzyme with the aid of glutaraldehyde on the G-PLA surface. The enzymatic biosensor was applied for the amperometric determination of glucose in blood plasma using chronoamperometry.

4.2 Experimental

4.2.1 Chemicals and samples

Uric acid (99% m/m), sodium nitrite (99% m/m), ferrocenecarboxylic acid (97% m/m) (FCA), and glucose oxidase from Aspergillus niger type VII (GOx) with declared activity of 100,000 units g-1 were obtained from Sigma Aldrich (St. Louis, USA). Potassium hexacyanoferrate(II) trihydrate, potassium chloride, acetic acid (99.7% m/v) from Synth (Diadema, Brazil), phosphoric acid (85% m/v) from QM (Cotia, Brazil), boric acid (99.8% m/m) and sodium hydroxide (98% m/m) were obtained from Panreac (Barcelona, Spain). Acetic, phosphoric and boric acids were used for preparation of the Britton-

Robinson (BR) buffer solution at the final concentration of 0.1 mol L^{-1} with pH values adjusted with sodium hydroxide.

Deionized water with a resistivity not lower than 18.2 M cm obtained from a Milli Q water purification system (Millipore, Bedford, MA, USA) was used in the preparation of all solutions. A 0.1 mol L^{-1} phosphate buffer solution (pH 7.0) was used as supporting electrolyte for amperometric detection of glucose. The stock solutions of UA and NIT were freshly prepared just before the experiments by dilution in 0.1 mol L^{-1} BR buffer (pH 2.0), which was selected as supporting electrolyte for voltammetric determination of UA and NIT based on a previous report (CAETANO et al., 2018).

The glucose biosensor was applied for the glucose analysis in blood plasma from bovine (Sigma-Aldrich, St. Louis, USA). UA and NIT were determined in saliva and urine collected from healthy volunteers following recommended procedures described in the literature (CAETANO et al., 2018).

4.2.2 Electrochemical instrumentation and measurements

The electrochemical measurements were all performed using a μ-Autolab Type III (Metrohm Autolab, Utrecht, Netherlands). The MPA technique was controlled by GPES 4.8 software, chronoamperometry by NOVA 2.1.2 software, and cyclic voltammetry and by NOVA 1.11 software, which also were used for data acquisition and treatment.

A 10-mL cell for chronoamperometric and cyclic voltammetric experiments and a 70-mL BIA cell for amperometric experiments were constructed by FDM 3D-printing using ABS filament as described in the literature (CARDOSO et al., 2018). The 3D-printed working electrode is placed at the bottom of both printed cells on a rubber O-ring which prevents leaks and defines the geometric area of the electrode (ID = 5.28 mm; area = 0.22 cm^2). A platinum wire was used as counter electrode and a miniaturized $Ag/AgCl/KCl_{sat}$. as reference electrode (PEDROTTI; ANGNES; GUTZ, 1996). In both printed cells, the counter and reference electrodes were placed in holes on the cell cover. An Eppendorf electronic micropipette (Multipette$^{\circ}$ E3) was used for reproducible-volume injections in the BIA system. The tip of the electronic micropipette was reproducible positioned in a hole on the BIA cell cover (2 mm distant from the working electrode). This electronic micropipette controls precisely the injection volume (from 10 to 1000μL) and injection rate (from 16.5 to 370 μL s^{-1}). All electrochemical measurements were performed in the presence of dissolved oxygen and at room temperature (25±2 ^{o}C).

4.2.3 Fabrication and treatment of 3D-printed G-PLA electrodes

The 3D-working electrodes were printed using an open source Graber i3 RepRap 3D-printer ("Graber i3 - RepRap," n.d.) and a graphene/PLA filament purchased from Black Magic 3D-(New York, USA) (CARDOSO et al., 2018) with a direct drive extruder

equipped with a 0.8 mm nozzle, a 40 mm × 40 mm × 40 mm square hollow cube with 0.80 mm wall thickness was printed. Then, after polishing with sandpaper, pieces of 20 mm × 20 mm were cut from the hollow cube sides (width = 0.80 mm) and set to be the final electrochemical working electrode (disposable surfaces). The printed sensors were treated by polishing with sandpaper (1200 grit) wet with deionized water for 30 s (CARDOSO et al., 2020). Then, the same polished surface was immersed in DMF for 10 min as proposed by (MANZANARES-PALENZUELA et al., 2018). For control, the unpolished surface was also treated with DMF for 10 min by immersion.

4.2.3.1 Fabrication of the glucose biosensor using 3D-printed G-PLA electrodes

The glucose biosensor was constructed by drop casting on the treated 3D-printed electrode, over a delimited area of 0.22 cm^2 by a vinyl adhesive. Firstly, 20 μL of 300 U mL^{-1} GOx solution (prepared with phosphate buffer solution pH 7.0) was dropped over the transducer surface. Then, after 2 h, 20 μL of 0.25% v/v glutaraldehyde was added over the GOx layer. After 20 min, the electrode was washed with deionized water and was ready to use.

4.2.3.2 Characterization of G-PLA electrode

The scanning electron microscopic (SEM) images of the G-PLA surfaces were acquired using a Vega 3 LMU (TESCAN, Brno-Kohoutovice, Czech Republic) operated at 20 kV.

4.3 Results and Discussion

4.3.1 Amperometric biosensing of glucose

As a proof-of-concept, the development of a glucose biosensor over the 3D-printed G-PLA surface was investigated for the analysis of biological fluid samples. The evaluation of GOx immobilization over the 3D-printed electrode was performed by cyclic voltammetric experiments, with and without glucose in solution, as shown in Figure 26 , in 0.1 mol L^{-1} phosphate buffer solution pH 7.0, in the presence of the electrochemical probe, FCA.

The behavior of the device in the presence of glucose presents typical electrochemical response of a second-generation biosensor, which is represented in in two-steps in Figure 27 . In the first step, flavin adenine dinucleotide (FAD) (active centre of the enzyme) acting as an electron mediator for glucose oxidation to glucolactone and reduced flavin adenine dinucleotide (FADH2). For this, FAD was converted FADH2, catalysing glucose oxidation.

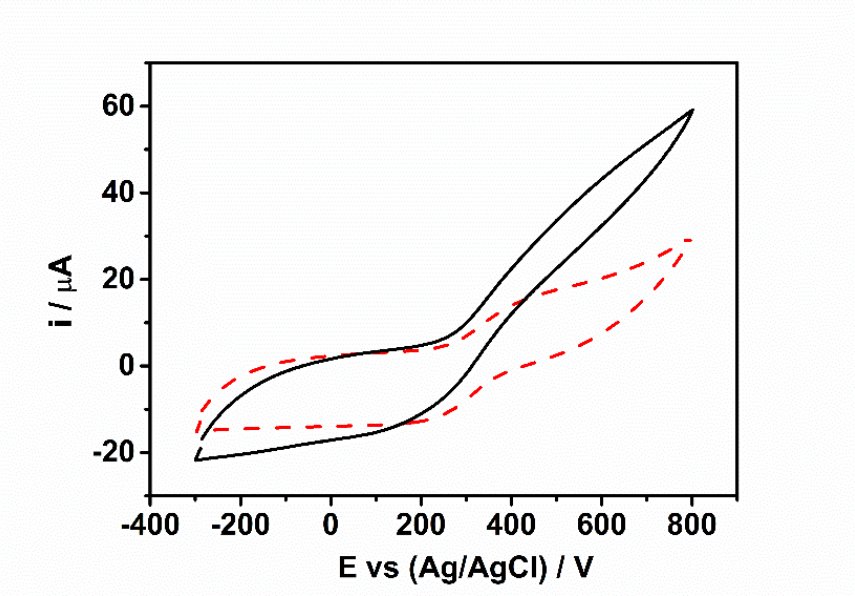

Figure 26 – Cyclic voltamogramms for solutions containing 1 mmol L^{-1} FCA in absence (red dashed line) and in the presence of 5 mmol L^{-1} glucose (black solid line). Supporting electrolyte: 0.1 mol L^{-1} phosphate buffer pH 7.0. Scan rate 50 mV s^{-1}.

Then, in the second step, the FADH2 was reverted again to FAD, and the electron involved in this oxidation was transferred to FCA, reducing Fe(III) to Fe(II)

The effect of pH on the electrode response was evaluated for different pH values (5.0, 6.0, 7.0 and 8.0) of a 0.1 mol L^{-1} phosphate solution. As can be seen in Figure 28 the highest current response of the 3D-printed biosensor in presence of glucose was obtained at pH 7.0, which was chosen in the further studies. Another important parameter studied was the enzyme concentration of the dispersion used in the electrode modification. The exposure of active sites is fundamental for the substrate catalysis. However, the excess of enzyme causes the presence of non-specific functional groups residues on electrode surface, resulting in steric impediment for the specific interactions with the substrate. On the other hand, the deficiency of enzyme on electrode surface limits the mediator action, decreasing the anodic current and the biosensor sensitivity. Figure 29 shows the results for different enzyme concentrations (2, 6, 10, 14 and 20 units per electrode), which shows the highest current obtained at 6 units per electrode. These results can be explained by the availability of oxygenated functional groups of the 3D-printed conductive G-PLA to cross-link with glutaraldehyde and GOx. (CARDOSO et al., 2018) demonstrated the predominance of carboxylic groups on G-PLA, which can be attributed to specific interactions with the cross-linking agent with high efficiency and, without the need for large amount of GOx. The glutaraldehyde, in turn establishes bonds with non-specific amino acids residues from the enzyme, increasing the exposure of FAD of active site for catalysis of substrate. The applied potential for the oxidation of FCA was also evaluated.

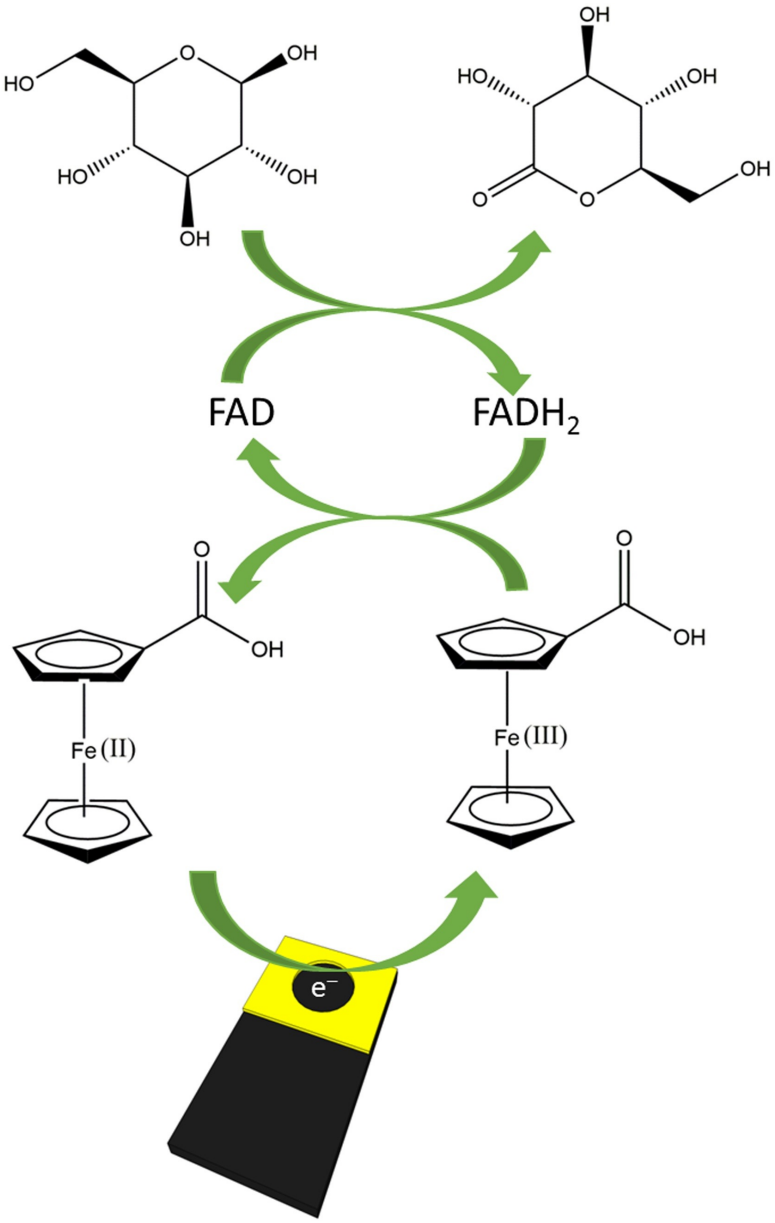

Figure 27 – Representation of the GOx biosensor in two steps to convert glucose into glucolactone mediated by FCA

Higher response was verified at +0.4 V (Figure 30) which was selected in order to provide the highest analytical response of the biosensor.

Figure 28, 29 and 30 show studies of pH, enzyme concentration and applied potential aiming to select the conditions which resulted in higher glucose responses.

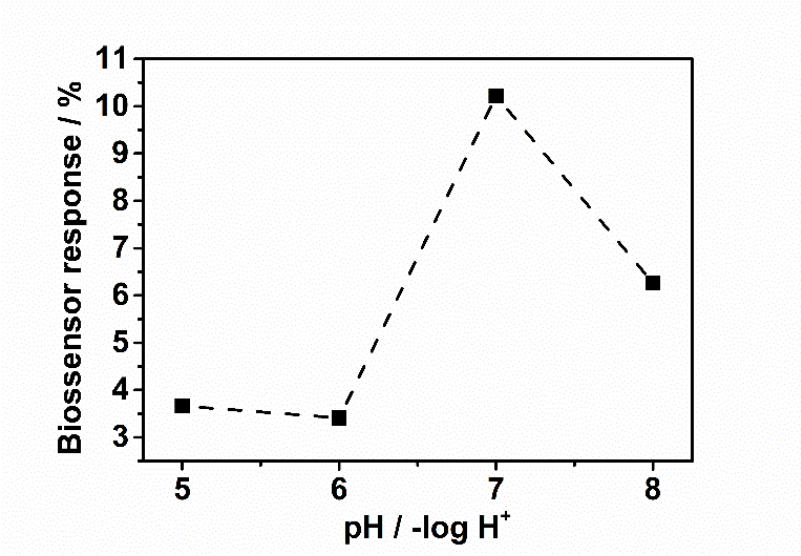

Figure 28 – Amperometric biosensor response as function of pH in 0.1 mol L^{-1} phosphate buffer, for 5 mmol L^{-1} glucose in presence of 1 mmol L^{-1} FCA.

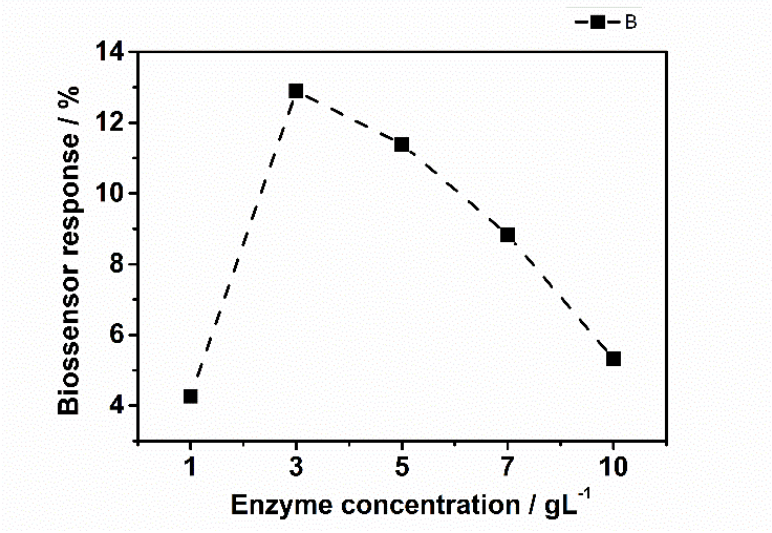

Figure 29 – Amperometric biosensor response for different enzyme concentration values (1.0, 3.0, 5.0, 7.0 and 10.0 mg m L^{-1}) used in electrode modification. Measures performed in 0.1 mol L^{-1} phosphate buffer pH 7.0, for 5 mmol L^{-1} glucose in presence of 1 mmol L^{-1} FCA.

The optimized biosensor was evaluated in the presence of increasing concentrations of glucose using chronoamperometric detection. Figure 31.A shows amperograms obtained

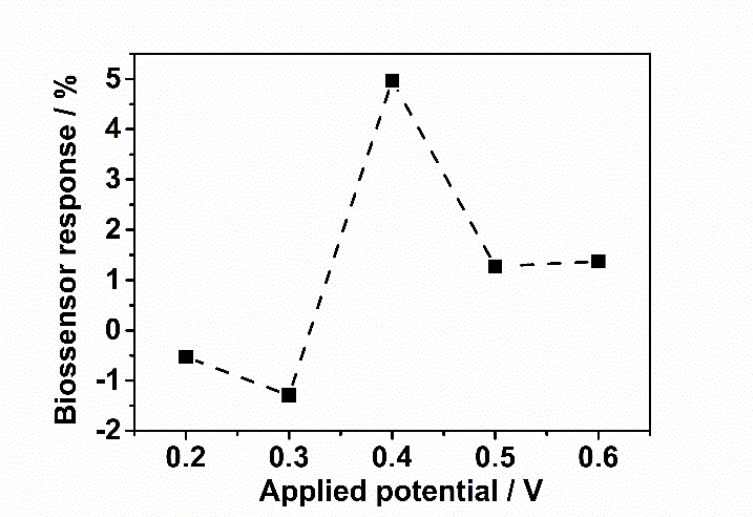

Figure 30 – Effect of different applied potential values (0.2, 0.3, 0.4, 0.5 and 0.6 V) on the amperometric biosensor response. Measurements performed in 0.1 mol L^{-1} phosphate buffer pH 7.0, for 5 mmol L^{-1} glucose in the presence of 1 mmol L^{-1} FCA.

at +0.4 V for increased concentrations of glucose and Figure 31.B shows the respective calibration curve presenting a linear relationship between glucose concentration and the limit current sampled at 60 s, represented by the equation, I(μA)= 0.80(±0.04) (μA) + 641(±1) (μA mmol L^{-1}) [glucose](mmol L^{-1}), R^2 = 0.998, with a limit of detection (LOD) of 15 μmol L^{-1}. The LOD was calculated by the 3S/slope, and S correspond to the standard deviation of 10 amperometric measurements performed in blank solution (FCA in supporting electrolyte, without glucose).

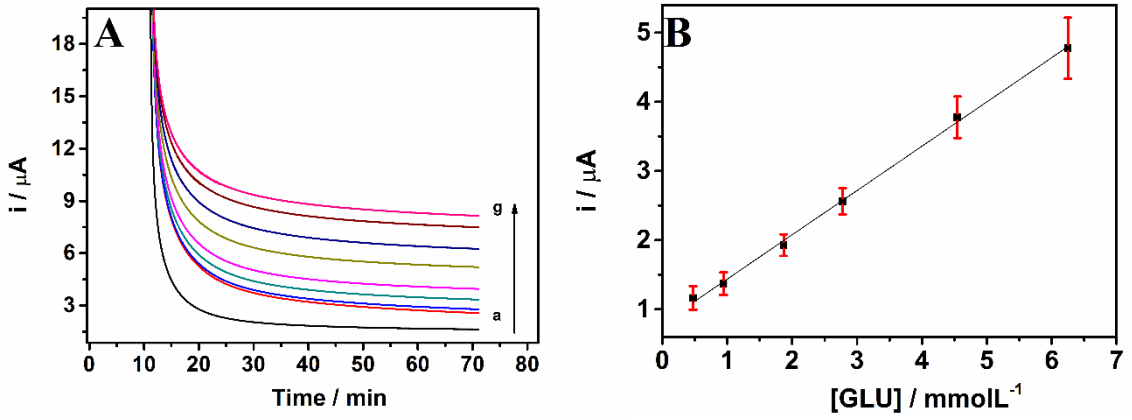

Figure 31 – (A) Amperometric curves obtained in the presence of: a) 0; b) 0.5; c) 1.0; d) 1.8; e) 2.8; f) 4.6 and g) 6.3 mmol L^{-1} glucose. (B) Linear regression obtained from glucose concentration versus limit current. Supporting electrolyte: 0.1 mol L^{-1} phosphate buffer (pH 7.0) with 1 mmol L^{-1} FCA. Error bars obtained from the standard deviation of 5 replicates for each glucose concentration.

The analytical performance for glucose detection was used as proof of concept for

the use of G-PLA as transducer for biosensor construction. Based on the comparison between the analytical parameters of this device and previewed published works, Table 8, it is possible infer that the 3D-printed G-PLA is a suitable material for the construction of sensing platforms based in biological materials. Although there are biosensors with better performance as can be seen in Table 8, the device constructed here has linear response and LOD applicable for the detection of glucose at levels commonly found in blood samples (i.e. from 4.0 mmol L^{-1} to 6.0 mmol L^{-1}) (WANG, 2008). In addition Table 8 compares the analytical characteristics of the 3D-printed G-PLA biosensor with glucose-oxidase (GOx)-based biosensors developed using other electrodic platforms reported in the literature.

Table 8 – Analytical characteristics of GOx based biosensors, including the proposed 3D-printed G-PLA biosensor.

Transducer	**Eletrochemical technique**	**Linear range (mmol L^{-1})**	**LOD (mmol L^{-1})**	**Ref.**
Au NEEs	CV	2.00 – 50.0	0.036	(CHEN et al., 2011)
SPCE	Amperometry	2.80 – 27.5	2.3	(HABTAMU; UGO, 2015)
GCE	Amperometry	2.00 – 16.0	2.0	(HUANG et al., 2018)
Au electrode	Amperometry	0.0020 – 6.66	0.0002	(LIN; WU; CHANG, 2019)
Au electrode	Amperometry	0.0020 – 3.00	7×10-5	(LIU, 1997)
Au electrode	CV	0.010 – 1.55	0.0022	(ZHANG et al., 2018))
3D-printed G-PLA electrode	Amperometry	0.50 – 6.30	0.015	**This work**

Au NEEs: gold nanoelectrodes ensembles; **CV**: cyclic voltammetry; **SPCE**: screen-printed carbon electrode; **GCE**: glassy carbon electrode.

The proposed 3D-printed G-PLA biosensor was applied for glucose determination in plasma from bovine before and after spiking with known amounts of glucose. The results are shown in Table 9 and acceptable recovery values were obtained (94-104%). The sensor was stable for 15 repetitive measurements.

Table 9 – Concentration of glucose in blood plasma sample obtained by the 3D-printed G-PLA biosensor before (1) and after (2-5) spiking with known concentration of glucose, and recovery values (n=3)

Experiments	**Spiked (mmol L^{-1})**	**Found (mmol L^{-1})**	**Recovery (%)**
1*	—	2.90 ± 0.07	—
2	6.3	8.82 ± 0.09	94
3	6.7	9.27 ± 0.09	95
4	7.2	7.79 ± 0.06	96
5	7.6	10.78 ± 0.05	104

*Pure blood plasma sample (not spiked).

Considering the presence of Na^+, K^+ and urea in blood plasma, their effects as potential interfering on biosensor response were tested. The variation of analytical signal for glucose detection presented a non-significative value of 0.3% in presence of both substances with concentrations 10 and 100 times greater than the target analyte. The precision of the biosensor was demonstrated by relative standard deviation (RSD) values of 5.0 mmol L^{-1} glucose detection, through experiments performed intra-day (n=5) and inter-day (n=10), with values of 3.7% and 4.2% being obtained, respectively.

The use of 3D-printed G-PLA as transducer presented attractive features, due to its good conductivity and the presence of oxygenated groups in the polymeric structure, which allowed the material modification via cross-link with a low amount of enzyme, resulting in high selectivity and stability for glucose detection as a proof-of-concept. Such results show great potential for the development of new biosensors using a 3D-printed G-PLA platform.

4.3.2 Voltammetric studies of UA and NIT

NIT and UA are relevant species in biological fluids, such as saliva and urine, and for this reason, they were selected as a proof-of-concept. The cyclic voltammetry of UA and NIT on the 3D-printed sensor reveals well-defined waves for NIT and UA (see Figure 32.6A and B, black lines). This result was expected based on recent papers that proposed the surface treatment of G-PLA 3D-printed sensors before electrochemical sensing either by mechanical polishing (CARDOSO et al., 2019) or by solvent immersion for 10 min (MANZANARES-PALENZUELA et al., 2018) to remove excess of PLA matrix. Therefore, the surfaces were treated by mechanical polishing for 30 s as new cyclic voltammograms were registered and presented in Figure 32(green lines). Moreover, the same polished G-PLA surfaces were submitted to immersion in DMF for 10 min (solvent treatment) and new cyclic voltammograms were recorded (Figure 32, blue lines).

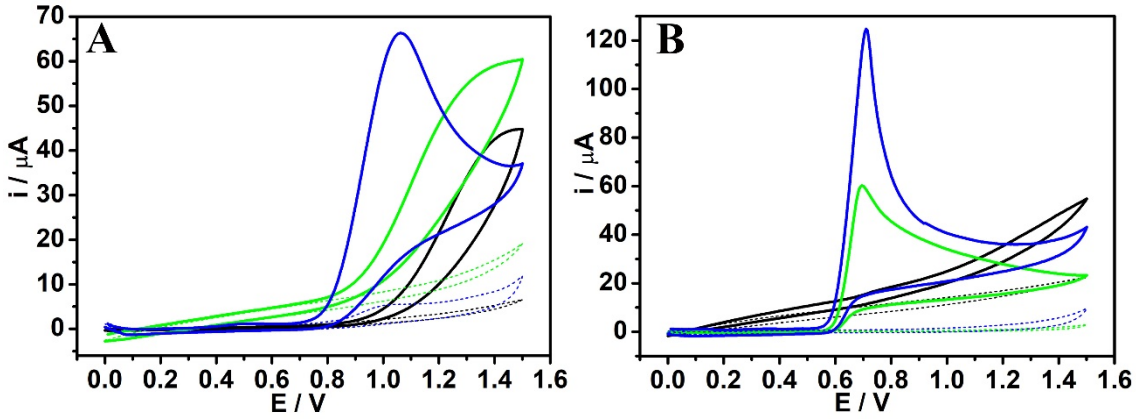

Figure 32 – Cyclic voltammograms for 1.0 mmol L^{-1} UA (A) and NIT (B) in 0.1 mol L^{-1} BR buffer pH 2 recorded on the 3D-printed G-PLA electrode (black), after mechanical polishing (green) and solvent-treated after polishing (blue). Dashed lines correspond to the respective blanks. Scan rate: 50 mV s^{-1}; step potential: 5 mV.

Figure 32 shows a well-defined peak for NIT at +1.1 V after both mechanical and solvent treatment. Both surface treatments improved the electrochemical properties of the sensor as the electrochemical oxidation of NIT was anticipated in comparison with untreated surface and after mechanical polishing. Figure 32.B shows well-defined peaks

for UA at +0.7 V on both treated G-PLA surfaces, with a higher (twice magnitude) current for the surface treated by mechanical polishing followed by solvent immersion. These results showed the positive effects of surface treatment of the 3D-printed sensor for the determination of both species. Therefore, the procedure involving mechanical polishing followed by solvent immersion was selected in further experiments. Aiming to understand the morphological changes of the surface after both treatments, Figure 33 presents the SEM images obtained for untreated and treated surfaces.

Figure 33 puts in evidence different levels of graphene nanoribbons exposure, which was previously confirmed using Raman spectroscopy (CARDOSO et al., 2018). The PLA matrix of untreated surface (Figure 33.A) overlaps the carbon structures preventing the sensor to actuate as expected, leading to low electron transfer and high resistivity. Once the treatment is performed with sandpaper (Figure 33.B) or solvent exposure after polishing (Figure 33.C), the graphene nanoribbons become more available to electron transfers, which increases the electrochemical performance of the 3D-printed electrode.

The normal concentration range of UA in blood is between 0.12 and 0.38 mmol L^{-1} while in urine this value should be lower than 4.50 mmol L^{-1} per day, otherwise excess of UA in urine may cause kidney stones (a disease called gout) (BALLESTA-CLAVER et al., 2011; ROSSINI et al., 2018). NIT concentration may change with the consumption of food rich in nitrate and nitrites (JAMES et al., 2015), but values higher than 1 mmol L^{-1} in urine may indicate urinary infection (SHIMONI et al., 2017). Considering normal concentration values of UA and NIT, the simultaneous determination of both species by MPA is proposed.

4.3.3 Amperometric determination of UA and NIT

The amperometric determination of UA and NIT was evaluated under flow conditions. For that, BIA was selected due to some advantages regarding cost, portability, speed and precision and the multiple-pulse amperometry (MPA) technique was selected as this technique enables the simultaneous of two or more analytes using a single working electrode (da Silva et al., 2011; FREITAS et al., 2016; GIMENES et al., 2013). First, the electrochemical behaviour of both target compounds was investigated under hydrodynamic conditions of the BIA-MPA system. Different potential pulses (from +0.4 to +1.3 V) were selected and continuously applied to the 3D-printed G-PLA working electrode positioned within the BIA cell in wall-jet configuration (BRETT; BRETT; MITOSERIU, 1995) and the current was monitored at each potential pulse. The hydrodynamic voltammograms shown in Figure 34.A (plots of average currents as a function of the applied potential pulse) were obtained separately for injection of solutions containing 10 μmol L⁻1 of UA or NIT.

As can be seen in Figure 34.A, the electrochemical oxidation of UA starts at approximately +0.55 V and NIT at around +0.85 V. These results allow us to conclude that

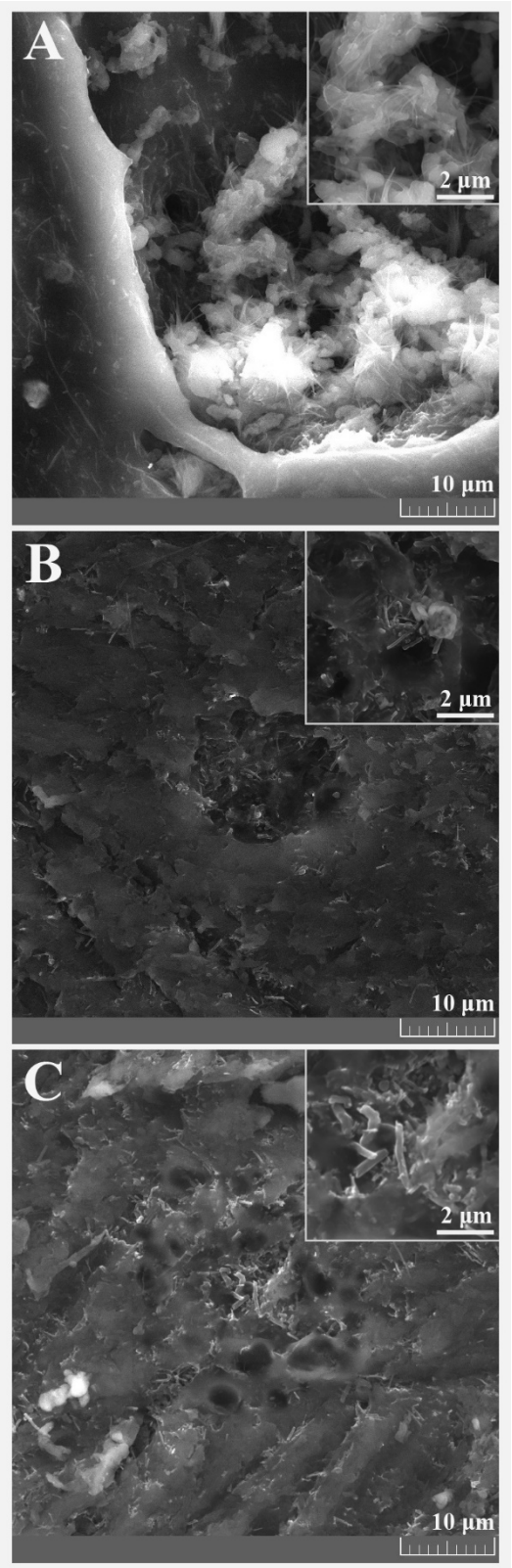

Figure 33 – SEM images of G-PLA surfaces: (A) untreated, (B) polished and (C) solvent treated after polishing.

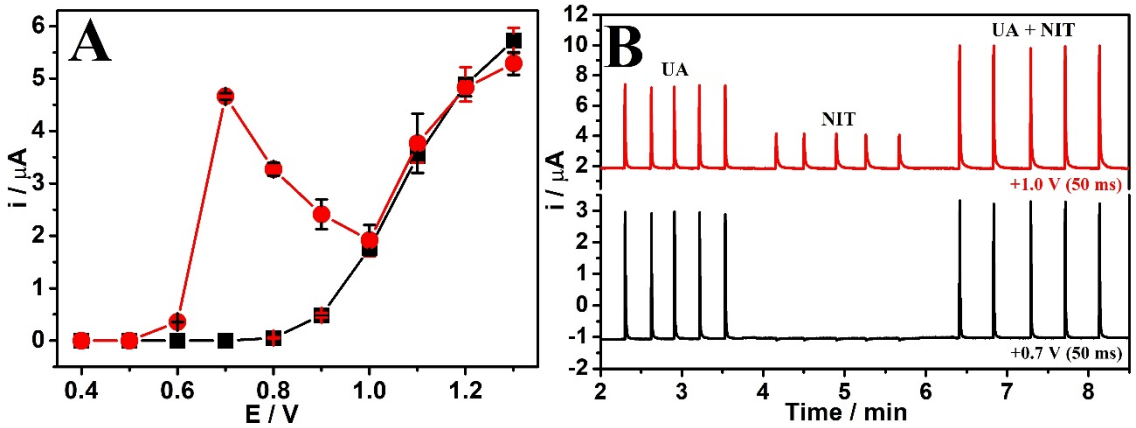

Figure 34 – (A) Hydrodynamic voltammograms obtained by plotting peak current values as a function of the corresponding applied potential pulses (70 ms each pulse). The solutions contained 10 μmol L^{-1} of UA (•) and NIT (■). (B) Amperometric responses (n=5) of solutions containing only UA (20 μmol L^{-1}), only NIT (20 μmol L^{-1}) and UA + NIT (20 μmol L^{-1} each). Supporting electrolyte: BR buffer pH 2; dispensing rate: 280 μL s^{-1}; injection volume: 100 μL.

potentials between +0.6 and +0.8 V are able to oxidize only UA without interference of NIT. At higher potentials than +0.8 V, both analytes are oxidized. Figure 34.B shows the amperograms obtained by BIA–MPA at potential levels of +0.7 V and +1.0 V (alternately applied to each 50 ms) for the injection (n = 5) of solutions containing only UA (20 μmol L^{-1}), only NIT (20 μmol L^{-1}), and both UA and NIT (20 μmol L^{-1} of each). These results demonstrate that in samples containing both UA and NIT, UA can be selectively detected at +0.7 V. However, the current from the oxidation of NIT cannot be directly accessed at +1.0 V (due to UA interference). This interference can be easily overcome using a correction factor (CF), as previously described (Da Silva et al., 2011; FREITAS et al., 2016; PEREIRA et al., 2013). The CF is necessary in order to obtain the exact oxidation current value of NIT at the potential of +1.0 V, because the UA oxidation currents are not the same at the two potential pulses (+0.7 V and +1.0 V). The CF was obtained by injecting a standard solution containing only UA in the BIA-MPA system and the following Equation 1:

$$CF_{UA} = \frac{i_{UA+1.0V}}{i_{UA+0.7V}} \tag{1}$$

In this way, when a solution containing UA and NIT is injected in the BIA-MPA system, the access to the oxidation current originated only from NIT (without interference of UA) can be obtained using Equation 2:

$$I_{NIT} = i_{+1.0V} - (CF.i_{+0.7V}) \tag{2}$$

In the next step, operational parameters of the BIA system (injected volume and dispensing rate) were optimized using the univariate method . Figure 35 shows the current variation (n=3) of UA monitored at the two potential pulses (+0.7 and +1.0 V red and green line respectively) as function the injected volume (A) and dispensing rate (B) in the BIA system using the 3D-printed G-PLA electrode. The variation of the CF value (i_{UA} at +1.0 V / i_{UA} at +0.7 V) is also plotted (blue lines).

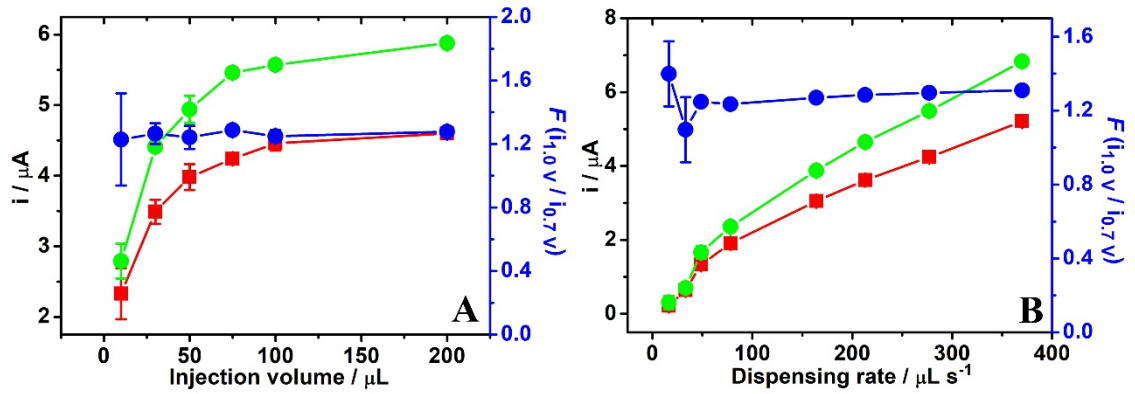

Figure 35 – Study of the injected volume (A) and dispensing rate (B) in the BIA system using the 3D-printed G-PLA electrode. Injections of 10, 30, 50, 75, 100 and 200 μL, dispensing rate 16.5, 33.2, 48.7, 78.1, 164, 213, 280 and 370 μL s^{-1} of standard solution of 20 μmol L^{-1} UA. Potential pulse: +0.70 V (■) and +1.0 V (•) for 50 ms. Correction factor (CF): iUA at +1.0 V / iUA at +0.7 V (•). Supporting electrolyte: 0.1 mol L^{-1} BR buffer solution (pH 2); in (A) dispensing rate: 280 μL s^{-1}; in (B) injection volume: 100 μL.

The oxidation currents of UA at +0.7 V and +1.0 V increased until 100 μL and reached a plateau after this volume (CF values were constant within this range of volumes, Figure 35.A), while the oxidation currents of UA at +0.7 V and +1.1 V increased gradually with the increase in the dispensing rate (CF values constant after 50 μL s^{-1}, Figure 35.B). The dispensing rate of 280 μL s^{-1} and the injection volume of 100 μL were selected in subsequent studies, keeping a stable CF (1.30 ± 0.02) value.

Once BIA-MPA parameters were selected, analytical curves for UA were obtained to evaluate the linear of the proposed amperometric method and also to verify if the CF values are constant within the varied concentration range. If the CF values vary significantly, NIT determination is compromised as it depends on the subtraction from UA signal multiplied by CF (see Equation 2). Figure 36.A shows the amperometric recording obtained at +0.7 and +1.0 V for increasing concentrations of UA (0.5 to 500 μmol L^{-1}) and Figure 36.B shows the corresponding analytical curves obtained at both potentials and the resulting CF value calculated for each concentration

Linear behavior between the current recorded at +0.7 V and the UA concentration from 0.5 up to 350 μmol L^{-1} (r = 0.997) is observed, while for the potential of +1.0 V, linearity is observed up to 500 μmol L^{-1} (r = 0.999). The CF value showed larger

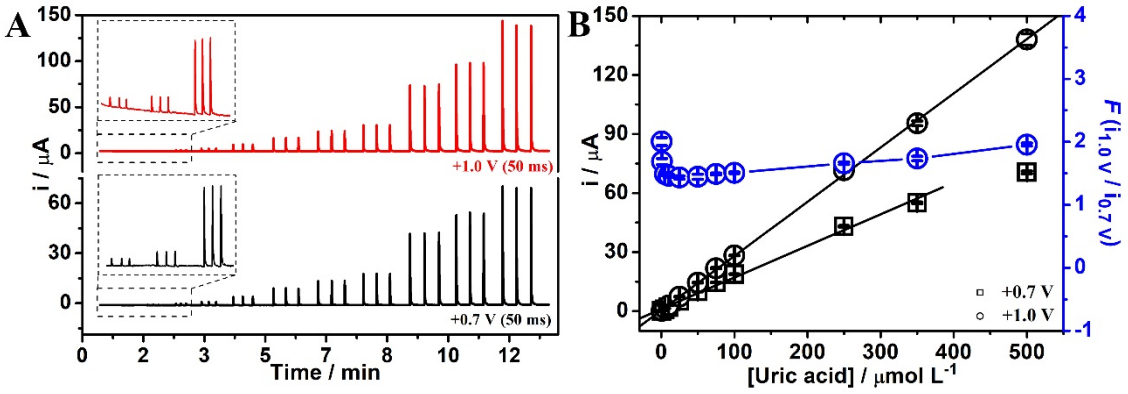

Figure 36 – Amperometric responses obtained after triplicate injections of solutions containing increasing concentrations of UA (0.5 to 500 µmol L-1) for study the correction factor. (B) Analytical curves obtained at () +0.7 V (0.5 - 350 molL-1) and at () +1.0 V (0.5 – 500 molL-1); the calculated correction factor for each concentration is plotted as blue (). Other conditions see Figure 34.

variation below 5 μmol L^{-1} while little variation was observed between 5 and 250 μmol L^{-1} (CF = 1.50 ± 0.08). Hence, this CF value can be applied for the determination of NIT in the presence of UA from 5 to 250 μmol L^{-1} using the proposed BIA-MPA method. It is worth mentioning that the CF must be determined for each calibration procedure (with injections of a solution containing only UA), because of small variations occurring between analyses conducted in different days. The success in NIT quantification depends, however, not only on the CF value to be applied in Equation 2, but also on the linear relationship between the concentration of this species and the oxidation current recorded at +1.0 V potential. Thus, the linear range study was investigated with solution injections of increasing concentrations of NIT. Figure 37.A show the currents obtained for injections of solutions of NIT (from 0.5 to 500 μmol L^{-1}) and Figure 37.B shows the linear behavior between the current recorded at +1.0 V and NIT concentration (r = 0.997). Thus, different from that observed for UA, NIT can be quantified over the entire concentration range studied (considering that the CF was obtained in a UA concentration range between 5 and 350 μmol L^{-1}).

Stability of the BIA-MPA method was studied by performing alternating measurements (n = 24) of solutions containing both UA + NIT (in equimolar ratio) of 10 μmol L^{-1} or 25 μmol L^{-1}. In this study, the RSD values (n = 24) were 3.5% (10 μmol L^{-1}) and 2.1% (25 μmol L^{-1}) for UA (at +0.7 V). For NIT (after using the CF) the values of RSD of 2.0% (10 μmol L^{-1}) and 1.1% (25 μmol L^{-1}) were found. The resulting amperograms are shown in Figure 38 These results show that the proposed method is highly precise and free from carryover effects.

After verifying the proposed BIA-MPA method enables the precise determination of UA and NIT using a CF value, analytical curves for the simultaneous determination of

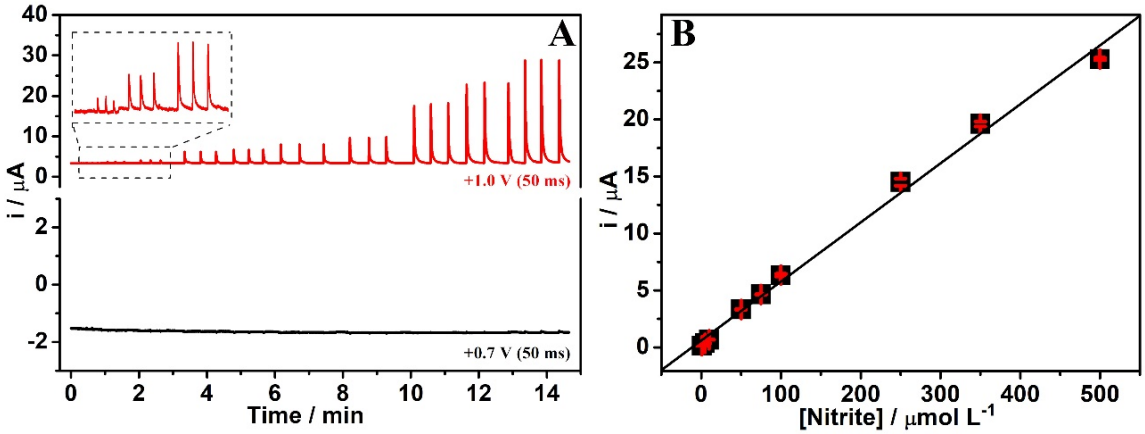

Figure 37 – (A) Amperometric responses obtained after triplicate injections of solutions containing increasing concentrations of NIT (0.5 to 500 μmol L^{-1}). (B) Analytical curve obtained at +1.0 V. Other conditions: see Figure 34.

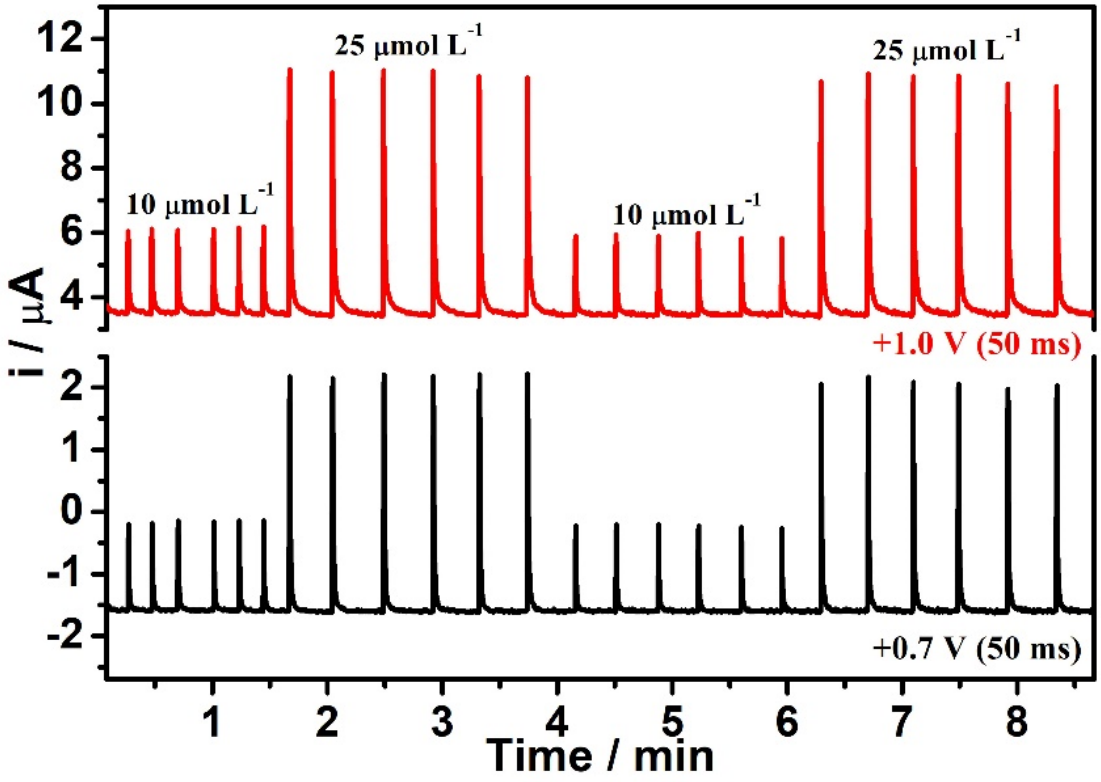

Figure 38 – Amperograms obtained from alternating injections (n=12) of standard solutions containing 10 + 10 μmol L^{-1} and 25 + 25 μmol L^{-1} of UA and NIT. Supporting electrolyte: 0.1 mol L^{-1} BR buffer solution (pH 2); dispensing rate: 280 μL s^{-1}; injection volume: 100 μL.

both analytes were obtained. Figure 39 presents the amperograms obtained at +0.7 V and +1.0 V for triplicate injections of solutions containing UA (a: used to obtain the CF value) followed by the triplicate injection of ten standard solutions containing increasing concentrations of both target UA and NIT (1-10: 0.5 – 250 μmol L^{-1}) and again a triplicate injection of UA (used to calculate the CF value). Both analytical curves show highly linear behavior within a wide concentration range of both analytes showing that MPA method there's no interference between both species and the simultaneous determination is feasible. Table 10 shows the analytical responses obtained by MPA-BIA.

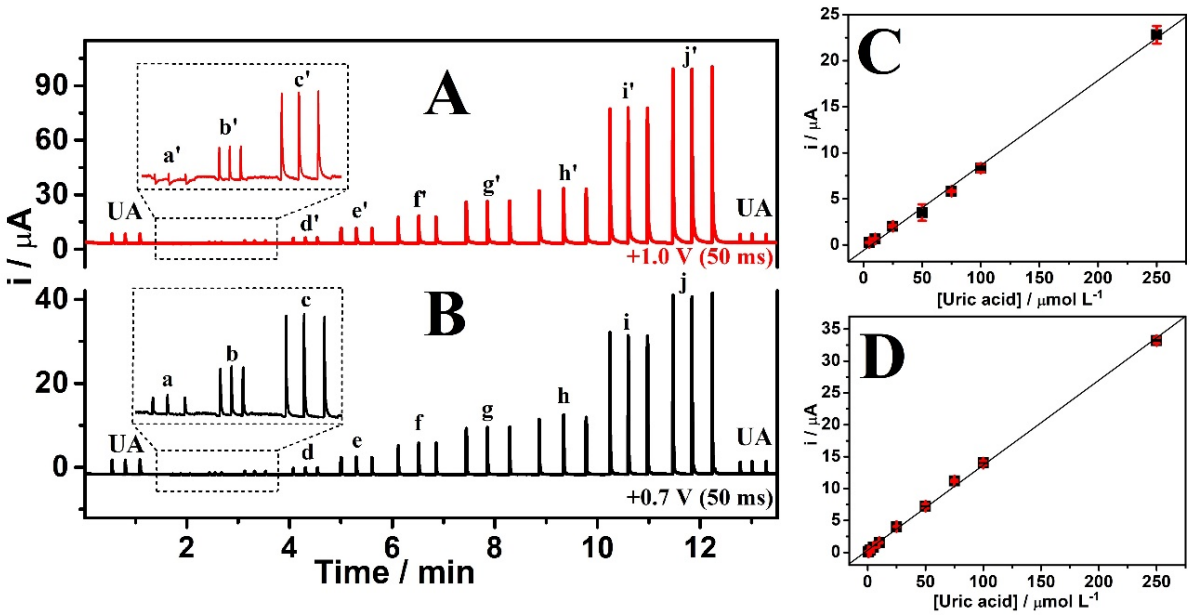

Figure 39 – Amperometric responses obtained at (A) +0.7 V and (B) +1.0 V after triplicate injections of solutions containing only UA used to obtain the CF value, followed by the triplicate injection of ten standard solutions containing simultaneously increasing concentrations of UA and NIT (black line = i_{UA}) and (red line = i_{UA+NIT}) (a-j: 0.5 – 250 μmol L^{-1}), and a triplicate injection of UA. (C) and (D) show the corresponding calibration curves for NIT and UA. Experimental conditions: see Figure 34.

The BIA-MPA presented satisfactory limit of detection values, precision, and linear ranges. Another important feature is sample throughput, which is a well-known advantage of flow methods such as BIA reaching values around 360 h^{-1}. The analysis of a real sample would require the standard analytical method so the analysis of one sample considering 4 additions of standard solutions would take 10 min (considering the injection time and supporting electrolyte replacement) resulting in a sample throughput of around 6 h^{-1}. The BIA method employs an electronic micropipette that injects quickly sample plugs (triplicate at a row by just pressing a button) and supporting electrolyte just needs to be replaced after 250 injections (the cell stands 25 mL of injected solutions plus 50 mL of supporting electrolyte).

Table 10 – Analytical parameters obtained by BIA-MPA.

Parameters	**BIA-MPA**	
	UA	**NIT**
Linear range (μmol L^{-1})	0.5 - 250	0.5 - 250
Slope (μA L μmolL^{-1})	0.1332	0.0922
LOD (μmol L^{-1})	0.02	0.03
R	0.9991	0.9986
RSD* (%)	2.1	1.1

*For concentration of 25 μmolL^{-1} of UA and NIT (n = 12) in BIA-MPA.

The proposed BIA-MPA method using the 3D-printed G-PLA sensor was applied for the simultaneous determination of UA and NIT in two biological samples, human urine and saliva. To evaluate if the sample matrix affects the accuracy of the method, recovery tests were performed by analysing the sample samples after spiking them with a known amount of UA and NIT. Samples were analysed by using a external calibration curve and by the standard addition method. Table 11 presents the obtained concentration values in pure and spiked samples as well as the calculated recovery values obtained by both methods. The proposed method using the 3D-printed sensor detected a measurable amount of NIT and UA in the urine sample while the concentration of both species in the saliva sample were below the respective LOD values. Recovery levels of the analytes in urine and saliva (spiked with 5 and 10 μmol L^{-1}) presented values between 70 and 172% using the external calibration curve. Using the standard addition method, the recovery values were between 70 and 120%. Acceptable values for the analysis of biological fluids should be between 80 and 120% (SIMON; BOOTH, 2004) and the values obtained using the standard addition method were within this acceptable range. Some recovery values using the external calibration curves were above this range (<12%), which indicates a possible sample matrix effect. To evaluate if if the sample matrix interferes in the determination of UA and NIT, the slope values of analytical curves obtained using standard solutions were compared with the ones obtained in the presence of saliva or urine samples. The results were statistically different, what explain the satisfactory results obtained by the standard addition method for the simultaneous determination of UA and NIT in biological samples using BIA-MPA and 3D-printed electrodes.

The normal concentration range of UA in urine is lower than 4.50 mmol L^{-1} per day, hence the amount found in the sample (4.6 ± 0.1 mmol L^{-1}) is alarming (BALLESTA-CLAVER et al., 2011; ROSSINI et al., 2018). On the other hand, NIT concentration higher than 1 mmol L^{-1} in urine may indicate urinary infection (SHIMONI et al., 2017) and the value found in the sample (5.0 ± 0.8 mmol L^{-1}) is much higher than this value. Urine containing a high amount of NIT indicates urinary tract infections and bacteriuria as excess of NIT may be a result of bacterial nitrate reductase activity (TSIKAS; SCHWARZ; STICHTENOTH,).

Table 11 – Concentrations of UA and NIT obtained by BIA-MPA method, recovery values for the spiked biological samples and respective standard deviation values (n=3) using the standard addition method

Standard addition method				
	Found (mmol L^{-1})	**Spiked (mmol L^{-1})**	**Recovery (mmol L^{-1})**	**Rec. (%)**
UA	5.5 ± 0.3	5	10 ± 0.3	109
	5.5 ± 0.3	10	17± 1.7	115
	5 ± 0.3	5	6 ± 0.9	120
	-	10	12 ± 1.1	120
NIT	7.7± 2	5	11 ±1.5	90
	7.7 ± 2	10	14 ± 1.9	70
	-	5	5 ± 1.0	100
	-	10	11 ± 1.2	110

4.4 Conclusions

We have shown the use of 3D-printing technology for rapid prototyping of electrochemical (bio)sensors for the analysis of biological fluids. We have demonstrated that the oxygenated group from carboxylic acid present at 3D-printed G-PLA provides suitable condition to enzyme immobilization by crosslinking with glutaraldehyde for a biosensor construction to glucose determination in plasma. The combined treatment by mechanical polishing followed by solvent immersion improves the electrochemical performance of 3D-printed G-PLA sensor for the detection of UA and NIT. SEM images showed that both treatments make the graphene nanoribbons more available from the PLA matrix and certainly contributes to the improved sensing properties of the 3D-printed sensor. The simultaneous determination of UA and NIT is demonstrated using BIA-MPA applied in biological fluids. The 3D-printed G-PLA sensor was successfully applied in urine and saliva using BIA-MPA with adequate recovery values for the analysis of spiked samples. This is the first demonstration of a 3D-printed device applied for sensing and biosensing in biological fluids. Therefore, this work shows great promises for the application of FDM 3D-printing technology to develop (bio)sensors for the analysis of biological samples, including perspectives for the development of wearable biosensors considering that 3D-printed G-PLA sensors are flexible, biodegradable and biocompatible. Moreover, this technology can be used to produce (bio)sensors in large-scale and different sizes, reducing costs of production, especially important for countries in the developing world.

4.5 Acknowledgements

The authors are thankful to FAPEMIG (PPM 00640-16), CAPES (001 and Pró-Forense 25/2014 23038.007073/2014-12), CNPq (307333/2014-0, 307271/2017-0, 427731/2018-

6 and 405546/2018-1), INCTBio (CNPq grant no. 465389/2014-7) and FAPESP (2016/10012-4) for financial support. The authors also are grateful to the Multiuser Laboratory of Chemistry Institute at the Universidade Federal de Uberlândia and FINEP for experiments involving scanning electron microscopy. This study was financed in part by the Coordenação de Aperfeiçoamento de Pessoal de Nível Superior – Brasil (CAPES) – Finance Code 001

Chapter 5

3D-printing pen vs desktop 3D-printers: fabrication of conductive PLA for TNT detection

This Chapter contains an adaption of the published paper entitled "3D-printing pen versus desktop 3D-printers: Fabrication of carbon black/polylactic acid electrodes for single drop detection of 2, 4, 6– trinitrotoluene by Rafael M. Cardoso , Diego P. Rocha , Raquel G. Rocha , Jéssica S. Stefano , Rodrigo A.B. Silva , Eduardo M. Richter, Rodrigo A.A. Muñoz available Online

Graphical Abstract

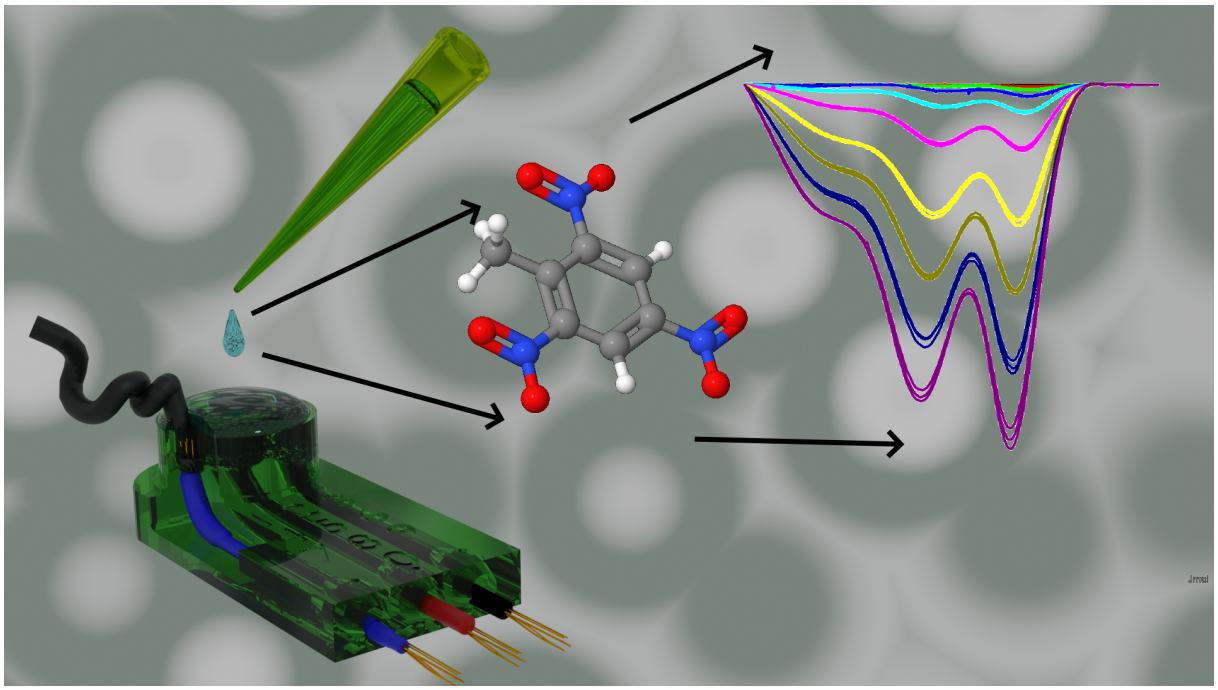

5.1 Introduction

This chapter demonstrates that a 3D-Pen can be used to manufacture electrochemical sensors by introducing conductive filaments (PLA with graphene or carbon black) over any desirable format and substrate. Commercially-available as a toy for children, the 3D-Pen can be considered a handheld FDM 3D-printer. Many designs, conductive filaments and substrates can be combined with a 3D-Pen to draw electrochemical sensors (e.g. medical point-of-care platforms) as well as other electrochemical devices for water splitting or energy storage (e.g. batteries or supercapacitors if filaments with superior conductivity are employed). It is noteworthy to mention the possible applications of 3D-Pen for teaching purpose using low consumables and materials. A communication entitled "Drawing electrochemical sensors using a 3D-printing pen" published in the Journal of the Brazilian Chemical Society demonstrates this idea (CARDOSO et al., 2020). Moreover, a video in Youtube illustrate the fabrication process (JBCS-YOUTUBE-CHANNEL, 2020). This Chapter compares the electrodes obtained by using the 3D-Pen with FDM 3D-printer.

5.2 Experimental section

5.2.1 Reagents and solutions

All solutions were prepared with deionized water (resistivity not lower than 18.2 MΩ cm) obtained from a Milli-Q water purification system (Millipore, Bedford, MA, USA). All reagents were analytical grade and used with no further purification. TNT was obtained from the military police of Minas Gerais state (Brazil) with purity higher than 96% (w/w). Dopamine (> 99%) was purchased from Acros (New Jersey, USA) and perchloric acid (70%) from Reagan (Rio de Janeiro, Brazil). Potassium ferrocyanide ($K_4[Fe(CN)_6]$) and potassium ferricyanide ($K_3[Fe(CN)_6]$) were purchased from CAAL (São Paulo, Brazil) and Proquimios (Rio de Janeiro, Brazil), respectively. TNT stock solution was prepared in HPLC-grade acetonitrile and further diluted in aqueous supporting electrolyte.

5.2.2 Instrumentation

Electrochemical measurements were performed using a μ-AUTOLAB type III potentiostat/galvanostat (Metrohm Autolab B. V., Utrecht, Netherlands) interfaced to a microcomputer and controlled by NOVA 1.12 software. A platinum wire and a laboratory-made $Ag|AgCl/KCl_{sat}$. electrode (PEDROTTI; ANGNES; GUTZ, 1996) were used as auxiliary and micro-reference electrodes, respectively, in the experiments using the single 3D-printed working-electrode device or for the electrochemical activation process

The 3D-Pen was purchased from Sanmersen (Shenzhen, China). Two desktop 3D-printers, an FDM RepRap custom build Prusa clone and an Anycubic Photon digital

UV light processing (DLP) purchased from ANYCUBIC Co., Ltd. (Shenzhen, China), were used in this work to prototype the substrates that worked as templates to guide the application of the molten thermoplastic by 3D-Pen for the fabrication of the electrodes in two designs, resulting in four different devices. ABS filament of 1.75 mm width was purchased from GTMAX 3D (São Paulo, Brazil) to feed the FDM 3D-printer, and a translucent green resin from ANYCUBIC Co (Shenzhen, China) was used in the DLP 3D-printer. A conductive carbon black/PLA thermoplastic filament (Proto-Pasta$^{\circ}$) obtained from ProtoPlant Inc. (Vancouver, Canada), with a resistivity of 30 Ω cm (FLOWERS et al., 2017), was used to prototype the conductive parts (electrodes) by the 3D-Pen or using the desktop FDM 3D-printer. A commercially-available screen-printed carbon electrode (SPE-d110) from Dropsens (Oviedo, Spain), in which the working electrode was made of a carbon ink, was used for comparison (nominal diameter of 4 mm of the working electrode according to the manufacturer).

5.2.3 Fabrication of the electrodes using the 3D-Pen

Two main designs to fabricate the electrodes were evaluated. The first one and simpler consisted in a single working electrode design (same design of a glassy-carbon disc electrode) and the second one, a three-electrode system on a planar substrate (similar to a commercial screen-printed electrode). The customized substrates of both designs were fabricated using two types of 3D-printers using different materials, fused deposition modelling (FDM) with ABS and digital UV light processing (DLP) with UV curable acrylic resin, resulting in four different electrochemical devices. Precise 3D-printed pieces (substrates) were fabricated to work as templates for the 3D-Pen extrusion of the conductive carbon black/PLA filament in a precise manner (independent of the user) and with minimum amount of filament. The process of electrode manufacturing using the 3D-Pen takes less than one minute as the molten filament quickly solidifies at room temperature.

Briefly, a 3D-Pen consists of a geared motor mounted for pushing filament along a filament guide tube towards a heated nozzle (190^{o}C). When the thermoplastic reaches the high temperature at the nozzle, the filament fuses and can be manually extruded. Figure 40 represents the 3D-Pen simplified mechanism for the construction of a three-electrode system on a planar 3D-printed substrate.

The models of all substrates were designed using Blender software 2.81a. For FDM slicing, Symplify3D® was used to generate the gcode files. The STL file used by both DLP and FDM 3D-printers was generated by ChituboxTM (Shenzhen, China). Both final working electrodes presented a nominal diameter of 3.8 mm and were named as WE-FDM and WE-DLP. Schemes of both electrode designs (WE-FDM and WE-DLP) are presented in Figure 41 (1 and 2, respectively). At the top side of the electrodes, the conductive filament is deposited by the 3D-Pen covering completely the empty hole and the exposed copper wires. Figure 41.3 and 4 show the three-electrode-system (TES) devices, consisting

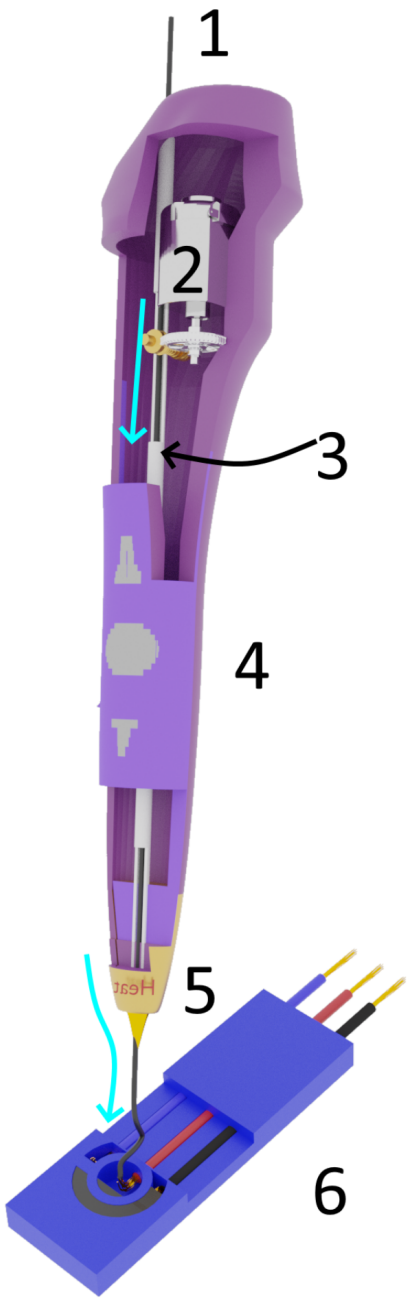

Figure 40 – Simplified representation of internal parts of the 3D-Pen and a scheme of the customized 3D-printed substrate of the three-electrode device (TES): (1) Conductive thermoplastic filament; (2) geared mechanism (5 V) motor; (3) filament guide tube; (4) command buttons; (5) heated nozzle (190 °C); and (6) illustrative cut of the FDM 3D-printed device showing wires and template holes to be filled by the filament

of a single strip with the three electrodes (working, reference and auxiliary). The shape is similar to a commercial screen-printed electrode. The substrate fabricated by FDM (TES-FDM) presented a working electrode diameter of 3.8 mm (Figure 41.3) while the one fabricated by TES-DLP had a diameter of 3.0 mm (Figure 41.4). All substrates were designed with axial holes to insert copper wires for the electrical contact of each electrode. Copper wires (4x26 American wire gauge, AWG) were acquired from local hardware store. The schemes shown in Figure 41.3 and Figure 41.4 also show the holes which are filled by the conductive filament using the 3D-Pen in such a way the copper wires are completely covered.

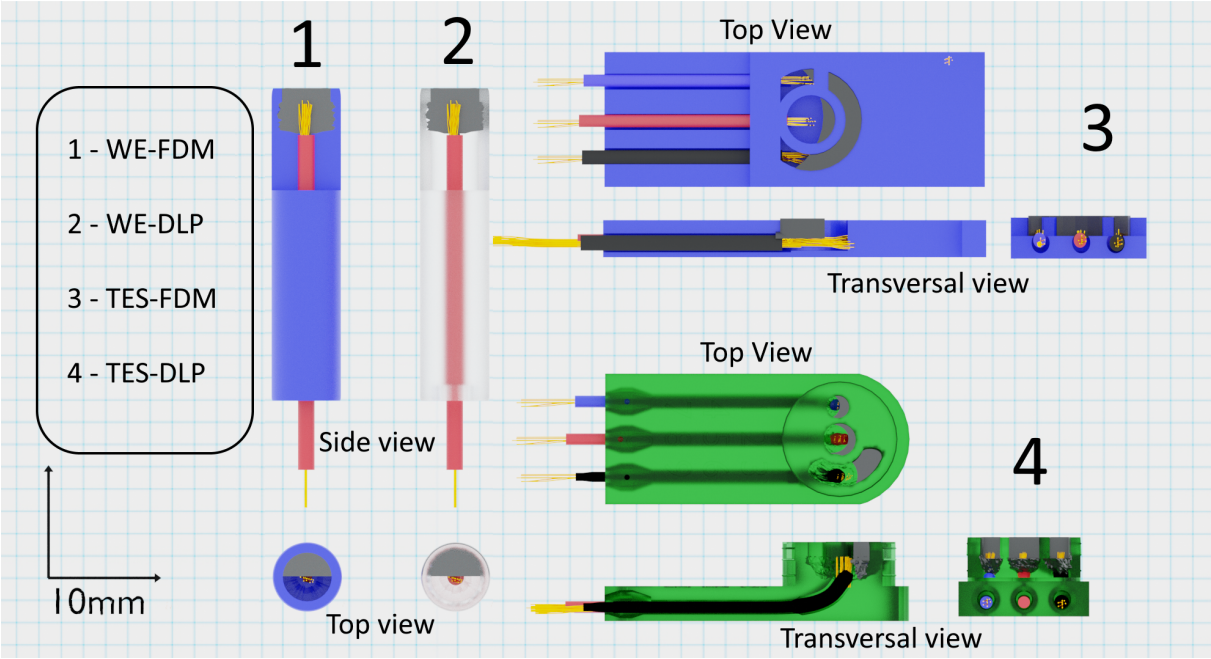

Figure 41 – Schematic orthogonal view of the electrochemical devices fabricated using a 3D-Pen and customized 3D-printing structures: (1 and 2) Side and top views of cylindrical working electrodes with the body 3D-printed by FDM (WE-FDM) or DLP (WE-DLP). with the holes partially filled by the conductive filament using the 3D-Pen; (3 and 4) Top and transversal views of the three-electrode-systems (TES) on planar substrates 3D-printed by FDM (TES-FDM) or DLP (TES-DLP). Holes in the substrates (electrodes location) are illustrated with partial filled of the conductive filament to facilitate identification of these regions.

The axial channels were made to fit the insulated copper wire while at one edge the insulation was removed to expose the copper wire as shown in detail in Figure 41 (all schemes). Over the holes containing the exposed copper wire, the conductive thermoplastic was inserted using the 3D-Pen to fill completely each hole, avoiding exposure of copper wires and any possible solution infiltration. The 3D-Pen conductive thermoplastic deposition was carried out at 190ºC. After deposition, the conductive thermoplastic fused

and became solid in less than 5 s at room temperature (~25ºC). After 5 min, the spare plastic over the planar surface was removed using an electric mini drill equipped with a sandpaper (gr80 for rotary tool) attached to a rubber wheel, and then the electrode was subjected to polishing on a 1200 grit sandpaper (for fine polishing) with deionized water. Real images of the four devices (TES-DLP, TES-FDM, WE-DLP, and WE-FDM) are shown in Figure 42. Zoom images of the TES-DLP device, which was used for TNT detection in a single drop of 100 μL, are presented in Figure 43. The protocol to produce the TES-FDM is available online at Youtube(JBCS-YOUTUBE-CHANNEL, 2020).

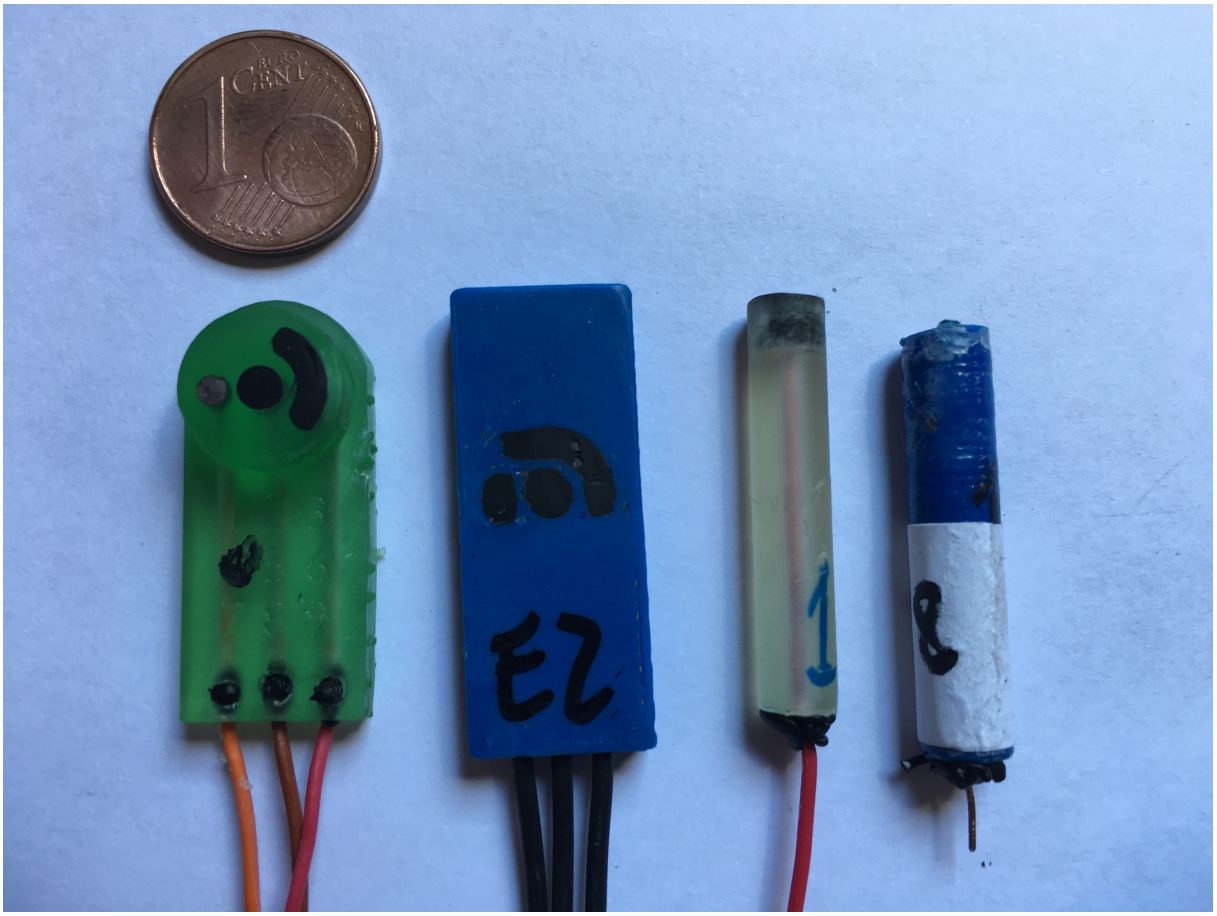

Figure 42 – Picture of the proposed devices. From left to right: TES-DLP, TES-FDM, WE-DLP, and WE-FDM.

Next, the working electrode in both designs (WE and TES) was electrochemically activated according to a recent protocol described in the literature for 3D-printed carbon black/PLA electrodes (RICHTER et al., 2019; ROCHA et al., 2020a). Briefly, the working electrode was treated in 0.5 mol L^{-1} NaOH by the application of +1.4 V for 200 s followed by -1.0 V for 200 s using Ag|AgCl|KCl^{sat} as reference electrode and a Pt wire as counter electrode. For both systems with 3 electrodes (TES-FDM and TES-DLP), all printed surfaces were simultaneously activated by connecting connected them as working electrode

during the activation step.

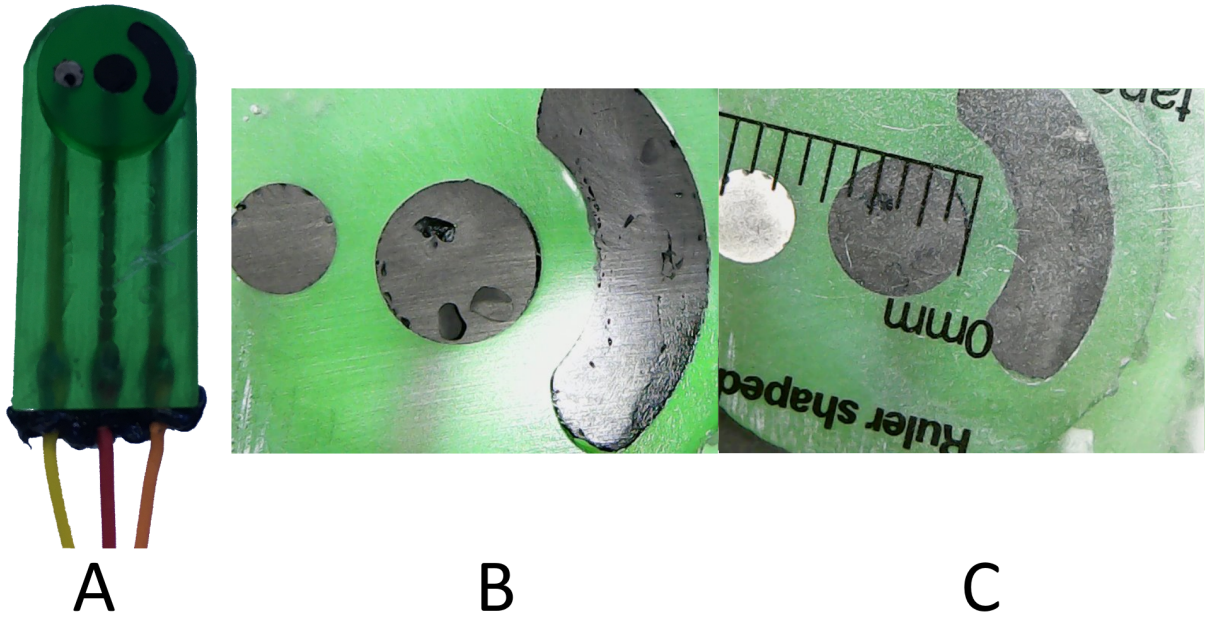

Figure 43 – Images of the TES-DLP device: complete view (A); zoom pictures with a Digital USB 1000X microscope over the three electrodes before (B) and after (C) silver electrodeposition. A ruler was placed in (C) indicating 1 cm scale.

5.2.4 Fabrication of the electrodes using a desktop FDM 3D-printer

The fabrication of carbon black/PLA electrodes using the FDM 3D-printer (instrument described in section 2.2) was based on previous works (CARDOSO et al., 2018) and chapters 2 to 4. Briefly, a rectangle hollow box shape (40 length x 40 width x 20 mm height) was 3D-printed using the conductive carbon black/PLA filament. 3D-printing parameters involved with vase mode on, one perimeter, zero infill, zero top and bottom layer and a single perimeter. The faces of the rectangle box formed by layer-by-layer deposition (layer height of 100 μm) of the filament in a vertical printing orientation were used as electrodes according to the previous optimization (CARDOSO et al., 2018; CARDOSO et al., 2020).

Each rectangular face was polished on a 1200 grit sandpaper wet with deionized water for 15 s (see Figure 8), then the faces were separated by cutting using a scissors (pieces of 20 mm x 40 mm). The 3D-printer was equipped with a 1 mm nozzle, heated at 205 ºC with cooling turned on before first layer and bed temperature at 65 ºC. The printing speed was set to 20 mm/s. The 20 x 40 mm rectangular pieces served as individual working

electrodes. One of them was assembled in a 3D-printed electrochemical cell (printed using ABS) and the same electrochemical treatment applied for the electrodes fabricated using the 3D-Pen of the preview subsection was applied for these 3D-printed electrodes.

5.3 Electrochemical measurements

All electrochemical measurements were performed in the presence of dissolved oxygen and at room temperature. Dopamine standard solution was prepared in aqueous solutions of 0.1 mol L^{-1} $HClO_4$ and the redox probe $[Fe(CN)_6]^{3-/4-}$ in 0.1 mol L^{-1} KCl. TNT stock solutions prepared in acetonitrile was diluted in 0.1 mol L^{-1} HCl as supporting electrolyte prior voltammetric measurements (the final concentration of acetonitrile was below 1% v/v).

5.4 Microscopic and spectroscopic characterizations

Raman spectra of the electrodes were obtained using a LabRAM HR Evolution – Horiba (λ = 532 nm). Moreover, scanning electron microscopy (SEM) measurements were performed in a Vega 3 -Tescan equipment (TESCAN, Brno-Kohoutovice, Czech Republic) operated at 20 kV. Atomic force microscopy (AFM) images were obtained using a Shimadzu scanning probe microscope (SPM-9600) using the tapping mode to study the electrode surfaces.

5.4.1 Safety note

TNT powder is insensitive to shock or friction, which reduces the risk of accidental detonation. In this work, few milligrams of the explosive were safely handled to prepare stock solutions in acetonitrile.

5.5 Results and discussion

5.5.1 Morphological analysis of carbon black/PLA electrodes: 3D-printing pen versus desktop 3D-printer

AFM measurements were obtained for the electrodes fabricated by the 3D-Pen Figure 44 to show the corresponding topological profile of surfaces. The images were obtained for the four designs, WE-FDM (A), WE-DLP (B), TES-FDM (C) and TES-DLP (D), after the electrochemical surface treatment applied for measurements, and compared with the one obtained for a commercial carbon screen-printed electrode (SPE) (E). The electrochemical performance of carbon SPE will be compared with the carbon black/PLA

electrodes fabricated using the 3D-Pen in the next section. The AFM images of electrodes fabricated using the 3D-Pen present an average roughness of 0.28 ± 0.07 μm, which is similar to the roughness surface of a carbon SPE (0.32 ± 0.09 μm, for n=3). For the next surface characterizations and comparison with carbon black/PLA electrodes fabricated using a desktop FDM 3D-printer, the WE-DLP device was selected to represent the carbon black/PLA electrodes fabricated by the 3D-Pen (as the only difference among the four electrodes is the design).

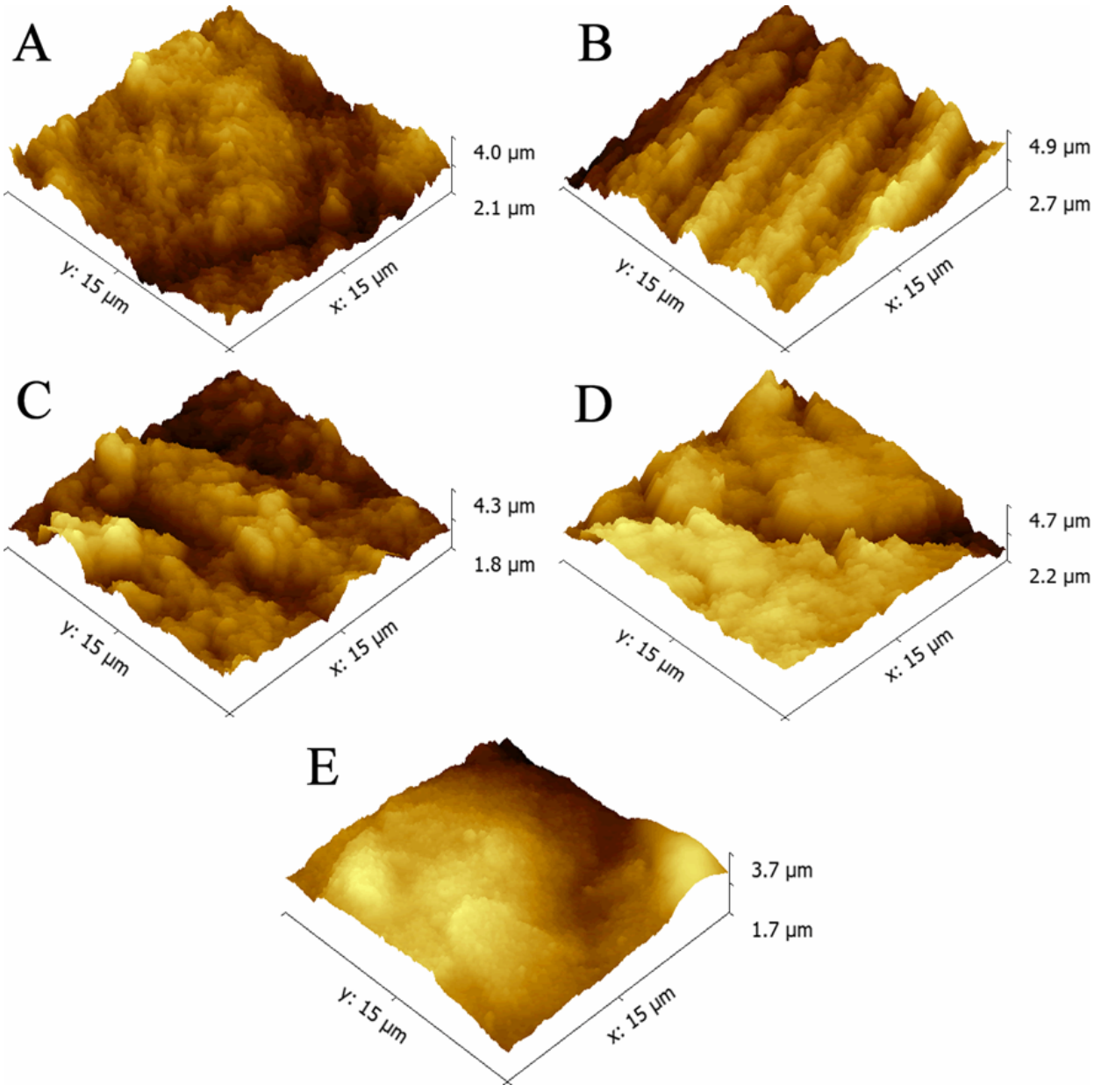

Figure 44 – AFM images for WE-FDM (A), WE-DLP (B), TES-FDM (C) and TES-DLP (D) (after electrochemical surface treatment) SPCE (E).

Previous papers have reported the use of desktop FDM 3D-printers to fabricate carbon black/PLA electrodes for the determination of dopamine and metals after surface

treatment to remove excess of PLA and expose the carbon black sites (JOÃO et al., 2020; RICHTER et al., 2019; ROCHA et al., 2020a). In order to verify if the different methods of fabrication of these electrodes affect their surface characteristics, morphological analysis using Raman spectroscopy and SEM was performed. Figure 45 shows the SEM images obtained for the carbon black/PLA electrodes fabricated by 3D-Pen and desktop 3D-printers, before and after electrochemical surface treatment.See Figure 46 for SEM images with less zoom.

The SEM images show some grooves in all surfaces obtained by both procedures (analyzing images on left). The procedure using the 3D-Pen required an additional polishing step to remove the excess of filament using a harder sandpaper (gr80), which probably is responsible for the generations of harder grooves seen in Figure 45.A and B. These images corroborate with the AFM topological profiles presented in Figure 44. On the other hand, the electrodes produced by the desktop 3D-printers presented thinner grooves (Figure 45.C and D). Figure 46 (A and C) shows additional SEM images in lower amplification of the electrodes fabricated by both procedures (B and D in (Figure 45 corresponds to B and D of Figure 46 for a better comparison).

These new images show larger fractures that can be found on the electrode surface fabricated by both procedures. Interestingly, the image of the FDM 3D-printed electrode presents parallel lines (grooves) interspaced in 100 μm, which is the exact value of layer thickness of the layer-by-layer 3D-printing deposition (vertical orientation print). Hence, these lines (grooves) are probably indicative of the layer-by-layer deposition and one of these grooves is highlighted in Figure 46 (lower part of the image). Comparing with the electrodes fabricated using the 3D-Pen, larger fractures are randomly observed in the image of (Figure 46 and the more amplified image (Figure 45 shows the grooves generated by the mechanical polishing (hard sandpaper gr80) as previously discussed.

When analyzing the effect of electrochemical surface treatment, it is more evident the degradation of the polymeric surface in the images on left in Figure 45.A and B for the electrodes fabricated using the 3D-Pen, where the grooves were more obvious after the treatment (Figure 45.B). Considering the electrodes produced by the desktop FDM 3D-printers, the images on right show more evidently the effect of surface treatment on the degradation of the PLA surface (Figure 45.C and D). The degradation of PLA by the electrochemical treatment using NaOH was previously demonstrated (RICHTER et al., 2019; ROCHA et al., 2020a).

Figure 47 shows the Raman spectroscopic measurements of the same surfaces presented in Figure 42. The spectra revealed the presence of D (1356 cm^{-1}) and G (1600 cm^{-1}) bands commonly found at carbon black particles (BOKOBZA; BRUNEEL; COUZI, 2015). The D band can be associated with the presence of defects and sp^3 type hybridization, while the G band is attributed to the presence of sp^2 carbon. The $I_{(D)}/I_{(G)}$ intensity ratio can be used to investigate the density of defects on the carbon structure. The electrochemical

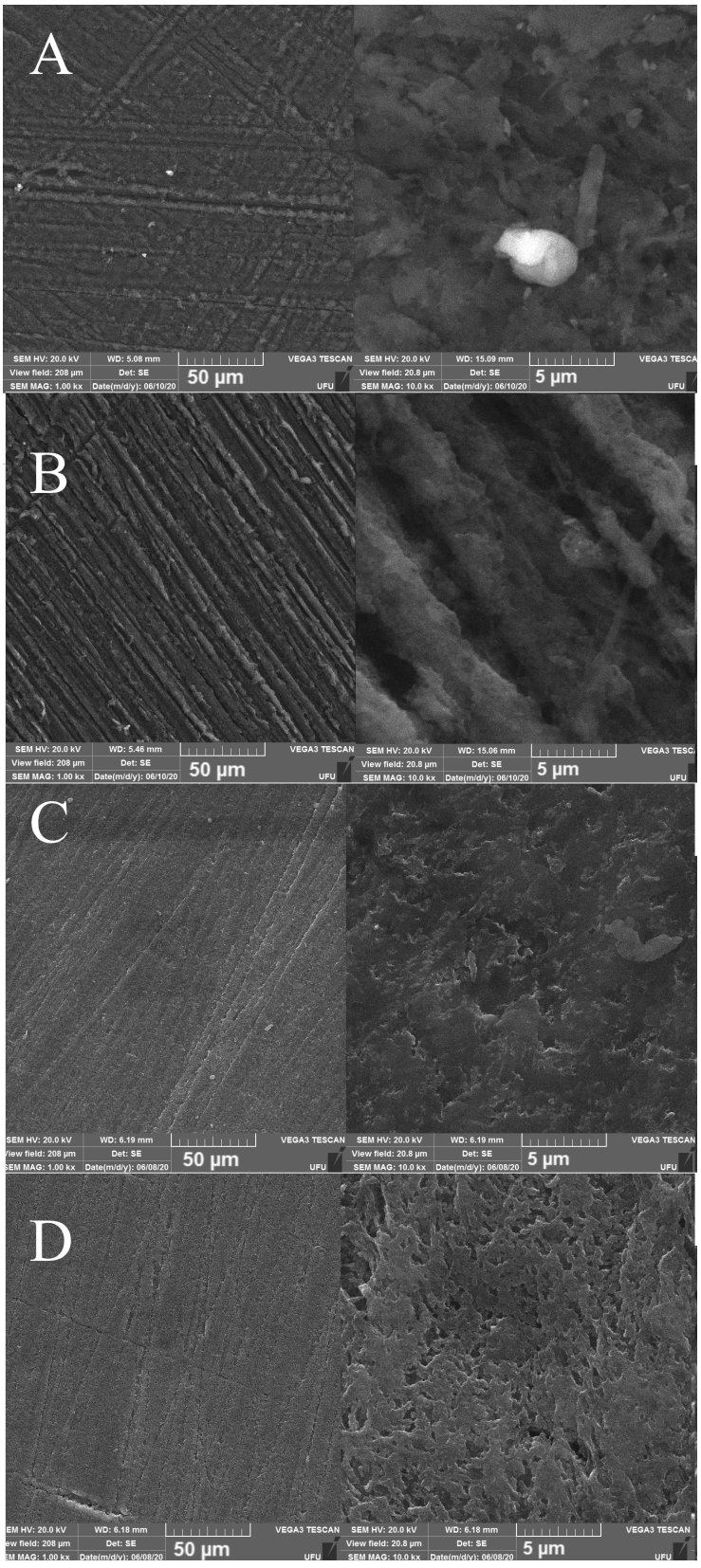

Figure 45 – SEM images (lower amplification on left and higher amplification on right) of the carbon black/PLA electrodes fabricated by 3D-Pen (A and B) and desktop 3D-printers (C and D), before (A and C) and after electrochemical surface treatment (B and D).

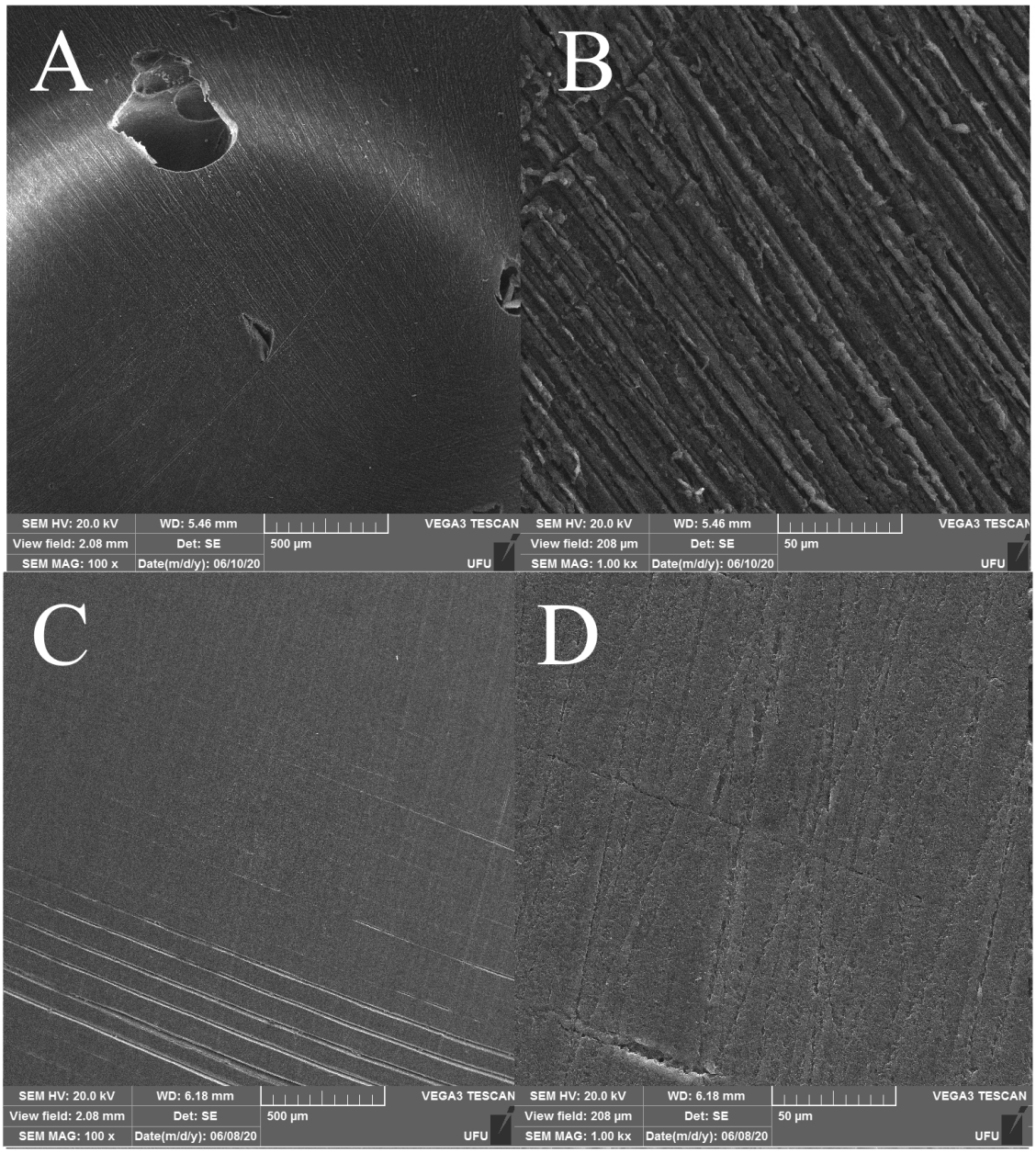

Figure 46 – SEM images (lower amplification on left and higher amplification on right) of the fabricated electrodes using the 3D-Pen (A and B) and using the desktop 3D-printer (C and D). These surfaces were electrochemically treated as described in the experimental section.

treatment of both electrode surfaces (fabricated using the 3D-Pen and the desktop 3D-printer) did not show significant differences of $I_{(D)}/I_{(G)}$ ratios in comparison with the values obtained for the untreated surfaces (3D-Pen: from 1.60 to 1.66; desktop 3D-printed: from 2.18 to 1.99, respectively, before and after treatment). However, there is a difference between the $I_{(D)}/I_{(G)}$ ratios of the electrodes fabricated by the desktop 3D-printer, which were slightly higher than the values obtained for the electrodes produced by the 3D-Pen. The higher $I_{(D)}/I_{(G)}$ ratio indicates higher presence of structural defects that may indicate improved electrochemical activity of such surfaces. Hence, the Raman spectra data suggest that the electrodes fabricated using a desktop FDM 3D-printer may present superior electrochemical performance. The next section compares the electrochemical properties of the carbon black/PLA electrodes fabricated by the 3D-Pen with electrodes fabricated using desktop 3D-printers.

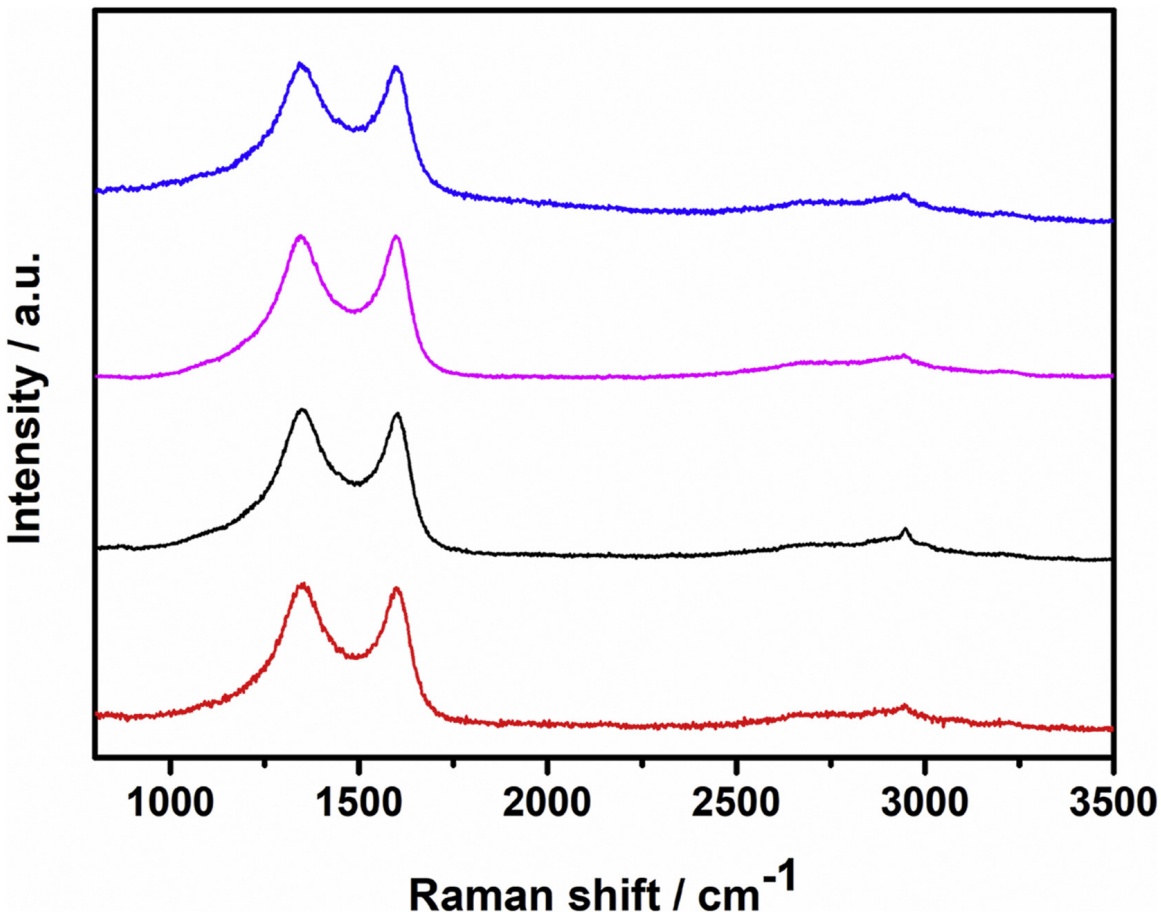

Figure 47 – Raman spectra for the 3D-Pen fabricated (WE-DLP) electrode before (blue) and after (pink) NaOH treatment and for the desktop FDM 3D-printed electrode before (black) and after (red) NaOH treatment.

5.5.2 Electrochemical characterization of carbon black/polylactic acid electrodes fabricated using 3D-Pen

Figure 51 shows the cyclic voltammograms for dopamine before and after the electrochemical activation of the working electrode presented in a TES-FDM device (using a carbon black/PLA pseudo-reference electrode). Dopamine is a model analyte used in previous works to evaluate the electrochemical performance of 3D-printed carbon electrodes (KALINKE et al., 2020). The amperometric profile observed during the activation process is shown in Figure 49.

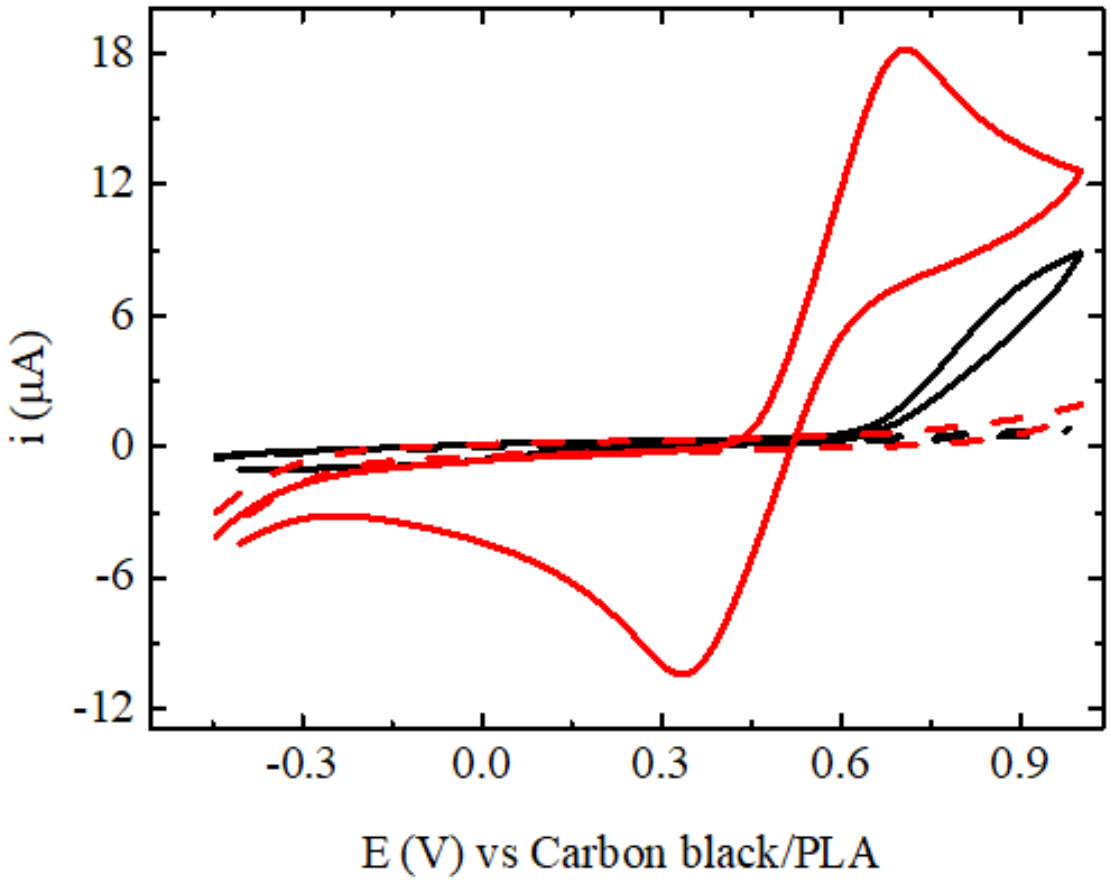

Figure 48 – Cyclic voltammograms recordings (vs carbon black/PLA pseudo-reference) in the presence of 1 mmol L^{-1} of dopamine before (black line) and after (red line) electrochemical activation of the TES-FDM; dashed lines are aqueous blank solutions (0.1 mol L^{-1} $HClO_4$).

This profile observed in Figure 49 was mandatory to consider the construction process a success, leading to substantial decrease in ΔE (from 1200 to 400 mV) and improvement of the voltammetric wave-shape. The chemical/electrochemical treatment of the carbon black/PLA surface in NaOH medium is responsible to make the carbon black conductive sites more available by removing excess of PLA. The electrochemical processes are likely

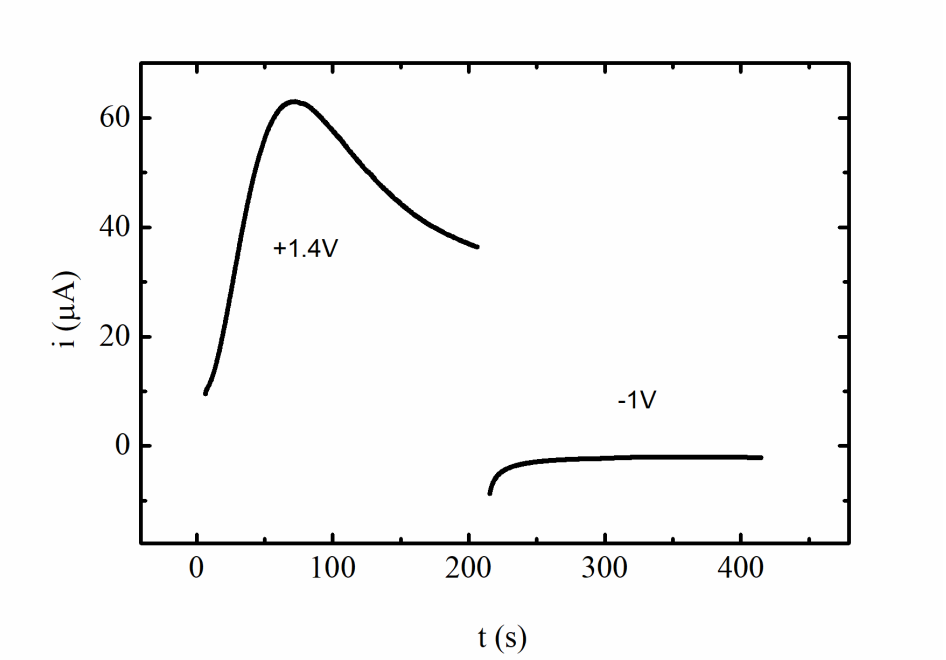

Figure 49 – Amperogram profile obtained during the electrochemical activation (+1.4 V for 200 s followed by -1.0 V for 200 s in 0.5 mol L^{-1} NaOH). All the three electrodes of the TES-FDM device were connected as single working electrode vs Ag|AgCl|$KCl_{(sat)}$ to perform the electrochemical activation.

to occur through these conductive sites and for this reason a higher electron transfer was observed after surface treatment (JOÃO et al., 2020; RICHTER et al., 2019; ROCHA et al., 2020a).

Considering the planar devices with three electrodes, the stability of the pseudo-reference electrode is crucial for repetitive electrochemical analytical measurements. The pseudo reference electrode in the TES devices was initially the native carbon black thermoplastic (carbon black/PLA pseudo-reference) as shown in Figure 49; however, potential variations on the electrochemical response depending on the target molecule due to interference in the pseudo-reference electrode have been previously demonstrated (RICHTER et al., 2019). To solve this inconvenience, the carbon black/PLA pseudo-reference electrode was modified by electrodeposition of silver from a commercial silver-plating solution, followed by a drop-casting of a concentrated liquid chlorine bleach. This procedure were performed according to a protocol described in the literature to generate the pseudo Ag|AgCl electrode (ROHAIZAD et al., 2019). To evaluate the stability of the Ag|AgCl pseudo-reference electrode, Figure 50 shows cyclic voltammograms (50 cycles) for $[Fe(CN)_6]^{3-/4-}$.

The voltammograms show the increase in anodic and cathodic currents of the redox probe in the first cycles which may indicate leaching of the Ag/AgCl pseudo reference electrode. After 50 cycles, the signal of the redox probe remained constant as also observed in the report that proposed such a procedure (JOÃO et al., 2020). Hence, it is

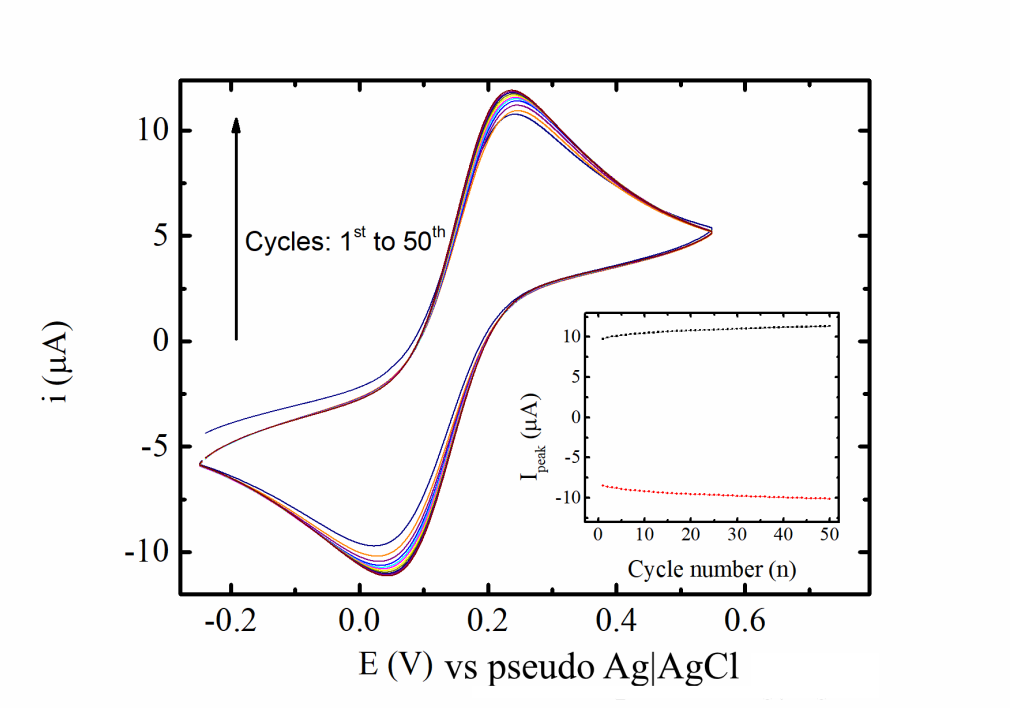

Figure 50 – Cyclic voltammetric recordings (from 1st to 50th cycles) of a stability experiment consisting of 50 continuous cycles in the presence of 1 mmol L^{-1} of the redox pair $[Fe(CN)_6]^{3-/4-}$ obtained on the TES-DLP device using the Ag|AgCl pseudo-reference electrode. Electrolyte: aqueous solution of 0.1 mol L^{-1} KCl; scan rate: 50 mV $s^{-}1$.

necessary to perform these voltammetric cycles to obtain a stable Ag/AgCl pseudo reference electrode. The silver pseudo-reference electrode reached RSD values of 4 % (both anodic and cathodic peak currents) within the 50 cycles.

To demonstrate the reproducibility of fabrication of the different devices using thermoplastic conductive electrodes by 3D-Pen, Figure 47 shows five overlapping cyclic voltammograms for $[Fe(CN)_6]^{3-/4-}$ obtained with five different devices, including the proposed WE-FDM, WE-DLP, TES-FDM, and TES-DLP systems and the commercially-available SPE-d110 (images of each device are presented as inset of Figure 42). Table 12 lists some electrochemical parameters obtained from data of Figure 43 Current values were divided by the respective geometric areas for a better comparison among the devices. Surface roughness obtained by AFM images (Figure 44) of the fabricated electrodes presented an average roughness of 0.28 ± 0.07 μm, which is statistically similar to the value found for the SPE (0.32 ± 0.09 μm). Hence, considering the surface roughness did not change in all electrodes, the estimation of current density values (μA cm^{-2}) was only valid for a comparison of the net current among the electrodes under a normalized electrode area.

When we compare the simpler designs consisting of a single working electrode (WE-FDM and WE-DLP), it is possible to note that the anodic peak potential of both designs presented similar behavior, with an oxidation peak at approximately 350 mV. Lower RSD

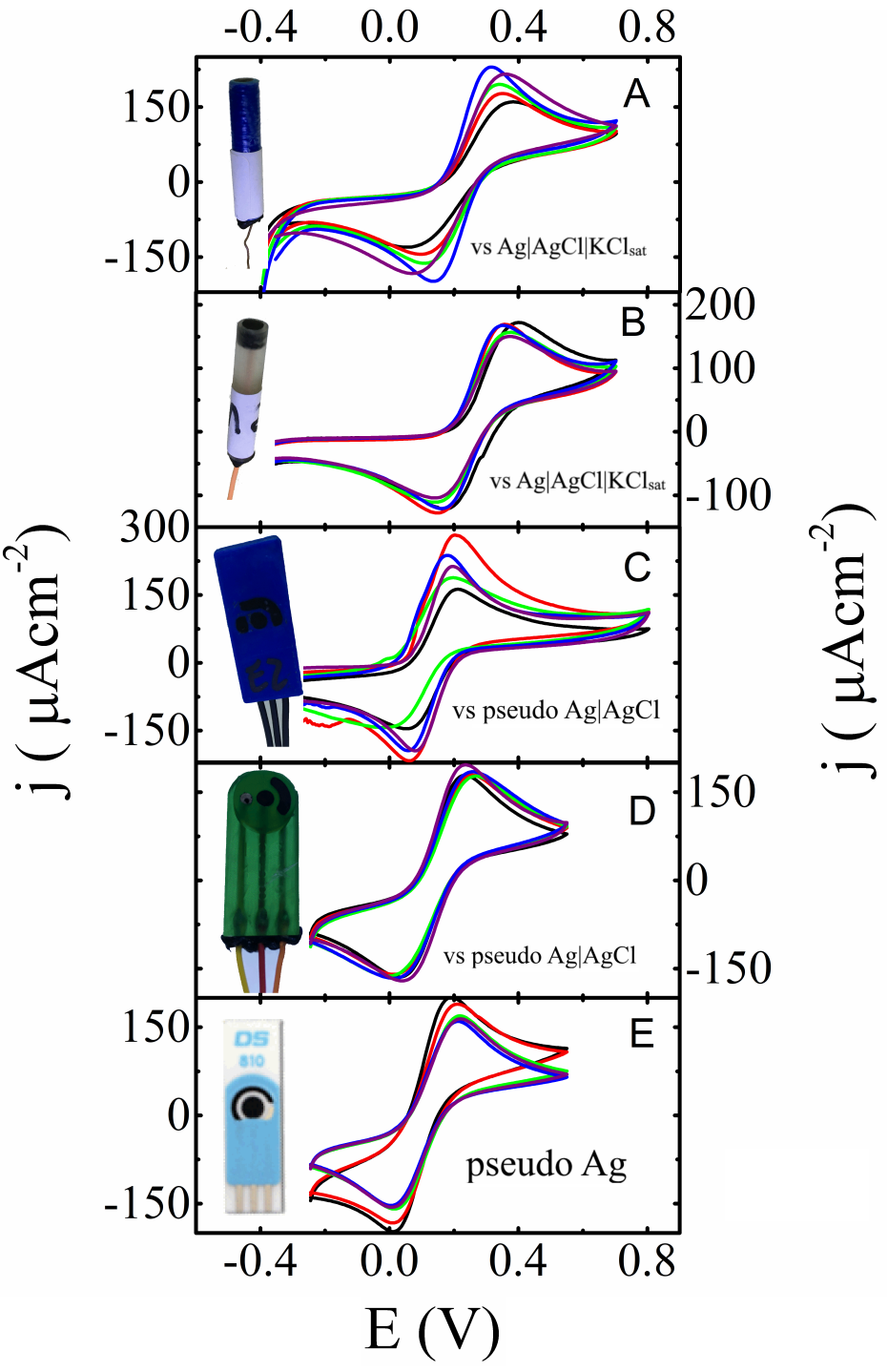

Figure 51 – Overlapping cyclic voltammograms of 1 mmol L^{-1} $[Fe(CN)_6]^{3-/4-}$ in aqueous 0.5 mol L^{-1} KCl obtained with: (A) WE-FDM; (B) WE-DLP; (C) TES-FDM; (D) TES-DLP; (E) SPE. Five responses correspond to the measures obtained in five different devices. Inset: real images of the devices.

Table 12 – Values (average ± SD) of peak-to-peak potential separation (ΔE), oxidation peak potential (Epa), current density (jpa), geometric measured area (A) and the respective relative standard deviation (RSD) values obtained from 5 units of each proposed device and compared with 5 units of commercial screen-printed electrodes (SPE).

Sensor type (n=5)	**ΔEp (mV)**	**Epa (mV)**	**jpa μAcm^{-2}**	**Geometric area (cm^2)**	**Inter-device RSD (Ep/Epa/jpa/A) (%)**
WE-FDM	224±40	340±26	120±19	0.118±0.002	18/8/16/2
WE-DLP	189±13	358±21	126±16	0.111±0.002	7/6/13/2
TES-FDM	134±24	193±10	137±31	0.091±0.007	18/5/23/7
TES-DLP	186±17	233±10	166±7	0.065±0.002	9/4/4/3
SPE-d110	179±14	179±14	160±12	0.13*	8/8/7/*

*area calculated according to manufacture documentation (inner diameter of 4 mm).

values of all parameters were verified for WE-DLP although the average geometric area presented similar values and standard deviation. Similarly, lower RSD values were verified using TES-DLP in comparison with TES-FDM. For these devices, the standard deviation of the geometric areas was lower for TES-DLP (3%) than TES-FDM (7%). Higher variation of the devices using theFDM 3D-printed substrates may be attributed to a deformability of the thermoplastic body (ABS) during the heated deposition step using the 3D-Pen. The temperature of the pen nozzle in the conductive thermoplastic deposition may cause small deformation on the area of the FDM 3D-printed substrate (body) during deposition, which did not occur when using the DLP 3D-printed substrates.

The cyclic voltammogram of the redox probe $[Fe(CN)_6]^{3-/4-}$ on a carbon black/PLA electrode fabricated by a desktop FDM 3D-printer was reported in the literature and a peak-to-peak separation of 151 mV was found (RICHTER et al., 2019). This value is within the range of values found for the electrodes fabricated using the 3D-Pen as shown in Table 12, especially considering the TES-FDM and TES-DLP devices. Hence, we can affirm the electrochemical activity of the electrodes fabricated either using a desktop FDM 3D-printer or a 3D-Pen towards the well-known redox probe $[Fe(CN)_6]^{3-/4-}$ is similar.

Although the SEM images show major surface differences of the electrodes originating from the different procedures and the slight difference in the $I_{(D)}/I_{(G)}$ ratios (data from Raman spectra) (surface characterization discussed in the previous section), the electrochemistry of the electrodes fabricated either using the 3D-Pen or the desktop 3D-printer is not significantly affected as shown in the voltammetric studies using the redox probe $[Fe(CN)_6]^{3-/4-}$.

The voltammetric profile for the redox probe obtained on the TES-DLP device was similar to the one obtained using the SPE (carbon working electrode). However, lower RSD values of current density and oxidation peak potential (as shown in Table 12) were obtained for the TES-DLP device, which indicates higher reproducibility than the com-

mercial SPE. This is a great advantage considering that part of the procedure involves the manipulation of a 3D-Pen. Due to its superior performance, TES-DLP was selected for TNT determination in single-drop solution.

5.5.3 TNT determination in a single drop on a planar three-electrode system (3D-Pen made)

In order to check the portability of proposed sensing device, the detection of TNT was carried out via square-wave voltammetry upon TES-DLP. The onsite detection of explosive residues is highly demanded (BOKOBZA; BRUNEEL; COUZI, 2015; ROHAIZAD et al., 2019; CASTRO et al., 2018). This device was selected among all others developed in this work due to the lower RSDs achieved during the intra-electrode studies and the presence of reference and auxiliary electrodes on the same device preventing any possible potential shift. The analysis was performed using a single-drop (100 μL) containing the analyte. This procedure reduces amount of solutions, samples and electrolyte, presenting quite favorable characteristics to green analytical chemistry. The voltammetric scans (n=3 for each concentration of TNT) are displayed in Figure 52 while inset is the respective analytical curve using average values (error bars are included for each point).

The SWV parameters as well as the background electrolyte were chosen based on a previous published work (CARDOSO et al., 2019). There was practically no variation in the electrochemical response in each triplicate for the increasing concentrations, showing that the proposed sensor is stable and presents satisfactory performance for TNT sensing. The proposed sensor provided a linear range of 5 to 500 μmol L^{-1}, a detection limit of 1.5 μmol L^{-1}, and RSD of 3.2% (n=10 for 100 μmol L^{-1}). The analytical features of the proposed sensor may not provide the best detectability in comparison with previous works that used graphene-based modified electrodes (CASTRO et al., 2018; TAN; CHUA; PUMERA, 2013; ZHANG et al., 2018) however, this is a low-cost device for TNT sensing in a droplet not previously described. Thus, these results show that the TES-DLP device is a low-cost and portable alternative platform to perform TNT detection with an extra advantage of reuse by polishing and renewing the surface (not possible if the electrode surface is chemically-modified). Experiments using the same electrode submitted to polishing and electrochemical activation were performed resulting in RSD values lower than 10% (n=3). Table 13 summarizes a literature overview for the electroanalytical sensing of TNT on a range of electrochemical platforms employing disposable and semi-disposable electrodes.

Disposable and semi-disposable electrodes have been widely used in the detection and determination of TNT (BHALLA; ZHAO; ZAZUBOVICH, 2011; CARDOSO et al., 2020; CASTRO et al., 2019; CAYGILL et al., 2013a; PESAVENTO et al., 2013; SINGH et al., 2016; WANG et al., 1998; WANG; THONGNGAMDEE; KUMAR, 2004; ZHANG et al.,

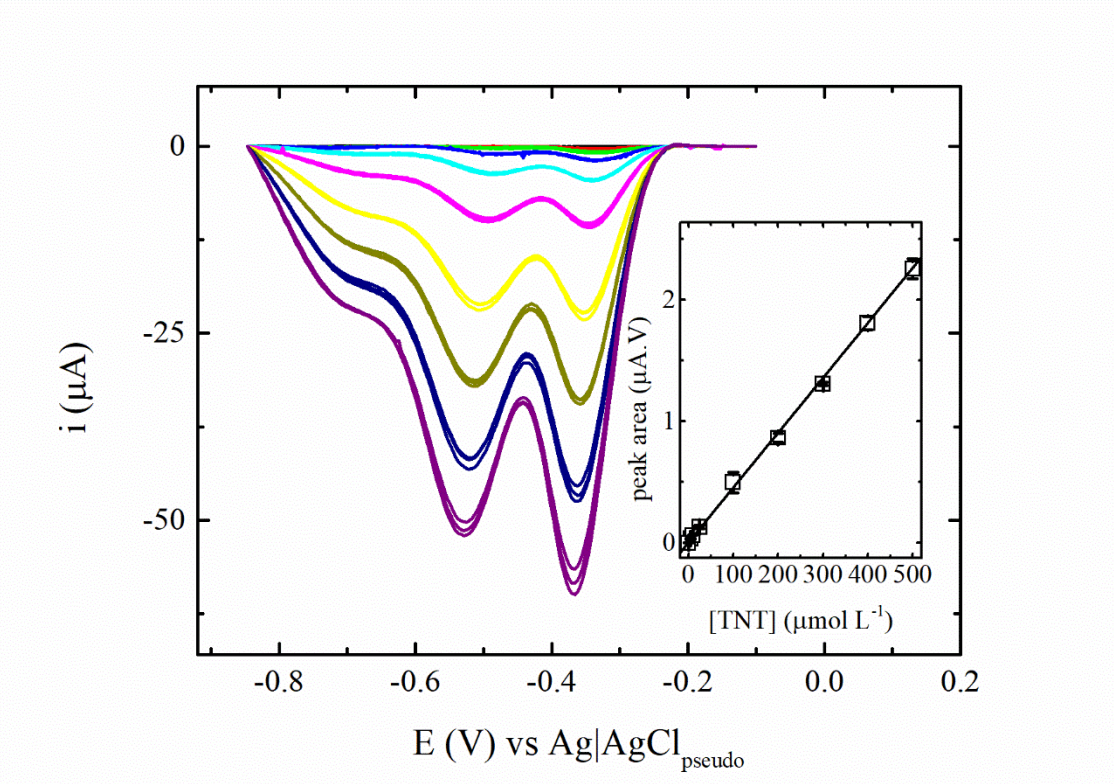

Figure 52 – Baseline-corrected square-wave voltammograms of triplicate scans of single-drops (100 μL) of crescent concentrations of TNT (from 5 to 500 μmol L^{-1}). The inset corresponds to the respective analytical curve (R^2>0.99) obtained using the area of the first peak at around -0.35 V vs Ag|AgCl pseudo reference. Electrochemical parameters: step potential of 4 mV, amplitude of 4 mV, frequency of 30 Hz, and 0.1 mol L^{-1} HCl as background electrolyte in 1% (v/v) acetonitrile.

Table 13 – Literature overview for electrochemical sensors of TNT produced on a range of electrochemical platforms employing disposable and semi-disposable electrodes.

Electrode[1]	**Detection technique**	**Linear range (μmol L^{-1})**	**LOD (μmol L^{-1})**	**Ref.**
PS II/Au-SPE	Photo-electrochemical	1 to 500	0.378	(BHALLA; ZHAO; ZAZUBOVICH, 2011)
SPCE	CV	1 to 200	0.4	(CAYGILL et al., 2013a)
CoPc/SPCE	CV	0 to 200	1 and 0.3*	(CAYGILL et al., 2013b)
Glyc-AgNPs/SPE	DPV	1x10-4 to 1x105	NM**	(SINGH et al., 2016)
PPf-SPCE	SWV	8.8 to 70.44***	4.4***	(WANG; THONGNGAMDEE; KUMAR, 2004)
SPCE	SWV	4.40 to 44.03***	0.88***	(WANG et al., 1998)
Pep-SPEs	Impedance	NM**	0.709	(ZHANG et al., 2015)
G-PLA	SWV	1 to 870	0.40	(CARDOSO et al., 2020); chapter 3
MIP-SPE	DPV	up to 20	0.5	(PESAVENTO et al., 2013)
GS	SWV	1 to 1300	0.06	(CASTRO et al., 2019)
TES-DLP	SWV	5 to 500	1.5	This work

*1 mol L^{-1} for the oxidative peak O1 and 0.3 μmol L^{-1} for the reductive peak R2.
**NM- not mentioned.
***Converted values considering the molar mass of TNT as 227.13 g mol^{-1}.

2015). It is possible to observe that screen-printed electrodes have been proposed and, in some cases, provided better electrochemical performance towards TNT sensing than the proposed protocol. Various of these works have utilized SPEs as substrates in the preparation of chemically modified electrodes (CAYGILL et al., 2013b; PESAVENTO et al., 2013; SINGH et al., 2016; WANG; THONGNGAMDEE; KUMAR, 2004) and biosensors (BHALLA; ZHAO; ZAZUBOVICH, 2011; ZHANG et al., 2015). Thus, although these sensors often present analytical performance superior, it must be emphasized that the electrode modification process provides some drawbacks, such as an increase in the steps of an analytical procedure (time-consuming) and in cost per analysis, moreover, in several cases leads to losses in reproducibility. Additionally, in the manufacture of the biosensors, molecules highly influenced by pH and temperature of the medium have been used and despite the increase in selectivity and detectability, depending on reaction conditions, losses in analytical performance may occur (BHALLA; ZHAO; ZAZUBOVICH, 2011; ZHANG et al., 2015). (Table 13) employed a 3D-printed graphene/PLA-based electrode for the TNT determination (CARDOSO et al., 2020), and it is possible to note that the analytical characteristics achieved are quite similar to those acquired in this work; however, a previous treatment step was applied by using a toxic organic solvent dimethylformamide (DMF) and larger solution volume for analysis, which is not in accordance with the principles of green chemistry. On the other hand, we developed a protocol that uses a basic aqueous solution for the treatment of the electrode surface and, in addition, it is worth mentioning that the TNT determination was performed in a single drop, being a complete environmentally-friendly protocol, since it does not use toxic organic solvents and provides a low consumption of reagents and sample.

Taking into consideration the time and cost of electrode fabrication and materials, the combination of additive manufacturing techniques (FDM and DLP) with 3D-Pen appears as an interesting alternative for the construction of integrated 3-in-1 electrochemical devices. Devices obtained with the conductive thermoplastic, wires and the FDM printed substrate reached values lower than \$0.50 (WE-FDM= \$0.13 and TES-FDM = \$0.38). Resin-based DLP 3D-printers presented almost the same production cost (WE-DLP= \$0.19 and TES-DLP= \$0.45).

Hence, the 3D-Pen can be used to manufacture electrodes over different substrates with a reduced cost and easy manufacturing operation and for this reason is promising in the fabrication of electrochemical sensors. These electrodes could be reused after a simple mechanical polishing at least three times, which was also reported for screen-printed electrodes (CUMBA et al., 2016; LEE; ARRIGAN; SILVESTER, 2016). However, commercial acquisition cost per unit of screen-printed electrodes is much higher than these values above-mentioned,. Additionally, typical technical problems not described in 3D-printing using new filaments, such as nozzle clogging, is much easily overcome using the 3D-printing pen as it is a hand-held device rapidly opened for cleaning. This statement is

crucial in the evaluation of the printability of novel conductive filaments and the 3D-Pen can be used quickly for such investigations. Moreover, other low-cost substrates could be applied in combination with a 3D-Pen to fabricate thermoplastic electrodes.

5.6 Conclusions

All proposed sensors manufactured using the 3D-Pen combined with customized FDM or DLP 3D-printed substrates achieved satisfactory performance compared with a commercially-available carbon SPE and desktop FDM 3D-printed electrodes. To demonstrated the potential of a 3D-Pen working with conductive filaments in the fabrication of electrochemical thermoplastic electrodes, we proposed two designs, a single working electrode and a three-electrode system on a planar substrate. Both devices presented low cost of fabrication (from \$0.13 to \$0.45) and were watertight leading to a long-term stability. Regarding inter-electrode precision, the TES-DLP presented excellent performance (RSD=4%), better than a commercial carbon SPE, even considering that the proposed procedure involves the handling of a 3D-Pen. High reproducibility of fabrication was possible due to the use 3D-printed templates. Considering the geometric areas of the working electrodes, the fabrication protocol is also very reproducible (RSD<7%). Electrochemical characterization showed similar properties to a screen−printed carbon electrode and desktop 3D-printed electrode. Raman spectroscopy and SEM images showed similar morphological characteristics of the electrodes fabricated by both procedures. The same techniques revealed PLA degradation after electrochemical treatment using NaOH of carbon black/PLA electrodes fabricated by both procedures (3D-Pen and desktop 3D-printer), which confirms PLA consumption as the main reason for the great improvement of electrochemical performance rather than increase in structural defects. The TES-DLP device was successfully applied for sensing TNT in a single drop, with sensing properties comparable to other electrochemical sensors except to electrodes that present surface chemical modification; however, such protocols are time-consuming and do not allow surface renewal after simple mechanical polishing as the proposed electrodes fabricated using the 3D-Pen. This work shows some possibilities of using a 3D-Pen to manufacture thermoplastic electrochemical sensors, however, many other designs can be explored as well as different low-cost substrates, such as recycled polymers or paper.

5.7 Acknowledgements

The authors are grateful to CNPq (427731/2018-6, 307271/2017-0, and 208504/2018-6), FAPEMIG (RED-00042-16 and APQ-03141-18), CAPES (001), and INCTBio (CNPq grant no. 465389/2014–7) for financial support. We are also thankful to the Institute of Physics (INFIS) of the Federal University of Uberlandia for Raman (Horiba

LabRAM HR Evolution Raman) spectroscopic measurements supported by the grant "Pró-Equipamentos" from the Brazilian agency CAPES and by FINEP and to Prof. Edson Nossol for helpful discussion on the morphological characterization of the electrodes. This study was financed in part by the Coordenação de Aperfeiçoamento de Pessoal de Nível Superior – Brasil (CAPES) – Finance Code 001

Chapter 6

Conclusion

This chapter contains all the conclusions obtained from this research, with limitations, perspectives and future investigations. In general the proposed sensors and cells developed using additive manufacture overcame expectations regarding electrodes prototyping and platform production. The low cost, easy operation and aparatus build on-demand are the highlights of the obtained results.

The 3D-printed electrodes have the advantage of very low cost, specially if built with a 3D-pen using Proto-Pasta filament. The price of acquisition of Black-Magic (G-PLA electrodes) filament is 10 times superior in US dollars when compared with the filament with carbon-black ($1 vs $0.1 per gram respectively)

The proposed electrodes based on FDM printers or 3D-pen have a limitation to organic solvents, for example, in alcoholic concentration up to 30%(v/v) the electrode will start to degrade. In other solvents such as acetonitrile, DMF or acetone no more than 5% (v/v) in aqueous solution is tolerated by the electrode.

6.1 Addressal of objectives

As previously mentioned, the purpose of this thesis is to demonstrate the potential of additive prototyping and manufacture of electroanalytical devices. The following objectives were addressed in this thesis:

1. All planar working electrodes commercially-available or custom-built with planar characteristics can be attached to the proposed multiuse (BIA, FIA, or batch) cell, as cited in Chapter III. As perspective, this cell was already improved and will be demonstrated in the next publications.

2. Another addressed objective is the promising results obtained with 3D-printed electrode, in the format of a strip, semi-flexible and inexpensive (0.3$ each).The electrode was subjected to a mechanical polishing, as a pre-treatment step, to renew

the electrode surface. The sensor showed applicability for catecholamines as a proof of concept, as well as for the redox probe hexaminruthenium(III).

3. The proposed strip sensor was evaluated to actuate as on demand explosive sampler and analyser. The graphene based thermoplastic electrode was able to reach high detectability of TNT residues by SWV and can be applied as a sampler in case of in field investigations in order to track the explosive production or include evidences for a crime investigation.

4. In clinical area, the G-PLA electrode was successfully applied at simultaneous quantification of NIT and UA in different biological samples. Urine and saliva were subjected to a simple dilution and then analyzed by pulsed amperometry, in a batch injection analysis system.

5. A biosensor was developed using the G-PLA electrode as substrate for an enzyme based device. Oxygenated groups from the electrode polymeric matrix provides suitable condition to enzyme immobilization by cross-linking with glutaraldehyde.

6. A 3D-printing pen was successfully used as a tool for sensors manufacture, where despite the fact that appears to be running in opposite direction of automated process, it can be a future solution for conductive thermoplastics, where the printability will not be an issue when working with higher carbonaceous ratio in proposed custom formulations of filaments.

Bibliography

AMBROSI, A.; PUMERA, M. 3D-printing technologies for electrochemical applications. **Chemical Society Reviews**, Royal Society of Chemistry, v. 45, n. 10, p. 2740–2755, 2016. ISSN 14604744. Disponível em: <http://dx.doi.org/10.1039/C5CS00714C>.

ANGNES, L. et al. Gold electrodes from recordable CDs. **Analytical Chemistry**, American Chemical Society, v. 72, n. 21, p. 5503–5506, 2000. ISSN 00032700. Disponível em: <http://pubs.acs.org/doi/abs/10.1021/ac000437p>.

BALLESTA-CLAVER, J. et al. Disposable luminol copolymer-based biosensor for uric acid in urine. **Analytica Chimica Acta**, v. 702, n. 2, p. 254–261, 2011. ISSN 00032670. Disponível em: <http://www.sciencedirect.com/science/article/pii/S0003267011009123>.

BHALLA, V.; ZHAO, X.; ZAZUBOVICH, V. Detection of explosive compounds using Photosystem II-based biosensor. **Journal of Electroanalytical Chemistry**, v. 657, n. 1-2, p. 84–90, 2011. ISSN 15726657. Disponível em: <http://www.sciencedirect.com/science/article/pii/S1572665711001639>.

Bin Hamzah, H. H. et al. The effects of printing orientation on the electrochemical behaviour of 3D printed acrylonitrile butadiene styrene (ABS)/carbon black electrodes. **Scientific Reports**, Springer US, v. 8, n. 1, p. 1–8, 2018. ISSN 20452322. Disponível em: <http://dx.doi.org/10.1038/s41598-018-27188-5>.

BOKOBZA, L.; BRUNEEL, J.-L.; COUZI, M. Raman Spectra of Carbon-Based Materials (from Graphite to Carbon Black) and of Some Silicone Composites. **C**, v. 1, n. 1, p. 77–94, 2015. ISSN 2311-5629.

BRETT, C. M.; BRETT, A. M. O.; MITOSERIU, L. C. Amperometric batch injection analysis: Theoretical aspects of current transients and comparison with wall-jet electrodes in continuous flow. **Electroanalysis**, v. 7, n. 3, p. 225–229, mar 1995. ISSN 15214109. Disponível em: <http://doi.wiley.com/10.1002/elan.1140070305>.

BROCENSCHI, R. F. et al. Use of a boron-doped diamond electrode to assess the electrochemical response of the naphthol isomers and to attain their truly simultaneous electroanalytical determination. **Electrochimica Acta**, Pergamon, v. 243, p. 374–381, jul 2017. ISSN 00134686. Disponível em: <http://www.sciencedirect.com/science/article/pii/S0013468617310162>.

BROWNE, M. P. et al. 3D Printed Graphene Electrodes' Electrochemical Activation. **ACS Applied Materials and Interfaces**, American Chemical Society, n. 46, p. 40294–40301, nov 2018. ISSN 19448252.

BROWNSON, D. A.; KELLY, P. J.; BANKS, C. E. In situ electrochemical characterisation of graphene and various carbon-based electrode materials: An internal standard approach. **RSC Advances**, Royal Society of Chemistry, v. 5, n. 47, p. 37281–37286, 2015. ISSN 20462069. Disponível em: <http://xlink.rsc.org/?DOI=C5RA03049Hhttp://dx.doi.org/10.1039/C5RA03049H>.

BRYAN, N. S. et al. Nitrite is a Signaling Molecule and Regulator of Gene Expression in Mammalian Tissues. **Nature Chemical Biology**, v. 1, n. 5, p. 290–297, 2005. ISSN 15524469. Disponível em: <https://doi.org/10.1038/nchembio734>.

BRYDSON, J. Plastics Based on Styrene. In: BRYDSON, J. A. B. T. P. M. S. E. (Ed.). **Plastics Materials**. Oxford: Butterworth-Heinemann, 1999. p. 425–465. ISBN 978-0-7506-4132-6. Disponível em: <http://www.sciencedirect.com/science/article/pii/B9780750641326500577>.

CAETANO, L. P. et al. Carbon-nanotube Modified Screen-printed Electrode for the Simultaneous Determination of Nitrite and Uric Acid in Biological Fluids Using Batch-injection Amperometric Detection. **Electroanalysis**, John Wiley & Sons, Ltd, v. 30, n. 8, p. 1862–1871, aug 2018. ISSN 15214109.

CARDOSO, R. M. et al. 3D-printed flexible device combining sampling and detection of explosives. **Sensors and Actuators B: Chemical**, Elsevier, v. 292, p. 308–313, 2019.

_____. Drawing Electrochemical Sensors Using a 3D Printing Pen. **Journal of the Brazilian Chemical Society**, scielo, v. 31, p. 1764 – 1770, 09 2020. ISSN 0103-5053. Disponível em: <http://www.scielo.br/scielo.php?script=sci_arttext&pid=S0103-50532020000901764&nrm=iso>.

_____.

_____. 3D printing for electroanalysis: From multiuse electrochemical cells to sensors. **Analytica Chimica Acta**, v. 1033, p. 49 – 57, 2018. ISSN 0003-2670. Disponível em: <http://www.sciencedirect.com/science/article/pii/S0003267018307864>.

_____. Multi-walled carbon nanotubes: Size-dependent electrochemistry of phenolic compounds. **Electrochimica Acta**, v. 176, p. 36–43, sep 2015. ISSN 00134686. Disponível em: <http://linkinghub.elsevier.com/retrieve/pii/S0013468615300281>.

_____. 3D-Printed graphene/polylactic acid electrode for bioanalysis: Biosensing of glucose and simultaneous determination of uric acid and nitrite in biological fluids. **Sensors and Actuators, B: Chemical**, v. 307, p. 127621, 2020. ISSN 09254005. Disponível em: <http://www.sciencedirect.com/science/article/pii/S0925400519318209>.

CASTRO, S. V. et al. Graphite sheet as a novel material for the collection and electrochemical sensing of explosive residues. **Talanta**, v. 203, p. 106–111, 2019. ISSN 00399140. Disponível em: <http://www.sciencedirect.com/science/article/pii/S0039914019305326>.

_____. Highly-sensitive voltammetric detection of trinitrotoluene on reduced graphene oxide/carbon nanotube nanocomposite sensor. **Analytica Chimica Acta**, v. 1035, p. 14–21, 2018. ISSN 18734324. Disponível em: <http://www.sciencedirect.com/science/article/pii/S0003267018308201>.

CAYGILL, J. S. et al. Disposable screen-printed sensors for the electrochemical detection of TNT and DNT. **Analyst**, The Royal Society of Chemistry, v. 138, n. 1, p. 346–352, 2013. ISSN 13645528. Disponível em: <http://dx.doi.org/10.1039/C2AN36351H>.

_____. Electrochemical Detection of TNT at Cobalt Phthalocyanine Mediated Screen-Printed Electrodes and Application to Detection of Airborne Vapours. **Electroanalysis**, John Wiley & Sons, Ltd, v. 25, n. 11, p. 2445–2452, nov 2013. ISSN 10400397. Disponível em: <https://doi.org/10.1002/elan.201300327>.

CHEN, C. et al. 3D-printed microfluidic devices: fabrication, advantages and limitations - a mini review. **Analytical Methods**, Royal Society of Chemistry, v. 8, n. 31, p. 6005–6012, 2016. ISSN 17599679. Disponível em: <http://dx.doi.org/10.1039/C6AY01671E>.

_____. High-performance amperometric biosensors and biofuel cell based on chitosan-strengthened cast thin films of chemically synthesized catecholamine polymers with glucose oxidase effectively entrapped. **Biosensors and Bioelectronics**, v. 26, n. 5, p. 2311–2316, 2011. ISSN 09565663. Disponível em: <http://www.sciencedirect.com/science/article/pii/S0956566310006846>.

CHIENG, B. W. et al. Effects of graphene nanoplatelets and reduced graphene oxide on poly(lactic acid) and plasticized poly(lactic acid): A comparative study. **Polymers**, v. 6, n. 8, p. 2232–2246, 2014. ISSN 20734360.

COCOVI-SOLBERG, D. J.; WORSFOLD, P. J.; MIRÓ, M. Opportunities for 3D printed millifluidic platforms incorporating on-line sample handling and separation. **TrAC - Trends in Analytical Chemistry**, v. 108, p. 13–22, 2018. ISSN 18793142. Disponível em: <http://www.sciencedirect.com/science/article/pii/S0165993618303005>.

CONTRASP. **Pesquisa nacional de ataque a bancos**. CONTRASP - Confederação Nacional de trabalhadores de segurança privada, 2018. Disponível em: <http://contrasp.org.br/wp-content/uploads/2018/01/RELATORIO-ANUAL-BANCOS.pdf>.

CREVILLEN, A. G. et al. The preferential electrocatalytic behaviour of graphite and multiwalled carbon nanotubes on enediol groups and their analytical implications in real domains. **Analyst**, v. 134, n. 4, p. 657–662, 2009. ISSN 13645528.

CUMBA, L. R. et al. Can the mechanical activation (polishing) of screen-printed electrodes enhance their electroanalytical response? **Analyst**, v. 141, n. 9, p. 2791–2799, 2016. ISSN 13645528.

Da Silva, R. A. B. et al. Batch injection analysis with amperometric detection: Application for simultaneous analysis using a single working electrode. **Analytical Methods**, The Royal Society of Chemistry, v. 3, n. 12, p. 2804–2808, dec 2011. ISSN 17599660. Disponível em: <http://xlink.rsc.org/?DOI=c1ay05395ghttp://dx.doi.org/10.1039/C1AY05395G>.

da Silva, R. A. B. et al. Development of a simple and fast electrochemical method to evaluate physical stress in athletes. **Electroanalysis**, v. 23, n. 11, p. 2601–2606, 2011. ISSN 10400397. Disponível em: <http://doi.wiley.com/10.1002/elan.201100326>.

DIAS, A. A. et al. Paper-based enzymatic reactors for batch injection analysis of glucose on 3D printed cell coupled with amperometric detection. **Sensors and Actuators, B: Chemical**, v. 226, p. 196–203, apr 2016. ISSN 09254005. Disponível em: <http://linkinghub.elsevier.com/retrieve/pii/S0925400515306225https://linkinghub.elsevier.com/retrieve/pii/S0925400515306225>.

DIXIT, C. K.; KADIMISETTY, K.; RUSLING, J. 3D-printed miniaturized fluidic tools in chemistry and biology. **TrAC - Trends in Analytical Chemistry**, Elsevier Ltd, v. 106, p. 37–52, 2018. ISSN 18793142. Disponível em: <http://www.sciencedirect.com/science/article/pii/S0165993618302449https://doi.org/10.1016/j.trac.2018.06.013>.

DONNET, J.-B. et al. Conducting Carbon Black. In: **Carbon Black**. [S.l.]: Routledge, 2018. p. 271–288.

DUL, S.; FAMBRI, L.; PEGORETTI, A. Fused deposition modelling with ABS-graphene nanocomposites. **Composites Part A: Applied Science and Manufacturing**, v. 85, p. 181–191, 2016. ISSN 1359835X. Disponível em: <http://www.sciencedirect.com/science/article/pii/S1359835X16300306>.

ECKMANN, A. et al. Probing the nature of defects in graphene by Raman spectroscopy. **Nano Letters**, v. 12, n. 8, p. 3925–3930, 2012. ISSN 15306984.

ELDER, B. et al. **Nanomaterial Patterning in 3D Printing**. 2020. 1–42 p.

ESCOBEDO, P. et al. Smartphone-based diagnosis of parasitic infections with colorimetric assays in centrifuge tubes. **IEEE Access**, v. 7, p. 185677–185686, 2019. ISSN 21693536.

FIORITO, P. A.; BRETT, C. M.; Córdoba De Torresi, S. I. Polypyrrole/copper hexacyanoferrate hybrid as redox mediator for glucose biosensors. **Talanta**, v. 69, n. 2 SPEC. ISS., p. 403–408, 2006. ISSN 00399140.

FLOWERS, P. F. et al. 3D printing electronic components and circuits with conductive thermoplastic filament. **Additive Manufacturing**, Elsevier B.V., v. 18, n. 2017, p. 156–163, 2017. ISSN 22148604. Disponível em: <http://dx.doi.org/10.1016/j.addma.2017.10.002>.

FOO, C. Y. et al. Three-Dimensional Printed Electrode and Its Novel Applications in Electronic Devices. **Scientific Reports**, Springer US, v. 8, n. 1, p. 1–11, 2018. ISSN 20452322. Disponível em: <http://dx.doi.org/10.1038/s41598-018-25861-3>.

FOSTER, C. W. et al. 3D Printed Graphene Based Energy Storage Devices. **Scientific Reports**, v. 7, n. October 2016, p. 42233, 2017. ISSN 20452322. Disponível em: <http://www.nature.com/articles/srep42233>.

_____. Additively manufactured graphitic electrochemical sensing platforms. **Chemical Engineering Journal**, v. 381, p. 122343, 2020. ISSN 13858947. Disponível em: <http://www.sciencedirect.com/science/article/pii/S1385894719317462>.

FRANCO, M. A. et al. An amperometric FIA system with carrier recycling: an environmentally friendly approach for atenolol determination in pharmaceutical formulations. **Analytical Methods**, v. 8, n. 48, p. 8420–8426, 2016. ISSN 17599679. Disponível em: <http://xlink.rsc.org/?DOI=C6AY02725C>.

FREITAS, J. M. et al. Simultaneous determination of three species with a single-injection step using batch injection analysis with multiple pulse amperometric detection. **Talanta**, Elsevier, v. 146, p. 670–675, jan 2016. ISSN 00399140. Disponível em: <http://linkinghub.elsevier.com/retrieve/pii/S0039914015300886http://dx.doi.org/10.1016/j.talanta.2015.06.048>.

GAO, J. et al. Simultaneous detection of glucose, uric acid and cholesterol using flexible microneedle electrode array-based biosensor and multi-channel portable electrochemical analyzer. **Sensors and Actuators, B: Chemical**, Elsevier, v. 287, n. January, p. 102–110, 2019. ISSN 09254005. Disponível em: <https://doi.org/10.1016/j.snb.2019.02.020>.

GIMENES, D. T. et al. Two new electrochemical methods for fast and simultaneous determination of codeine and diclofenac. **Talanta**, v. 116, p. 1026–1032, nov 2013. ISSN 00399140. Disponível em: <http://www.ncbi.nlm.nih.gov/pubmed/24148511http://linkinghub.elsevier.com/retrieve/pii/S0039914013006784>.

_____. Flow-injection amperometric method for determination of diclofenac in pharmaceutical formulations using a boron-doped diamond electrode. **Electroanalysis**, v. 23, n. 11, p. 2521–2525, 2011. ISSN 10400397.

GNANASEKARAN, K. et al. 3D printing of CNT- and graphene-based conductive polymer nanocomposites by fused deposition modeling. **Applied Materials Today**, Elsevier, v. 9, p. 21–28, dec 2017. ISSN 23529407. Disponível em: <http://ac.els-cdn.com/S2352940717300586/1-s2.0-S2352940717300586-main.pdf?{_}tid=4e94b702-5651-11e7-9fae-00000aab0f6c{&}acdnat=1498029467{_}ae80e6e1e966e472ba000f6a25409220https://www.sciencedirect.com/science/article/pii/S2352940>.

GROSS, B. C. et al. Evaluation of 3d printing and its potential impact on biotechnology and the chemical sciences. **Analytical Chemistry**, v. 86, n. 7, p. 3240–3253, 2014. PMID: 24432804. Disponível em: <https://doi.org/10.1021/ac403397r>.

GUO, J. Uric acid monitoring with a smartphone as the electrochemical analyzer. **Analytical Chemistry**, v. 88, n. 24, p. 11986–11989, 2016. ISSN 15206882.

GUSMÃO, R. et al. The capacitance and electron transfer of 3d-printed graphene electrodes are dramatically influenced by the type of solvent used for pre-treatment. **Electrochemistry Communications**, Elsevier, v. 102, p. 83–88, 2019.

GUSMÃO, R. et al. The capacitance and electron transfer of 3D-printed graphene electrodes are dramatically influenced by the type of solvent used for pre-treatment. **Electrochemistry Communications**, Elsevier, v. 102, n. April, p. 83–88, 2019. ISSN 13882481. Disponível em: <http://www.sciencedirect.com/science/article/pii/S1388248119300852https://doi.org/10.1016/j.elecom.2019.04.004>.

HABTAMU, H. B.; UGO, P. Miniaturized Enzymatic Biosensor via Biofunctionalization of the Insulator of Nanoelectrode Ensembles. **Electroanalysis**, John Wiley & Sons, Ltd, v. 27, n. 9, p. 2187–2193, sep 2015. ISSN 15214109. Disponível em: <https://doi.org/10.1002/elan.201500115>.

HAMZAH, H. H. et al. **3D printable conductive materials for the fabrication of electrochemical sensors: A mini review**. Elsevier B.V, 2018. 27–31 p. Disponível

em: <https://doi.org/10.1016/j.elecom.2018.09.006http://www.sciencedirect.com/science/article/pii/S1388248118302212>.

HERMANN, H.; GEBAUER, J.; KONIECZNY, P. Industrial nitration of toluene to dinitrotoluene. In: _____. **Nitration**. [s.n.]. cap. 21, p. 234–249. Disponível em: <https://pubs.acs.org/doi/abs/10.1021/bk-1996-0623.ch021>.

HONEYCHURCH, K. C. Cheap and disposable gold and silver electrodes: Trends in the application of compact discs and digital versatile discs for electroanalytical chemistry. **TrAC - Trends in Analytical Chemistry**, Elsevier, v. 93, p. 51–66, aug 2017. ISSN 18793142. Disponível em: <http://www.sciencedirect.com/science/article/pii/S0165993617301255?via{\%}3Di>.

HONEYCHURCH, K. C.; RYMANSAIB, Z.; IRAVANI, P. Anodic stripping voltammetric determination of zinc at a 3-D printed carbon nanofiber–graphite–polystyrene electrode using a carbon pseudo-reference electrode. **Sensors and Actuators, B: Chemical**, Elsevier B.V., v. 267, p. 476–482, 2018. ISSN 09254005. Disponível em: <https://doi.org/10.1016/j.snb.2018.04.054>.

HU, F. et al. Study on the application of reduced graphene oxide and multiwall carbon nanotubes hybrid materials for simultaneous determination of catechol, hydroquinone, p-cresol and nitrite. **Analytica Chimica Acta**, Elsevier B.V., v. 724, n. 2, p. 40–46, 2012. ISSN 00032670.

HUANG, T. et al. Oxidative polymerization of 5-hydroxytryptamine to physically and chemically immobilize glucose oxidase for electrochemical biosensing. **Analytica Chimica Acta**, v. 1013, p. 26–35, 2018. ISSN 18734324. Disponível em: <http://www.sciencedirect.com/science/article/pii/S0003267018302095>.

HULL, C. **Apparatus for production of three dimensional objects by Stereolithography**. Google Patents, 1986. 62–66 p. Disponível em: <https://www.google.nl/patents/US4575330>.

IIJIMA, S. Helical microtubules of graphitic carbon. **Nature**, Nature Publishing Group, v. 354, n. 6348, p. 56–58, 1991. ISSN 00280836.

IRKHAM; WATANABE, T.; EINAGA, Y. Hydroxide Ion Oxidation in Aqueous Solutions Using Boron-Doped Diamond Electrodes. **Analytical Chemistry**, American Chemical Society, v. 89, n. 13, p. 7139–7144, jul 2017. ISSN 15206882. Disponível em: <http://pubs.acs.org/doi/abs/10.1021/acs.analchem.7b01102>.

JAMES, P. E. et al. Nitrate pharmacokinetics: Taking note of the difference. **Nitric Oxide - Biology and Chemistry**, v. 48, p. 44–50, 2015. ISSN 10898611. Disponível em: <http://www.sciencedirect.com/science/article/pii/S1089860315002086>.

JBCS-YOUTUBE-CHANNEL. **Drawing Electrochemical Sensors Using a 3D Printing Pen**. 2020. Disponível em: <https://www.youtube.com/watch?v=ty4-tjpeKig&feature=youtu.be>.

JOÃO, A. F. et al. Additive-manufactured sensors for biofuel analysis: copper determination in bioethanol using a 3D-printed carbon black/polylactic electrode. **Analytical and Bioanalytical Chemistry**, v. 412, n. 12, p. 2755–2762, 2020. ISSN 16182650.

KALINKE, C. et al. Comparison of activation processes for 3D printed PLA-graphene electrodes: Electrochemical properties and application for sensing of dopamine. **Analyst**, The Royal Society of Chemistry, v. 145, n. 4, p. 1207–1218, 2020. ISSN 13645528. Disponível em: <http://dx.doi.org/10.1039/C9AN01926J>.

KATIC, V. et al. 3D Printed Graphene Electrodes Modified with Prussian Blue: Emerging Electrochemical Sensing Platform for Peroxide Detection. **ACS Applied Materials and Interfaces**, American Chemical Society, v. 11, n. 38, p. 35068–35078, sep 2019. ISSN 19448252. Disponível em: <https://doi.org/10.1021/acsami.9b09305>.

KATSELI, V.; ECONOMOU, A.; KOKKINOS, C. Single-step fabrication of an integrated 3D-printed device for electrochemical sensing applications. **Electrochemistry Communications**, Elsevier, v. 103, n. May, p. 100–103, 2019. ISSN 13882481. Disponível em: <https://linkinghub.elsevier.com/retrieve/pii/S138824811930116Xhttps://doi.org/10.1016/j.elecom.2019.05.008>.

_____. A novel all-3D-printed cell-on-a-chip device as a useful electroanalytical tool: Application to the simultaneous voltammetric determination of caffeine and paracetamol. **Talanta**, Elsevier B.V., v. 208, n. July 2019, p. 120388, 2020. ISSN 00399140. Disponível em: <https://doi.org/10.1016/j.talanta.2019.120388>.

KRONTHALER, M. et al. Laser cutting in the production of lithium ion cells. **Physics Procedia**, v. 39, p. 213 – 224, 2012. ISSN 1875-3892. Laser Assisted Net shape Engineering 7 (LANE 2012). Disponível em: <http://www.sciencedirect.com/science/article/pii/S187538921202559X>.

LEE, J.; ARRIGAN, D. W.; SILVESTER, D. S. Achievement of Prolonged Oxygen Detection in Room-Temperature Ionic Liquids on Mechanically Polished Platinum Screen-Printed Electrodes. **Analytical Chemistry**, v. 88, n. 10, p. 5104–5111, 2016. ISSN 15206882.

LI, M. et al. Recent developments and applications of screen-printed electrodes in environmental assays-A review. **Analytica Chimica Acta**, v. 734, p. 31–44, jul 2012. ISSN 00032670. Disponível em: <http://linkinghub.elsevier.com/retrieve/pii/S0003267012007295>.

LIN, M. J.; WU, C. C.; CHANG, K. S. **Effect of poly-l-lysine polycation on the glucose oxidase/ferricyanide composite-based second-generation blood glucose sensors**. 2019.

LIU, S.; JU, H. Reagentless glucose biosensor based on direct electron transfer of glucose oxidase immobilized on colloidal gold modified carbon paste electrode. **Biosensors and Bioelectronics**, v. 19, n. 3, p. 177–183, 2003. ISSN 09565663.

LIU, Y. Immobilization of glucose oxide with the blend of regenerated silk and poly(vinyl alcohol) and its application too 1, 1-dimethylferrocene-meaiating glucose sensor. **Applied Biochemistry and Biotechnology - Part A Enzyme Engineering and Biotechnology**, v. 62, n. 2-3, p. 105–117, 1997. ISSN 02732289. Disponível em: <http://www.ncbi.nlm.nih.gov/pubmed/9170249>.

López Marzo, A. M.; MAYORGA-MARTINEZ, C. C.; PUMERA, M. 3D-printed graphene direct electron transfer enzyme biosensors. **Biosensors and**

Bioelectronics, v. 151, p. 111980, 2020. ISSN 18734235. Disponível em: <http://www.sciencedirect.com/science/article/pii/S0956566319310577>.

LUO, L. et al. Simultaneous determination of epinephrine and uric acid at ordered mesoporous carbon modified glassy carbon electrode. **Analytical Methods**, v. 4, n. 8, p. 2417–2422, 2012. ISSN 17599660. Disponível em: <http://xlink.rsc.org/?DOI=c2ay25168j>.

MACDONALD, N. P. et al. Comparing microfluidic performance of three-dimensional (3d) printing platforms. **Analytical chemistry**, ACS Publications, v. 89, n. 7, p. 3858–3866, 2017.

MADHUVILAKKU, R. et al. Glassy carbon electrodes modified with reduced graphene oxide-MoS2-poly (3, 4-ethylene dioxythiophene) nanocomposites for the non-enzymatic detection of nitrite in water and milk. **Analytica Chimica Acta**, v. 1093, p. 93–105, 2020. ISSN 18734324. Disponível em: <http://www.sciencedirect.com/science/article/pii/S0003267019311146>.

MANZANARES-PALENZUELA, C. L. et al. Proteinase-sculptured 3D-printed graphene/polylactic acid electrodes as potential biosensing platforms: Towards enzymatic modeling of 3D-printed structures. **Nanoscale**, The Royal Society of Chemistry, v. 11, n. 25, p. 12124–12131, 2019. ISSN 20403372. Disponível em: <http://dx.doi.org/10.1039/C9NR02754H>.

_____. 3D-Printed Graphene/Polylactic Acid Electrodes Promise High Sensitivity in Electroanalysis. **Analytical Chemistry**, American Chemical Society, v. 90, n. 9, p. 5753–5757, may 2018. ISSN 15206882. Disponível em: <https://doi.org/10.1021/acs.analchem.8b00083>.

MATSUMOTO, K. et al. Simultaneous determination of glucose, fructose, and sucrose in mixtures by amperometric flow injection analysis with immobilized enzyme reactors. **Analytical Chemistry**, v. 60, n. 2, p. 147–151, 1988. PMID: 3348480. Disponível em: <https://doi.org/10.1021/ac00153a010>.

METTERS, J. P.; KADARA, R. O.; BANKS, C. E. New directions in screen printed electroanalytical sensors: An overview of recent developments. **Analyst**, v. 136, n. 6, p. 1067–1076, mar 2011. ISSN 13645528. Disponível em: <http://www.ncbi.nlm.nih.gov/pubmed/21283890http://xlink.rsc.org/?DOI=c0an00894j>.

_____. Electroanalytical properties of screen printed graphite microband electrodes. **Sensors and Actuators, B: Chemical**, v. 169, p. 136–143, 2012. ISSN 09254005.

MILENIUS, D. L. **ABS extrusion compositions**. Google Patents, 1979. Disponível em: <https://patents.google.com/patent/US4150009A/en>.

MONTI, L. D. et al. Endothelial nitric oxide synthase polymorphisms are associated with type 2 diabetes and the insulin resistance syndrome. **Diabetes**, v. 52, n. 5, p. 1270–1275, may 2003. ISSN 00121797. Disponível em: <http://diabetes.diabetesjournals.org/content/52/5/1270.abstract>.

MUÑOZ, R. A.; MATOS, R. C.; ANGNES, L. Amperometric determination of dipyrone in pharmaceutical formulations with a flow cell containing gold electrodes from recordable

compact discs. **Journal of Pharmaceutical Sciences**, v. 90, n. 12, p. 1972–1977, 2001. ISSN 00223549.

MURRAY, R. W. Chemically Modified Electrodes. **Accounts of Chemical Research**, American Chemical Society, v. 13, n. 5, p. 135–141, may 1980. ISSN 15204898. Disponível em: <https://doi.org/10.1021/ar50149a002>.

NEWMAN, J. D.; TURNER, A. P. Home blood glucose biosensors: A commercial perspective. **Biosensors and Bioelectronics**, v. 20, n. 12, p. 2435–2453, 2005. ISSN 09565663.

NI, Y. et al. A review of 3D-printed sensors. **Applied Spectroscopy Reviews**, v. 52, n. 7, p. 623–652, 2017. ISSN 1520569X.

NICHOLSON, R. S. Theory and Application of Cyclic Voltammetry for Measurement of Electrode Reaction Kinetics. **Analytical Chemistry**, v. 37, n. 11, p. 1351–1355, 1965. ISSN 15206882.

NOVOTNÝ, F. et al. Preserving Fine Structure Details and Dramatically Enhancing Electron Transfer Rates in Graphene 3D-Printed Electrodes via Thermal Annealing: Toward Nitroaromatic Explosives Sensing. **ACS Applied Materials and Interfaces**, American Chemical Society, v. 11, n. 38, p. 35371–35375, sep 2019. ISSN 19448252. Disponível em: <https://doi.org/10.1021/acsami.9b06683>.

OLIVEIRA, A. G.; MUNOZ, R. A. A.; ANGNES, L. Disposable graphite foil based electrodes and their application in pharmaceutical analysis. **Electroanalysis**, WILEY-VCH Verlag, v. 22, n. 12, p. 1290–1296, jun 2010. ISSN 10400397. Disponível em: <http://dx.doi.org/10.1002/elan.200900548>.

OLIVEIRA, L. C. A. de; SOUTO, R. C. F. Prevalence of urinary tract infection in ambulatory patients and its relationship to nitrite values and leukocytes. **Revista Brasileira de Análises Clínicas**, v. 50, n. 3, p. 237–243, 2018. ISSN 2448-3877.

OLIVEIRA, T. D. C. et al. A batch injection analysis system with square-wave voltammetric detection for fast and simultaneous determination of naphazoline and zinc. **Talanta**, Elsevier, v. 152, p. 308–313, may 2016. ISSN 00399140. Disponível em: <http://linkinghub.elsevier.com/retrieve/pii/S0039914016300972>.

O'NEIL, G. D. et al. Single-step fabrication of electrochemical flow cells utilizing multi-material 3D printing. **Electrochemistry Communications**, Elsevier, v. 99, n. November 2018, p. 56–60, 2019. ISSN 13882481. Disponível em: <https://doi.org/10.1016/j.elecom.2018.12.006>.

PANG, Y. et al. Additive Manufacturing of Batteries. **Advanced Functional Materials**, John Wiley & Sons, Ltd, v. 30, n. 1, p. 1906244, jan 2020. ISSN 16163028. Disponível em: <https://doi.org/10.1002/adfm.201906244>.

PEDROTTI, J. J.; ANGNES, L.; GUTZ, I. G. Miniaturized Reference Electrodes with Microporous Polymer Junctions. **Electroanalysis**, VCH Verlagsgesellschaft mbH, v. 8, n. 7, p. 673–675, jul 1996. ISSN 10400397. Disponível em: <http://doi.wiley.com/10.1002/elan.1140080713http://dx.doi.org/10.1002/elan.1140080713>.

PEREIRA, P. F. et al. Fast and simultaneous determination of nimesulide and paracetamol by batch injection analysis with amperometric detection on bare boron-doped diamond electrode. **Diamond and Related Materials**, v. 39, p. 41–46, oct 2013. ISSN 09259635. Disponível em: <http://linkinghub.elsevier.com/retrieve/pii/S0925963513001507>.

PESAVENTO, M. et al. Voltammetric platform for detection of 2,4,6-trinitrotoluene based on a molecularly imprinted polymer. **Analytical and Bioanalytical Chemistry**, v. 405, n. 11, p. 3559–3570, 2013. ISSN 16182642. Disponível em: <https://doi.org/10.1007/s00216-012-6553-y>.

POLLI, H. et al. Degradation behavior and kinetic study of ABS polymer. **Journal of Thermal Analysis and Calorimetry**, v. 95, n. 1, p. 131–134, 2009. ISSN 13886150. Disponível em: <https://doi.org/10.1007/s10973-006-7781-1>.

PRATER, T. et al. 3D Printing in Zero G Technology Demonstration Mission: complete experimental results and summary of related material modeling efforts. **International Journal of Advanced Manufacturing Technology**, v. 101, n. 1-4, p. 391–417, 2019. ISSN 14333015. Disponível em: <https://doi.org/10.1007/s00170-018-2827-7>.

RAVI, A. K.; DESHPANDE, A.; HSU, K. H. An in-process laser localized pre-deposition heating approach to inter-layer bond strengthening in extrusion based polymer additive manufacturing. **Journal of Manufacturing Processes**, v. 24, p. 179–185, 2016. ISSN 15266125. Disponível em: <http://www.sciencedirect.com/science/article/pii/S1526612516301013>.

RAYMUNDO-PEREIRA, P. A. et al. Thin Films and Composites Based on Graphene for Electrochemical Detection of Biologically-relevant Molecules. **Electroanalysis**, John Wiley & Sons, Ltd, v. 30, n. 9, p. 1888–1896, sep 2018. ISSN 15214109. Disponível em: <https://doi.org/10.1002/elan.201800283>.

RICCI, F.; PALLESCHI, G. Sensor and biosensor preparation, optimisation and applications of Prussian Blue modified electrodes. **Biosensors and Bioelectronics**, v. 21, n. 3, p. 389–407, 2005. ISSN 09565663.

RICHTER, E. M. et al. Complete Additively Manufactured (3D-Printed) Electrochemical Sensing Platform. **Analytical Chemistry**, American Chemical Society, v. 91, n. 20, p. 12844–12851, sep 2019. ISSN 15206882. Disponível em: <https://doi.org/10.1021/acs.analchem.9b02573>.

ROBERTS, L. D. et al. Inorganic nitrate promotes the browning of white adipose tissue through the nitrate-nitrite-nitric oxide pathway. **Diabetes**, v. 64, n. 2, p. 471–484, feb 2015. ISSN 1939327X. Disponível em: <http://diabetes.diabetesjournals.org/content/64/2/471.abstract>.

ROCHA, D. P. et al. Chemically versus electrochemically reduced graphene oxide: Improved amperometric and voltammetric sensors of phenolic compounds on higher roughness surfaces. **Sensors and Actuators, B: Chemical**, Elsevier B.V., v. 254, p. 701–708, jan 2018. ISSN 09254005. Disponível em: <http://www.sciencedirect.com/science/article/pii/S0925400517312777http://dx.doi.org/10.1016/j.snb.2017.07.070https://linkinghub.elsevier.com/retrieve/pii/S0925400517312777>.

_____. Improved electrochemical detection of metals in biological samples using 3D-printed electrode: Chemical/electrochemical treatment exposes carbon-black conductive sites. **Electrochimica Acta**, v. 335, p. 135688, 2020. ISSN 00134686. Disponível em: <http://www.sciencedirect.com/science/article/pii/S0013468620300797>.

ROCHA, R. G. et al. Production of 3d-printed disposable electrochemical sensors for glucose detection using a conductive filament modified with nickel microparticles. **Analytica Chimica Acta**, Elsevier, 2020.

RODRÍGUEZ-PANES, A.; CLAVER, J.; CAMACHO, A. M. The influence of manufacturing parameters on the mechanical behaviour of PLA and ABS pieces manufactured by FDM: A comparative analysis. **Materials**, v. 11, n. 8, 2018. ISSN 19961944.

ROGERS, C. I. et al. 3D printed microfluidic devices with integrated valves. **Biomicrofluidics**, v. 9, n. 1, p. 1–9, 2015. ISSN 19321058. Disponível em: <http://dx.doi.org/10.1063/1.4905840>.

ROHAIZAD, N. et al. 3D-printed Ag/AgCl pseudo-reference electrodes. **Electrochemistry Communications**, Elsevier, v. 103, p. 104–108, may 2019. ISSN 13882481. Disponível em: <https://www.sciencedirect.com/science/article/pii/S1388248119301183>.

ROSSINI, E. L. et al. Simultaneous determination of renal function biomarkers in urine using a validated paper-based microfluidic analytical device. **Analytica Chimica Acta**, v. 997, p. 16–23, 2018. ISSN 18734324. Disponível em: <http://www.sciencedirect.com/science/article/pii/S0003267017311777>.

RYMANSAIB, Z. et al. All-Polystyrene 3D-Printed Electrochemical Device with Embedded Carbon Nanofiber-Graphite-Polystyrene Composite Conductor. **Electroanalysis**, v. 28, n. 7, p. 1517–1523, 2016. ISSN 15214109.

SAGLAM, S. et al. Electrochemical determination of tnt, dnt, rdx, and hmx with gold nanoparticles/poly (carbazole-aniline) film–modified glassy carbon sensor electrodes imprinted for molecular recognition of nitroaromatics and nitramines. **Analytical chemistry**, ACS Publications, v. 90, n. 12, p. 7364–7370, 2018.

SANOIT, J. D. et al. Electrochemical diamond sensors for tnt detection in water. **Electrochimica acta**, Elsevier, v. 54, n. 24, p. 5688–5693, 2009.

SANTOS, P. L. dos et al. Enhanced performance of 3D printed graphene electrodes after electrochemical pre-treatment: Role of exposed graphene sheets. **Sensors and Actuators, B: Chemical**, Elsevier, v. 281, n. November 2018, p. 837–848, feb 2019. ISSN 09254005. Disponível em: <https://doi.org/10.1016/j.snb.2018.11.013https://www.sciencedirect.com/science/article/pii/S0925400518319609?via{\%}3Di>.

SEAH, T. H. et al. Towards graphane applications in security: The electrochemical detection of trinitrotoluene in seawater on hydrogenated graphene. **Electroanalysis**, v. 26, n. 1, p. 62–68, 2014. ISSN 15214109.

SHAO, Y. et al. Graphene based electrochemical sensors and biosensors: A review. **Electroanalysis**, John Wiley & Sons, Ltd, v. 22, n. 10, p. 1027–1036, may 2010. ISSN 10400397. Disponível em: <https://doi.org/10.1002/elan.200900571>.

SHIMONI, Z. et al. Sensitivity of the dipstick in detecting bacteremic urinary tract infections in elderly hospitalized patients. **PLoS ONE**, Public Library of Science, v. 12, n. 10, p. e0187381, oct 2017. ISSN 19326203. Disponível em: <https://doi.org/10.1371/journal.pone.0187381>.

SILVA, T. A. et al. **Electrochemical biosensors based on nanostructured carbon black: A review**. [S.l.]: Hindawi Limited, 2017.

SIMON, W.; BOOTH, B. Analytical Method Validation. n. 2, p. 165–185, 2004.

SINGH, S. et al. Electrochemical sensing of nitro-aromatic explosive compounds using silver nanoparticles modified electrochips. **Analytical Methods**, The Royal Society of Chemistry, v. 8, n. 39, p. 7158–7169, 2016. ISSN 17599679. Disponível em: <http://dx.doi.org/10.1039/C6AY01945E>.

STEFANO, J. S. et al. Highly sensitive amperometric detection of drugs and antioxidants on non-functionalized multi-walled carbon nanotubes: Effect of metallic impurities? **Electrochimica Acta**, v. 240, p. 80–89, 2017. ISSN 00134686. Disponível em: <http://www.sciencedirect.com/science/article/pii/S0013468617308083>.

STOZHKO, N. et al. A nanostructured sensor based on gold nanoparticles and nafion for determination of uric acid. **Biosensors**, v. 8, n. 1, p. 5–10, 2018. ISSN 20796374.

TAN, S. M.; CHUA, C. K.; PUMERA, M. Graphenes prepared from multi-walled carbon nanotubes and stacked graphene nanofibers for detection of 2,4,6-trinitrotoluene (TNT) in seawater. **Analyst**, The Royal Society of Chemistry, v. 138, n. 6, p. 1700–1704, 2013. ISSN 13645528. Disponível em: <http://dx.doi.org/10.1039/C3AN00089C>.

TASHKHOURIAN, J.; DANESHI, M.; NAMI-ANA, S. F. Simultaneous determination of tyrosine and tryptophan by mesoporous silica nanoparticles modified carbon paste electrode using H-point standard addition method. **Analytica Chimica Acta**, v. 902, p. 89–96, 2016. ISSN 18734324. Disponível em: <http://www.sciencedirect.com/science/article/pii/S0003267015013161>.

TIAN, X. et al. Emerging 3D-Printed Electrochemical Energy Storage Devices: A Critical Review. **Advanced Energy Materials**, v. 7, n. 17, p. 1–17, 2017. ISSN 16146840.

TORMIN, T. F. et al. Fast simultaneous determination of BHA and TBHQ antioxidants in biodiesel by batch injection analysis using pulsed-amperometric detection. **Talanta**, v. 99, p. 527–531, sep 2012. ISSN 00399140. Disponível em: <http://linkinghub.elsevier.com/retrieve/pii/S0039914012004912>.

TRIGUEIRO, A. **Mais de 2,5 mil caixas eletrônicos são destruídos pelo Brasil em três anos**. Globo, 2012. Disponível em: <http://glo.bo/QBCpO9>.

TSIKAS, D.; SCHWARZ, A.; STICHTENOTH, D. O. simultaneous measurement of [15n]nitrate and [15n]nitrite enrichment and concentration in urine by gas chromatography mass spectrometry as pentafluorobenzyl derivatives. **Analytical Chemistry**, American Chemical Society, n. 6, p. 2585–2587, mar. ISSN 00032700.

VANĚČKOVÁ, E. et al. 3D printed polylactic acid/carbon black electrodes with nearly ideal electrochemical behaviour. **Journal of Electroanalytical Chemistry**, Elsevier B.V, v. 857, p. 113745, 2020. ISSN 15726657. Disponível em: <https://doi.org/10.1016/j.jelechem.2019.113745>.

_____. Copper electroplating of 3D printed composite electrodes. **Journal of Electroanalytical Chemistry**, v. 858, p. 113763, 2020. ISSN 15726657. Disponível em: <http://www.sciencedirect.com/science/article/pii/S1572665719310318>.

_____. UV/VIS spectroelectrochemistry with 3D printed electrodes. **Journal of Electroanalytical Chemistry**, v. 857, p. 113760, 2020. ISSN 15726657. Disponível em: <http://www.sciencedirect.com/science/article/pii/S1572665719310288>.

WAHEED, S. et al. 3D printed microfluidic devices: Enablers and barriers. **Lab on a Chip**, Royal Society of Chemistry, v. 16, n. 11, p. 1993–2013, may 2016. ISSN 14730189. Disponível em: <http://xlink.rsc.org/?DOI=C6LC00284F>.

WALTERS, J. G. et al. Trace Analysis of Heavy Metals (Cd, Pb, Hg) Using Native and Modified 3D Printed Graphene/Poly(Lactic Acid) Composite Electrodes. **Electroanalysis**, John Wiley & Sons, Ltd, v. 32, n. 4, p. 859–866, feb 2020. ISSN 15214109. Disponível em: <https://doi.org/10.1002/elan.201900658>.

WANG, J. Electrochemical glucose biosensors. **Chemical Reviews**, American Chemical Society, v. 108, n. 2, p. 814–825, feb 2008. ISSN 00092665. Disponível em: <https://doi.org/10.1021/cr068123a>.

WANG, J. et al. Screen-printed voltammetric sensor for TNT. **Talanta**, v. 46, n. 6, p. 1405–1412, 1998. ISSN 00399140. Disponível em: <http://www.sciencedirect.com/science/article/pii/S0039914098000058>.

WANG, J.; THONGNGAMDEE, S.; KUMAR, A. Highly stable voltammetric detection of nitroaromatic explosives in the presence of organic surfactants at a polyphenol-coated carbon electrode. **Electroanalysis**, John Wiley & Sons, Ltd, v. 16, n. 15, p. 1232–1235, aug 2004. ISSN 10400397. Disponível em: <https://doi.org/10.1002/elan.200302948>.

WANG, L. F.; RHIM, J. W.; HONG, S. I. Preparation of poly(lactide)/poly(butylene adipate-co-terephthalate) blend films using a solvent casting method and their food packaging application. **LWT - Food Science and Technology**, v. 68, p. 454–461, 2016. ISSN 00236438. Disponível em: <http://www.sciencedirect.com/science/article/pii/S0023643815304199>.

WANG, X. et al. 3D printing of polymer matrix composites: A review and prospective. **Composites Part B: Engineering**, v. 110, p. 442–458, 2017. ISSN 13598368. Disponível em: <http://www.sciencedirect.com/science/article/pii/S1359836816321230>.

WIRTH, D. M. et al. Electrolysis Activation of Fused-Filament-Fabrication 3D-Printed Electrodes for Electrochemical and Spectroelectrochemical Analysis. **Analytical Chemistry**, American Chemical Society, v. 91, n. 9, p. 5553–5557, may 2019. ISSN 15206882. Disponível em: <https://doi.org/10.1021/acs.analchem.9b01331>.

WONG, A. et al. An Overview of Pesticide Monitoring at Environmental Samples Using Carbon Nanotubes-Based Electrochemical Sensors. **C—Journal of Carbon**

Research, v. 3, n. 4, p. 8, mar 2017. ISSN 2311-5629. Disponível em: <http://www.mdpi.com/2311-5629/3/1/8>.

ZEN, J. M.; CHEN, P. J. A selective voltammetric method for uric acid and dopamine detection using clay-modified electrodes. **Analytical Chemistry**, American Chemical Society, v. 69, n. 24, p. 5087–5093, dec 1997. ISSN 00032700. Disponível em: <https://doi.org/10.1021/ac9703562>.

_____. An Ultrasensitive Voltammetric Method for Dopamine and Catechol Detection Using Clay-Modified Electrodes. **Electroanalysis**, v. 10, n. 1, p. 12–15, jan 1998. ISSN 10400397. Disponível em: <http://doi.wiley.com/10.1002/{\%}28SICI{\%}291521-4109{\%}28199801{\%}2910{\%}3A1{\%}3C12{\%}3A{\%}3AA>.

ZHANG, D. et al. Smartphone-based portable biosensing system using impedance measurement with printed electrodes for 2,4,6-trinitrotoluene (TNT) detection. **Biosensors and Bioelectronics**, Biosensor National Special Laboratory, Key Laboratory for Biomedical Engineering of Education Ministry, Department of Biomedical Engineering, Zhejiang University, Hangzhou 310027, PR China; Cyber Innovation Joint Research Center, Zhejiang University, Hang, v. 70, p. 81–88, 2015. ISSN 18734235. Disponível em: <http://europepmc.org/abstract/MED/25796040https://doi.org/10.1016/j.bios.2015.03.004>.

ZHANG, Q. et al. Biomineralization-mimetic preparation of robust metal-organic frameworks biocomposites film with high enzyme load for electrochemical biosensing. **Journal of Electroanalytical Chemistry**, v. 823, p. 40–46, 2018. ISSN 15726657. Disponível em: <http://www.sciencedirect.com/science/article/pii/S1572665718302698>.

ZHANG, R. et al. Graphene Nanoribbon-Supported PtPd Concave Nanocubes for Electrochemical Detection of TNT with High Sensitivity and Selectivity. **Analytical Chemistry**, American Chemical Society, v. 87, n. 24, p. 12262–12269, dec 2015. ISSN 15206882. Disponível em: <https://doi.org/10.1021/acs.analchem.5b03390>.

_____. Nitrogen and sulfur co-doped graphene nanoribbons: A novel metal-free catalyst for high performance electrochemical detection of 2, 4, 6-trinitrotoluene (TNT). **Carbon**, v. 126, p. 328–337, 2018. ISSN 00086223. Disponível em: <http://www.sciencedirect.com/science/article/pii/S0008622317310436>.

ZHAO, N. et al. Polylactide (PLA)/layered double hydroxides composite fibers by electrospinning method. **Journal of Physics and Chemistry of Solids**, v. 69, n. 5-6, p. 1564–1568, 2008. ISSN 00223697. Disponível em: <http://www.sciencedirect.com/science/article/pii/S0022369707006646>.

ZHU, C. et al. Highly compressible 3D periodic graphene aerogel microlattices. **Nature Communications**, Nature Publishing Group, v. 6, apr 2015. ISSN 20411723.

Annex

ANNEX A

Curriculum summary

All published works by the author of this thesis are listed below.

A.1 Thesis related papers

Published works in this section are related to this thesis.

- Cardoso, R. M., Mendonça, D. M., Silva, W. P., Silva, M. N., Nossol, E., da Silva, R. A., ... Muñoz, R. A. **(2018)**. 3D printing for electroanalysis: from multiuse electrochemical cells to sensors. **Analytica chimica acta**, 1033, 49-57.

- Cardoso, R. M., Castro, S. V., Silva, M. N., Lima, A. P., Santana, M. H., Nossol, E., ... Munoz, R. A. **(2019)**. 3D-printed flexible device combining sampling and detection of explosives.**Sensors and Actuators B: Chemical**, 292, 308-313.

- Cardoso, R. M., Silva, P. R., Lima, A. P., Rocha, D. P., Oliveira, T. C., do Prado, T. M., ... Muñoz, R. A. **(2020)**. 3D-Printed graphene/polylactic acid electrode for bioanalysis: Biosensing of glucose and simultaneous determination of uric acid and nitrite in biological fluids. **Sensors and Actuators B: Chemical**, 307, 127621.

- Cardoso, R. M., Kalinke, C., Rocha, R. G., dos Santos, P. L., Rocha, D. P., Oliveira, P. R., ... Munoz, R. A. **(2020)**. Additive-manufactured (3D-printed) electrochemical sensors: A critical review. **Analytica Chimica Acta** .

- Cardoso, R. M., Castro, S. V., Stefano, J. S., Muñoz, R. A. **(2020)**. Drawing Electrochemical Sensors Using a 3D Printing Pen. **Journal of the Brazilian Chemical Society**, 31(9), 1764-1770.

- Cardoso, R. M., Rocha, D. P., Rocha, R. G., Stefano, J. S., Silva, R. A., Richter, E. M., Muñoz, R. A. **(2020)**. 3D-printing pen versus desktop 3D-printers: Fabrication of carbon black/polylactic acid electrodes for single-drop detection of 2, 4, 6-trinitrotoluene. **Analytica Chimica Acta**, 1132, 10-19.

A.2 PDSE - International visitor scholar related papers

Published works related to the "Programa Institucional de Doutorado Sanduíche no Exterior", PDSE nº 88881.188561/2018-01.

- ❏ Cardoso, R. M., Santos, R. O. D., Munoz, R. A., Garcia, C. D., Blanes, L. **(2020)**. A Multi-Pump Magnetohydrodynamics Lab-On-A-Chip Device for Automated Flow Control and Analyte Delivery. **Sensors**, 4909, 20(17), 4909.

- ❏ Reed, P. A., Cardoso, R. M., Muñoz, R. A., Garcia, C. D. **(2020)**. Pyrolyzed cotton balls for protein removal: Analysis of pharmaceuticals in serum by capillary electrophoresis. . **Analytica Chimica Acta**

Collaboration works developed during PhD program.

A.3 Additional published papers

- ❏ Garcia Cardozo, C., Melo Cardoso, R., Matheus Guimarães Selva, T., Evaristo de Carvalho, A., Torres Pio dos Santos, W., Regis Longo Cesar Paixão, T., Amorim Bezerra da Silva, R. **(2017)**. Batch Injection Analysis-Multiple Pulse Amperometric Fingerprint: A Simple Approach for Fast On-site Screening of Drugs. **Electroanalysis**, 29(12), 2847-2854.

- ❏ Rocha, D. P., Dornellas, R. M., Cardoso, R. M., Narciso, L. C., Silva, M. N., Nossol, E., ... Munoz, R. A. **(2018)**. Chemically versus electrochemically reduced graphene oxide: improved amperometric and voltammetric sensors of phenolic compounds on higher roughness surfaces. **Sensors and Actuators B: Chemical**, 254, 701-708.

- ❏ Rocha, D. P., Cardoso, R. M., Mendonça, D. M., Richter, E. M., da Silva, S. G., Batista, A. D., Muñoz, R. A. **(2018)**. Solenoid Micro-pumps: A New Tool for Sample Introduction in Batch Injection Analysis Systems with Electrochemical Detection. **Electroanalysis**, 30(1), 180-186.

- ❏ Rocha, D. P., Silva, M. N., Cardoso, R. M., Castro, S. V., Tormin, T. F., Richter, E. M., ... Munoz, R. A. **(2018)**. Carbon nanotube/reduced graphene oxide thin-film nanocomposite formed at liquid-liquid interface: characterization and potential electroanalytical applications**Sensors and Actuators B: Chemical**. , 269, 293-303.

- ❏ Silva, L. A. J., Stefano, J. S., Cardoso, R. M., Prado, N. S., Soares, P. H. T., Nossol, E., ... Richter, E. M. **(2019)**. Evaluation of graphite sheets for production

of high-quality disposable sensors. **Journal of Electroanalytical Chemistry**, 833, 560-567.

- ❏ Mendonça, D. M., Rocha, D. P., Dutra, G. S., Cardoso, R. M., Batista, A. D., Richter, E. M., Munoz, R. A. **(2019)**. 3D-printed Portable Platform for Mechanized Handling and Injection of Microvolumes Coupled to Electrochemical Detection. **Electroanalysis**, 31(4), 771-777.

- ❏ João, A. F., Squissato, A. L., Fernandes, G. M., Cardoso, R. M., Batista, A. D., Muñoz, R. A. **(2019)**. Iron (III) determination in bioethanol fuel using a smartphone-based device. **Microchemical Journal**, 146, 1134-1139.

- ❏ Richter, E. M., Rocha, D. P., Cardoso, R. M., Keefe, E. M., Foster, C. W., Munoz, R. A., Banks, C. E. **(2019)**. Complete additively manufactured (3D-printed) electrochemical sensing platform. **Analytical chemistry**, 91(20), 12844-12851.

- ❏ Castro, S. V., Cardoso, R. M., Santana, M. H., Richter, E. M., Munoz, R. A. **(2019)**. Graphite sheet as a novel material for the collection and electrochemical sensing of explosive residues. **Talanta**, 203, 106-111.

- ❏ Silva, S. C., Cardoso, R. M., Richter, E. M., Munoz, R. A., Nossol, E. **(2020)**. Reduced graphene oxide/multi-walled carbon nanotubes/prussian blue nanocomposites for amperometric detection of strong oxidants. **Materials Chemistry and Physics**, 250, 123011.

- ❏ Castro, S. V., Lima, A. P., Rocha, R. G., Cardoso, R. M., Montes, R. H., Santana, M. H., ... Munoz, R. A. **(2020)**. Simultaneous determination of lead and antimony in gunshot residue using a 3D-printed platform working as sampler and sensor. **Analytica Chimica Acta**, 1130, 126-136.

- ❏ Rocha, R. G., Cardoso, R. M., Zambiazi, P. J., Castro, S. V., Ferraz, T. V., Aparecido, G. D. O., ... Richter, E. M. **(2020)**. Production of 3D-printed disposable electrochemical sensors for glucose detection using a conductive filament modified with nickel microparticles. **Analytica Chimica Acta**, 1132, 1-9.

- ❏ Rocha, R. G., Stefano, J. S., Cardoso, R. M., Zambiazi, P. J., Bonacin, J. A., Richter, E. M., Munoz, R. A. **(2020)**. Electrochemical synthesis of Prussian blue from iron impurities in 3D-printed graphene electrodes: Amperometric sensing platform for hydrogen peroxide. **Talanta** , 219, 121289.

A.4 Book Chapters

- ❏ Squissato, A. L., Rocha, D. P., Cardoso, R. M., Tormin, T. F., Munoz, R. A. **(2019)**. Nanomaterial-Based Electrochemical Sensors for Environmental and En-

ergy Applications. In Nanomaterials Design for Sensing Applications (pp. 197-228). **Elsevier**.

ANNEX **B**

Front Cover ACA

Volume 1118 29 JUNE 2020 ISSN 0003-2670

ELSEVIER

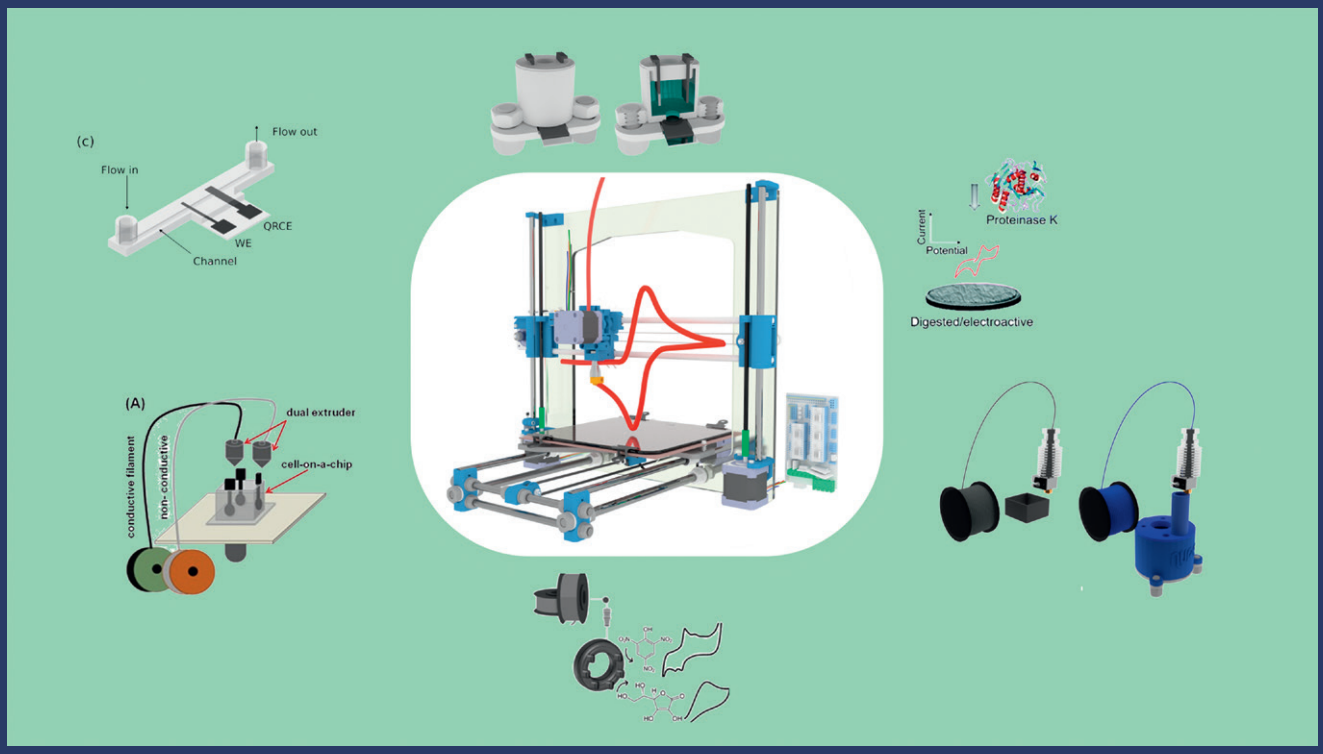

Analytica Chimica Acta

AN INTERNATIONAL JOURNAL DEVOTED TO ALL BRANCHES OF ANALYTICAL CHEMISTRY

Additive-manufactured (3D-printed) electrochemical sensors: A critical review

Rafael M. Cardoso, Cristiane Kalinke, Raquel G. Rocha, Pamyla L. dos Santos, Diego P. Rocha, Paulo R. Oliveira, Bruno C. Janegitz, Juliano A. Bonacin, Eduardo M. Richter, Rodrigo A.A. Munoz

(Published in pages 73–91 of this issue)

ANNEX C

Copyright

License Details

This Agreement between Federal University of Uberlândia -- Rafael Cardoso ("You") and Elsevier ("Elsevier") consists of your license details and the terms and conditions provided by Elsevier and Copyright Clearance Center.

Print Copy

License Number	4900240987190
License date	Sep 01, 2020
Licensed Content Publisher	Elsevier
Licensed Content Publication	Biosensors and Bioelectronics
Licensed Content Title	Sensor and biosensor preparation, optimisation and applications of Prussian Blue modified electrodes
Licensed Content Author	F. Ricci,G. Palleschi
Licensed Content Date	Sep 15, 2005
Licensed Content Volume	21
Licensed Content Issue	3
Licensed Content Pages	19
Type of Use	reuse in a thesis/dissertation
Portion	figures/tables/illustrations
Number of figures/tables/illustrations	1
Format	both print and electronic
Are you the author of this Elsevier article?	No
Will you be translating?	No
Title	Development, fabrication and application of electrochemical devices using 3D printing.
Institution name	Federal University of Uberlandia
Expected presentation date	Oct 2020
Order reference number	Scheme 1
Portions	General overview for PB-based biosensor with an oxidase enzyme.
Requestor Location	Federal University of Uberlândia Avenida Alexandre Ribeiro Guimaraes Number 365 Apartment 302 Uberlandia, Minas Gerais MG 38408050 Brazil Attn: Federal University of Uberlândia
Publisher Tax ID	GB 494 6272 12
Customer VAT ID	BR08778495601
Total	**0.00 USD**

BACK

Additive-manufactured (3D-printed) electrochemical sensors: A critical review

Author:
Rafael M. Cardoso,Cristiane Kalinke,Raquel G. Rocha,Pãmyla L. dos Santos,Diego P. Rocha,Paulo R. Oliveira,Bruno C. Janegitz,Juliano A. Bonacin,Eduardo M. Richter,Rodrigo A.A. Munoz

Publication: Analytica Chimica Acta

Publisher: Elsevier

Date: 29 June 2020

3D printing for electroanalysis: From multiuse electrochemical cells to sensors

Author:
Rafael M. Cardoso,Dianderson M.H. Mendonça,Weberson P. Silva,Murilo N.T. Silva,Edson Nossol,Rodrigo A.B. da Silva,Eduardo M. Richter,Rodrigo A.A. Muñoz

Publication: Analytica Chimica Acta

Publisher: Elsevier

Date: 29 November 2018

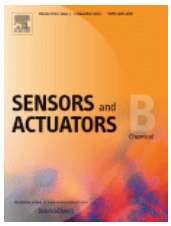

3D-printed flexible device combining sampling and detection of explosives

Author:
Rafael M. Cardoso,Sílvia V.F. Castro,Murilo N.T. Silva,Ana P. Lima,Mário H.P. Santana,Edson Nossol,Rodrigo A.B. Silva,Eduardo M. Richter,Thiago R.L.C. Paixão,Rodrigo A.A. Muñoz

Publication: Sensors and Actuators B: Chemical

Publisher: Elsevier

Date: 1 August 2019

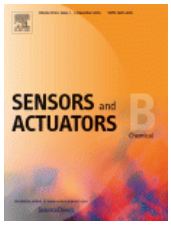

3D-Printed graphene/polylactic acid electrode for bioanalysis: Biosensing of glucose and simultaneous determination of uric acid and nitrite in biological fluids

Author:
Rafael M. Cardoso,Pablo R.L. Silva,Ana P. Lima,Diego P. Rocha,Thiago C. Oliveira,Thiago M. do Prado,Elson L. Fava,Orlando Fatibello-Filho,Eduardo M. Richter,Rodrigo A.A. Muñoz

Publication: Sensors and Actuators B: Chemical

Publisher: Elsevier

Date: 15 March 2020

3D-printing pen versus desktop 3D-printers: Fabrication of carbon black/polylactic acid electrodes for single-drop detection of 2,4,6-trinitrotoluene

Author:
Rafael M. Cardoso,Diego P. Rocha,Raquel G. Rocha,Jéssica S. Stefano,Rodrigo A.B. Silva,Eduardo M. Richter,Rodrigo A.A. Muñoz

Publication: Analytica Chimica Acta

Publisher: Elsevier

Date: 2 October 2020